Max Planck Graduate Center
mit der Johannes Gutenberg-Universität

MAX-PLANCK-GESELLSCHAFT

JOHANNES GUTENBERG UNIVERSITÄT MAINZ

JG|U

NUCLEAR MIGRATION THROUGH RING CANALS AND ITS ROLE IN CLONAL REPRODUCTION IN UNISEXUAL WHIPTAIL LIZARDS *ASPIDOSCELIS*

Dissertation

Zur Erlangung des akademischen Grades eines

„Doctor rerum naturalium“ (Dr. rer. nat) der Fachbereiche:

08 – Physik, Mathematik und Informatik

09 – Chemie, Pharmazie, Geographie und Geowissenschaften

10 – Biologie

Universitätsmedizin

vorgelegt von

Nadine Denise Bobon

Geb. am 06.02.1990 in Hagen

Mainz, 31.Oktober 2024

1. Berichterstatter:

2. Berichterstatter:

Tag der mündlichen Prüfung: 10.12.2024

Declaration

I hereby declare that I wrote the dissertation submitted without any unauthorized external assistance and used only sources acknowledged in the work. All textual passages which are appropriated verbatim or paraphrased from published and unpublished texts as well as all information obtained from oral sources are duly indicated and listed in accordance with bibliographical rules. In carrying out this research, I complied with the rules of standard scientific practice as formulated in the statutes of Johannes Gutenberg-University-Mainz to ensure standard scientific practice.

Mainz, 31. October 2024

Table of Contents

LIST OF ABBREVIATIONS

DAPI	4′,6-diamidino-2-phenylindole
ddRADseq	double digest Restriction-site Associated DNA sequencing
FACS	Fluorescence-Activated Cell Sorting
GVs	Germinal Vesicles
IF	Immunofluorescence
MKLP1	Mitotic Kinesin-Like Protein 1
NE	Nuclear Envelope
PCA	Principal Component Analysis
SC	Synaptonemal Complex
SCP1	Synaptonemal Complex Protein 1
SCP3	Synaptonemal Complex Protein 3
SNPs	Single Nucleotide Polymorphisms

LIST OF TABLES

LIST OF FIGURES

ABSTRACT

Asexual reproduction is often seen as a "dead end" in evolutionary terms. However, parthenogenetic species of whiptail lizards in the genus *Aspidoscelis* are remarkable in their unique speciation through clonal reproduction. Multiple hybridization events have led to polyploid all-female lineages that maintain high levels of heterozygosity over generations. Adaptations in oogenesis, to produce ploidy-elevated oocytes, enable the production of unreduced eggs in the absence of male fertilization. In this study we present evidence of a series of events that facilitate the migration of whole nuclei through ring canals during Prophase I in *Aspidoscelis* lizards. This process results in allopolyploid oocytes, which allow for the pairing of identical chromosomes thus enabling the continuation of meiosis. The described observation is a well-known phenomenon in the plant kingdom, known as cytomixis, and can be seen as conserved strategy for clonal reproduction in asexual species. Our investigations into the co-localization patterns of SCP1 and SCP3—two major components of the synaptonemal complex—in pachytene-like and diplotene oocytes provide strong evidence for the necessity of nuclear migration events occurring prior to synapsis in parthenogenetic species with distinct genome compositions. This was confirmed in the diploid *A. neomexicanus*, triploid *A. uniparens*, and tetraploid *A. townsendae*. Furthermore, we demonstrate that in cases of a more “balanced” genome, comprising of two genomes each of the parental species, ploidy elevation is not always necessary. This is evidenced by the presence of non-ploidy-elevated diplotene oocytes in tetraploid Sono. As a consequence, a rare instance of ploidy loss from 4N to 2N within one generation due to the development of a non-elevated oocyte through meiosis was detected. Additionally, we noted chromosome abnormalities in another *Sono* individual, suggesting a transition from 4N to 3N. We hypothesize that atypical synapsis patterns between similar but non-identical homeologous chromosomes in *Sono* may result in an unequal distribution of genes or chromosome fragments in this individual. Overall, this study reveals a mechanism of nuclear migration, which allows for identical chromosome pairing in parthenogenetic *Aspidoscelis* lizards to produce offspring with maintained heterozygosity over generations. Furthermore, the study points out the influence of genome composition for meiosis and offspring.

ZUSAMMENFASSUNG

Die asexuelle Fortpflanzung wird oft als eine Sackgasse genetischer Vielfalt in der Evolution angesehen. Parthenogenetische Peitschenschwanzrennechsen der Gattung *Aspidoscelis* stellen jedoch ein bemerkenswertes Beispiel für die Artbildung durch klonale Fortpflanzung dar. Mehrere Hybridisierungsereignisse haben zu polyploiden reinweiblichen Linien geführt, die über Generationen hinweg ein hohes Maß an Heterozygotie aufrechterhalten. Anpassungen in der Oogenese, führen im Diplotän, zur Produktion von Oozyten mit erhöhter Ploidiestufe, die die Bildung unreduzierter Eizellen in Abwesenheit männlicher Befruchtung ermöglichen. In dieser Studie identifizierten wir eine Abfolge von Ereignissen, die die Migration ganzer Zellkerne durch Ringkanäle während der Prophase I in *Aspidoscelis*-Arten belegt. Dieser Prozess führt zu allopolyploiden Oozyten, die die Paarung identischer Chromosomen ermöglichen und somit die Fortsetzung der Meiose aufrechterhalten. Die beschriebene Beobachtung ähnelt einem Phänomen aus dem Pflanzenreich, welches als Cytomixis bekannt ist. Somit kann die Migration von Zellkernen als konservierter Mechanismus für klonale Fortpflanzung in asexuellen Arten betrachtet werden. Unsere Untersuchungen fokussierten sich auf die Kolokalisierung der Proteine SCP1 und SCP3, zwei Hauptkomponenten des Synaptonemalen Komplexes (SC), in pachytän-ähnlichen und diplotänen Oozyten. Die beobachteten Muster der Kolokalisierung beider Proteine bestätigten die Notwendigkeit einer Zellkernwanderung, die vor der Synapse in parthenogenetischen Arten mit unterschiedlichen Genomkompositionen stattfinden. Dies wurde in dieser Arbeit bei der diploiden Art *A. neomexicanus*, der triploiden Art *A. uniparens* und der tetraploiden Art *A. townsendae* belegt. Darüber hinaus zeigen wir, dass in Fällen einer ‚ausgewogeneren' Genomzusammensetzung, die aus je zwei Genomen von zwei Elternarten besteht, die Verdopplung der Ploidie in Oozyten im Pachytän nicht zwingend erforderlich ist. Das einzigartige Vorkommen diploider Oozyten im Diplotän bei tetraploiden *Sono* belegt dies. Daraus ergibt sich eine Reduktion der Ploidie von 4N auf 2N in der nachfolgenden Generation. Zudem stellten wir in einem weiteren *Sono*-Individuum Chromosomenanomalien sowie einen Verlust der Ploidie von 4N auf 3N fest und vermuten, dass atypische Synapsismuster zwischen ähnlichen, aber nicht identischen Chromosomen zu einer ungleichen Verteilung von Genen oder Chromosomenfragmenten geführt haben. Insgesamt zeigt diese Studie den Mechanismus, der die identische Chromosomenpaarung bei parthenogenetischen *Aspidoscelis*-Arten sichert, um Nachkommen mit erhaltener Ploidie und Heterozygotie zu erzeugen. Zusätzlich wird der Einfluss von Genomzusammensetzung auf die Meiose und die Nachkommenschaft analysiert.

I. INTRODUCTION

I.I. Parthenogenesis and hybridization in whiptail lizards *Aspidoscelis*

Whiptail lizards of the genus *Aspidoscelis*, formerly *Cnemidophorus*, (Squamata: Teiidae) consist of approximately 50 bisexual and parthenogenetic species, mainly distributed in arid and semiarid regions, such as deserts, grasslands and scrublands of the southwestern United States and Mexico (Reeder et al., 2002).

Morphologically they are characterized by their long, slender bodies, and varying in a range of colors from brown, gray and green to more vibrant hues with patterns of stripes, spots or a combination of both (Fig.1). Notably, their long, whip-like tail can detach and continue moving, to distract predators. *Aspidoscelis* lizards are diurnal and are known for their speed and agility.

One of their key features, is the occurrence of parthenogenetic all-female species originated by interspecific hybridization of ancestral sexual species (Wright et al., 1983). Unisexual reproduction is documented in more than 80 vertebrate taxa, but reptiles, particularly within the Teiidae family and snakes, are unique for the occurrence of true obligate parthenogenesis (Kearney et al., 2009). True obligate parthenogenesis is defined as reproduction when females produce unreduced eggs in the absence of any male contribution which result in viable offspring (Neaves & Baumann 2011). In the genus *Aspidoscelis*, cases of true obligate parthenogenesis are observed in species originating from historical hybridization events, such as *A. neomexicanus*, which is the result of a hybridization event between *A. arizonae* and *A. marmoratus* (Fig. 2). Facultative parthenogenesis is when reproduction can occur with or without sexual reproduction and is limited to the sexual species of this genus, such as *A. marmoratus* or *A. arizonae* (Ho et al., 2024). Even though, parthenogenesis is often referred to as “dead-end” in evolution caused by the potential loss of genetic diversity, parthenogenetic species do not exhibit significant reductions in fecundity or survival despite the lack of genetic recombination (Newton et al, 2016; Fujita et al., 2020). In fact, parthenogenesis can also be a highly effective strategy to produce large numbers of offspring in a stable environment or colonize new environments quickly, where mates are rare. The success of true obligate parthenogenesis can be seen in *A. neomexicanus*, which is colonizing its environment for approximately 200,000 years (Barley et al., 2022). As these species have been taxonomically reclassified many times, this thesis follows the *Aspidoscelis* taxonomy described by Barley et al., 2022. Currently, research is being conducted to determine whether the subspecies *A. inornatus arizonae* can be reclassified into two separate species.

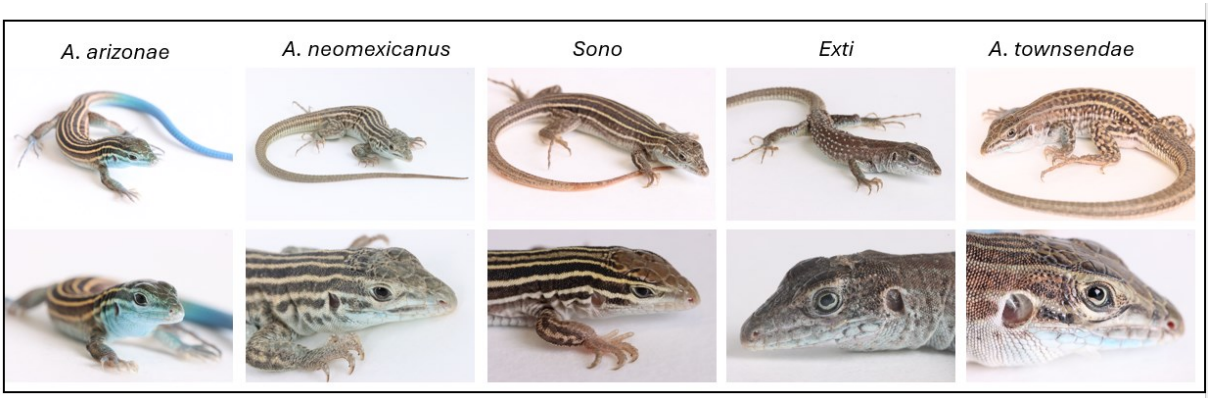

Figure 1: Overview of different lizard species. From left to right: sexual diploid male of *A. arizonae*; parthenogenetic diploid female *A. neomexicanus*; parthenogenetic tetraploid females: Sono, Exti and *A. townsendae.* Pictures were taken by Alara Ö.

The basis of all parthenogenetic lizards goes back to hybridization events between sexual progenitors; thus, they are inheriting a perpetually hybrid genome, composed of at least one haploid genome from each parental species (Fujita et al., 2020). This happened in overlapping territories in the wild, as well as in captivity in the laboratory (Lutes et al., 2011). Additional rounds of hybridization have generated a network of polyploid lineages such as triploids and tetraploids due to backcrossing with one of the parental species or a third species (Lutes et al., 2011) (Fig. 2) and shows how allopolyploidy speciation via hybridization can be seen as the driving force in diversification in *Aspidoscelis* (Cole, 1997; Dessauer & Cole, 1986). In general, these hybridization events are possible because the species involved are not highly divergent from each other (Lowe & Wright, 1966; Manning et al, 2005). Ancestral sexual species are often homozygous for specific alleles at numerous loci, and therefore combining the alleles of the ancestral species is resulting in parthenogenetic offspring with a high level of heterozygosity as each allele now originates from a genome of a different species (Neaves & Baumann, 2011). The combination of two or more genomes in a hybrid species also results in a great diversity in chromosome number and structure in parthenogenetic species (Barley et al., 2022; Barley et al., 2024). The maintenance of heterozygosity observed in asexual *Aspidoscelis* species has been confirmed through allozyme analysis by Dessauer and Cole, who used electrophoresis of tissue proteins to demonstrate that all individuals within a lineage possess identical allele combinations. Their findings concluded that each individual within a lineage represents a genetic clone with ‘fixed’ heterozygosity (Dessauer & Cole, 1986).

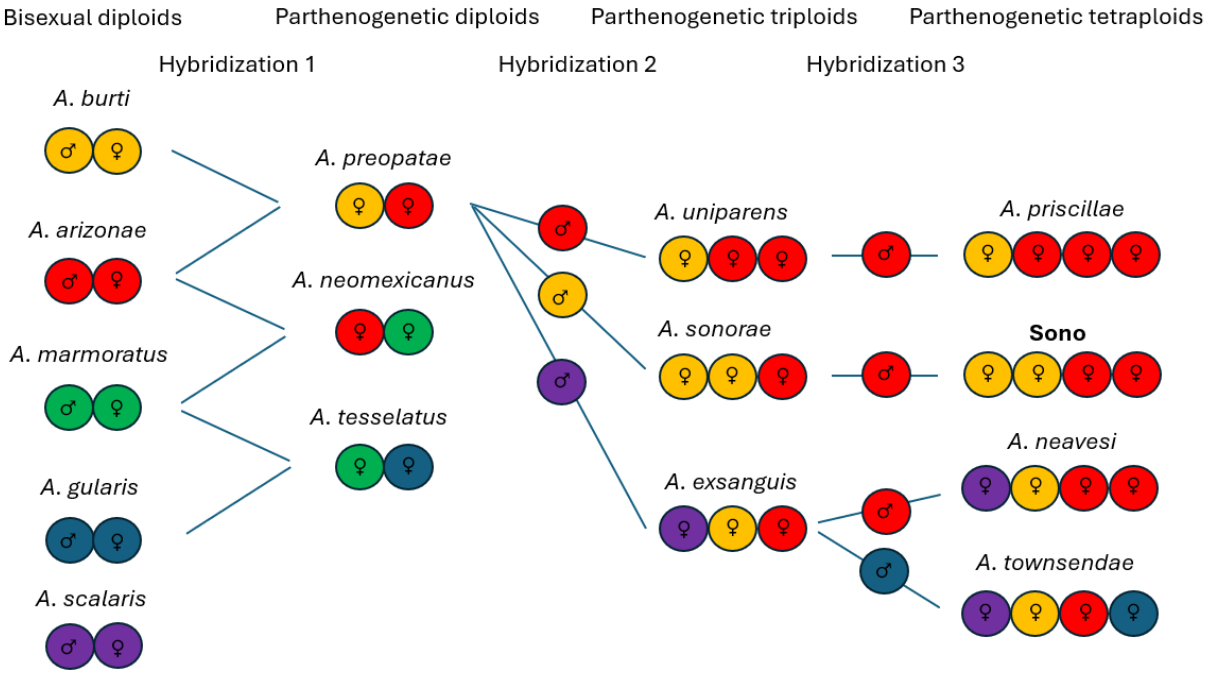

Figure 2: Network of different hybridization events between sexual and asexual species of *Aspidoscelis*. Each color represents a distinct species, and each genome is represented by a circle. Sexual species are marked with ♂♀, parthenogenetic all-females are marked with ♀♀ respectively.

I.II. Modifications of oogenesis in parthenogenetic *Aspidoscelis*

In contrast to sexual reproduction, the parthenogenetic pathway requires a modification of oogenesis, to generate eggs with a full set of chromosomes in the absence of fertilization (Lutes et al., 2010). Their findings demonstrate that parthenogenetic species are entering the diplotene stage of meiosis with twice the number of chromosomes. This bypasses the need for genetic contribution from males and as a result, the normal meiotic program produces the expected diploid eggs. This was confirmed through fluorescent in situ hybridization (FISH) using peptide-nucleic acid (PNA) and locked-nucleic acid (LNA) probes in germinal vesicles (GVs). This revealed an important deviation to the normal canonical meiotic pathways; in parthenogenetic species chromosome pairing and recombination takes place between identical chromosomes instead of homologous chromosomes (Fig. 3) (Lutes et al., 2010).

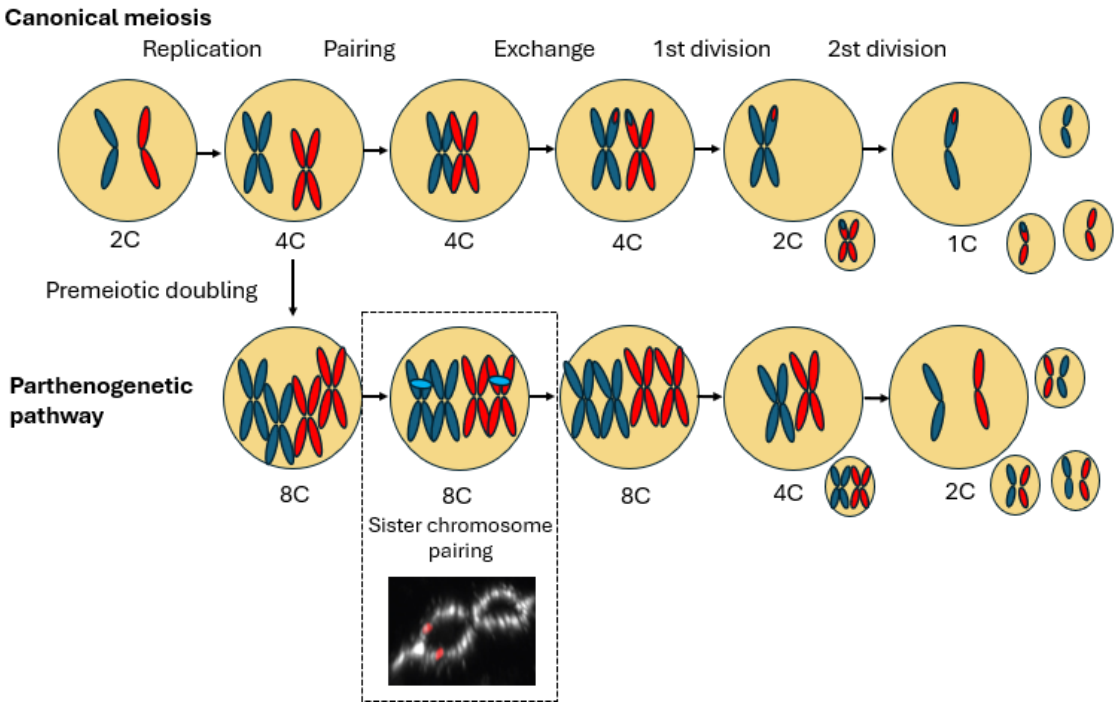

Figure 3: Comparison of sexual and parthenogenetic pathway of meiosis. Canonical meiosis allows for pairing of homologous chromosomes and results in a haploid gamete and three polar bodies (sexual reproduction). In the parthenogenetic pathway, the premeiotic doubling of chromosomes leads to 8C cells in diploid species. Identical chromosome pairing occurs between homeologous and produces diploid gametes with three polar bodies, which maintain heterozygosity and eliminates the need for fertilization. Adapted from Lutes et al., 2010.

Further investigations were done in the germinal beds, a structure within the ovaries of lower vertebrates containing all stages of germ cell development such as primordial cells and early primary follicles (Fig. 4A), focusing on staining against the Synaptonemal Complex Protein-3 (SCP3) (Fig. 4B). SCP3 localizes to the axial elements of the complex (red), prior to synapsis. The axial elements turn into lateral elements when synapsis occurs. SCP1 is a component of the central element (green). In contrast to SCP3 which is already visible before synapsis occurs, the presence of SCP1 is restricted to chromosomes synonymous with synapsis (Krester et al., 1994).

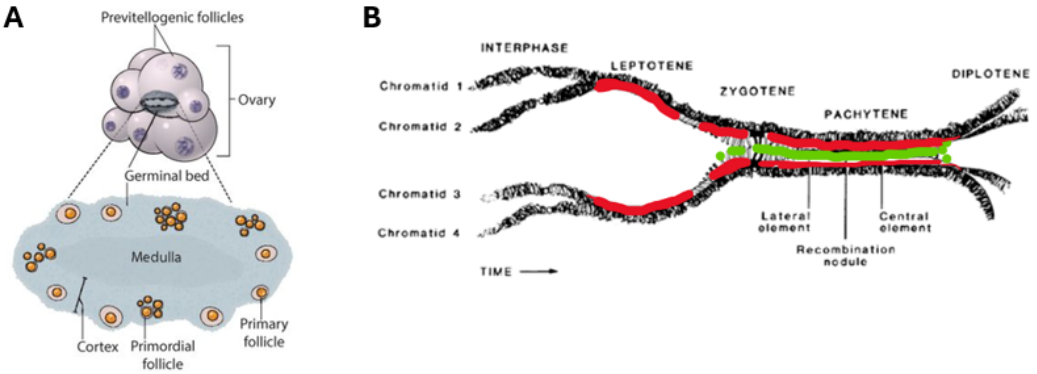

Figure 4: Schematics of ovaries and the Synaptonemal complex. **A:** Schematic of ovaries including previtellogenic follicles and the germinal bed, which is found in reptiles (Newton et al., 2016). **B:** Diagram of the synaptonemal complex (SC). The Diagram was adapted from de Kretser DM, Kerr JB. The cytology of the testes. In: Knobil E, Neill JD, eds. The physiology of reproduction, 2nd ed. New York: Raven Press, 1994).

Newton et al., 2016 cloned and purified SCP3 from sexually reproducing *Aspidoscelis gularis* and raised polyclonal antibodies against it. This antibody was used for all further studies (including this work) and allows for identification of cells in each stage of meiotic prophase (Fig. 5A).

The DNA content of pachytene-like and early diplotene cells were quantified and compared from sexual and parthenogenetic species to determine the time point at which the ploidy increase occurs (Fig. 5B). This led to the observation that in parthenogenetic species, diploid oocytes enter the early stages of prophase I in large numbers, 75% - 83% of cells accumulate at the pairing stage and fail to progress further because synapsis is impaired due to differences of homeologous chromosomes (Fig. 5C). Only a rare number of pseudo-tetraploid cells are progressing into diplotene and therefore the earlier assumption of a tetraploid germline in parthenogenetic species could be eliminated (Newton et al., 2016). Furthermore, investigations of homeologous chromosomes in *A. neomexicanus* obtained by SIM reveal the occurrence of unpaired and a majority of partially paired chromosomes (Fig. 5D). The partial pairing is generally located near the chromosome ends in 4C state oocytes. Only one case of complete pairing was observed in this study. Their findings confirmed that synapsis of homeologous chromosomes is impaired in non-elevated 4C oocytes in *A. neomexicanus*.

These brought up that structural differences and sequence divergence between ancestral homeologous chromosomes in asexual species might cause the arrest at the pairing state for those oocytes that haven’t doubled their DNA content.

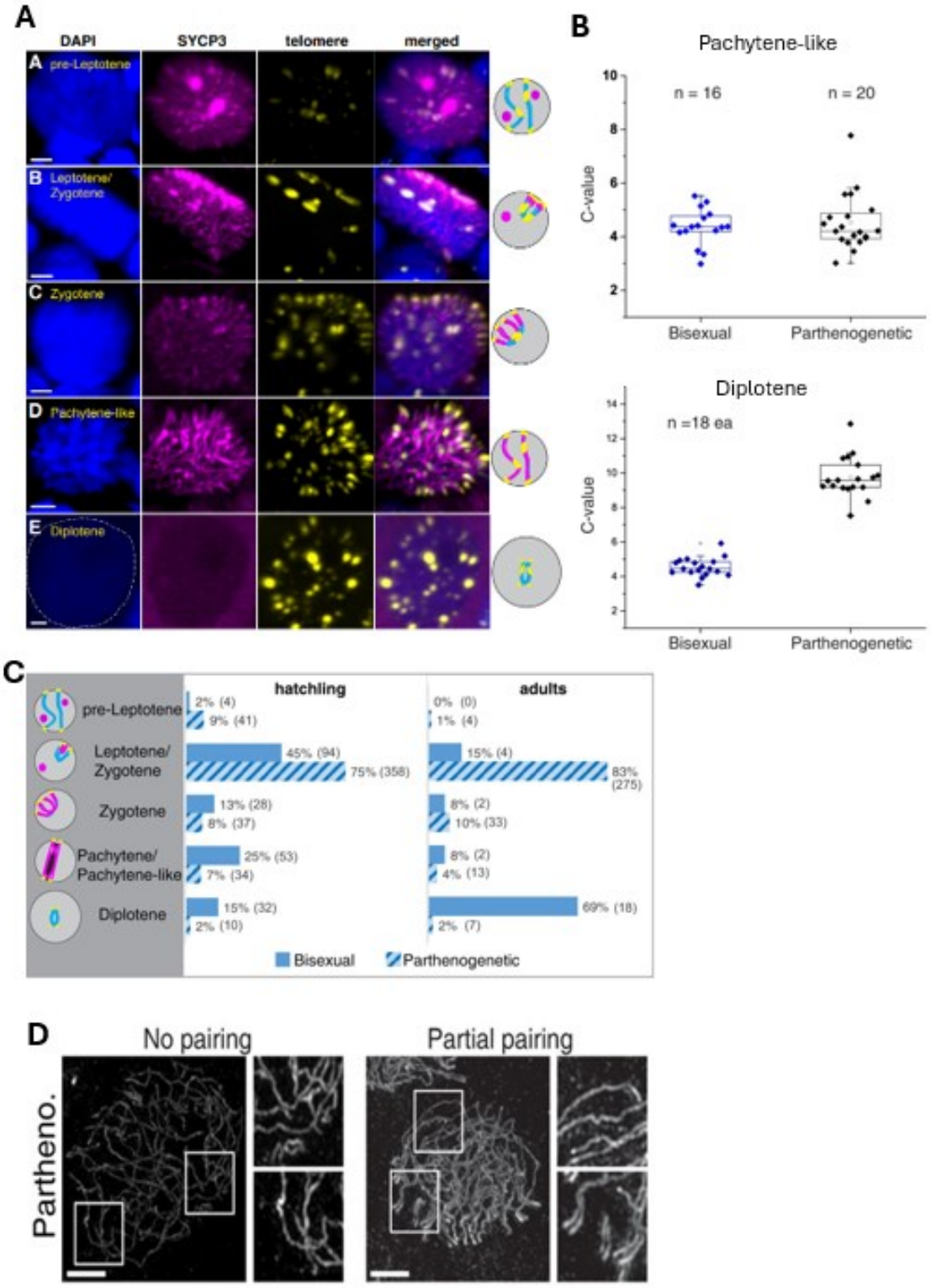

Figure 5: Investigations of meiotic Prophase I**: A**: Different stages of Prophase I in parthenogenetic species *A. neomexicanus*. Pre-Leptotene to Leptotene can be characterized by few SCP3 loci. Leptotene to Zygotene stage oocytes can be identified by partial SCP3 staining of chromosomes axes, the telomeres are clustering at the nuclear periphery at Late-Zygotene. Oocytes with cells showing extended tracks of chromosomes by SCP3 and a dissolving of telomere clustering defines pachytene oocytes. In Diplotene, SCP3 staining, and a characteristic pattern of telomeres is missing. **B**: DNA content analysis of pachytene-like (top) and diplotene oocytes (bottom) of the same species as in A. **C**: Occurrence of oocytes across Prophase I in hatchlings and adults of *A. inornatus* (solid blue) and *A. neomexicanus* (striped). **D:** Structured illumination microscopy (SIM) of SYCP3 threads resolves lateral elements on paired chromosomes. Unpaired and partially paired chromosomes from *A. neomexicanus* hatchling. Scale bars: 2 µm. Figure adapted from Newton et al., 2016.

I.III. The synteny of homeologous chromosomes

The assumption of the inability of homeologous chromosomes to synapse without prior DNA duplication if the hybrid genome composition is too distinct, is supported by considering the chromosome structures of the species involved. The karyotypes of the parental species show a haploid genome comprised of 23 chromosomes. The number of macro, mid-sized and micro chromosomes vary by species due to fission and fusion events that have occurred during the evolutionary history within this genus (Cole et al., 1988). *A. neomexicanus* inherited 23 chromosomes each from either parental species (Fig. 6A). The syntenic average gap-compressed percent identity of 94.67% across the entire chromosome length of *A. marmoratus* and *A. arizonae* (unpublished data from David Ho) indicates a high degree of heterozygosity due to its hybrid origin (Britten, 2002). Several fusion and fission events have occurred between the individual chromosomes over time (Fig. 6B). One fusion event involving chromosomes 2, 22, and 23 of *A. marmoratus* resulted in the formation of the present-day chromosome 1 in *A. arizonae*. A second fusion event of the two mid-sized chromosomes 2 and 3 of *A. arizonae* resulted in the present-day macro-chromosome 1 in *A. marmoratus* and a third fusion of two mid-sized chromosomes 4 and 13 of *A. arizonae* resulted in syntenic macro-chromosome 3 of present-day *A. marmoratus.* These observations of differences in chromosome architecture are consistent with descriptions of Reeder et al., 2002 and Lutes et al., 2010.

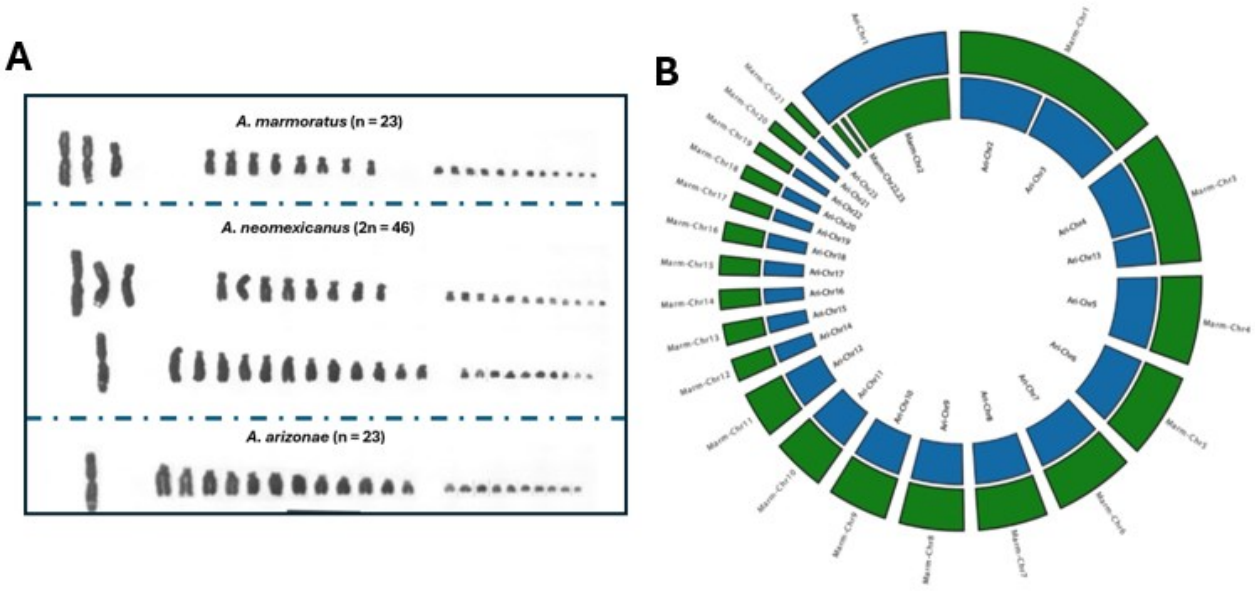

Figure 6: Chromosomal differences in *A. neomexicanus*: **A:** Karyotypes of *A. marmoratus* in a haploid state (n=23) at the top, *A. neomexicanus* in a diploid state (n=46) middle, and *A. arizonae* in a haploid state (n=23) bottom. Figure adapted from Cole et al., 1988. **B:** Circos plot showing fissions and fusions between the 23 chromosomes of *A. marmoratus* (green) and *A. arizonae* (blue). Circos plot was generated by David Ho and Aaron Odell (Unpublished data).

For a better understanding of the influence of genome composition on synapsis pattern between chromosomes, this work includes investigations on triploid *A. uniparens* and two tetraploid species. Tetraploid *A. townsendae* comprises of four distinct genomes from four ancestral species (Fig. 2). Similar to the tetraploids *A. neavesi* and *A. priscillae*, *A. townsendae* was successfully created in the lab (Cole et al., 2023). The next step was to test if it is possible to create a tetraploid with a "balanced" genome composition comprising of two similar genomes each and to see its consequences in regard to chromosome pairing during synapsis and ploidy in the offspring generation (Fig. 2).

The "balanced" Sono genome comprises of two genomes each of *A. arizonae* and *A. burti*. The synteny analysis conducted by David Ho reveals a consistent 1:1 syntenic pattern between all 23 chromosomes of *A. burti* and their corresponding chromosomes in *A. arizonae* (Fig. 7, unpublished data). This observation aligns with the recently published evolutionary network of whiptail lizards by Barely et al. (2022), indicating that *A. burti* and *A. arizonae* share a more recent common ancestor than *A. arizonae* and *A. marmoratus*. This indicates that the genome composition within Sono (burti x arizonae) is more similar than the genome composition within *A. neomexicanus* (marmoratus x arizonae).

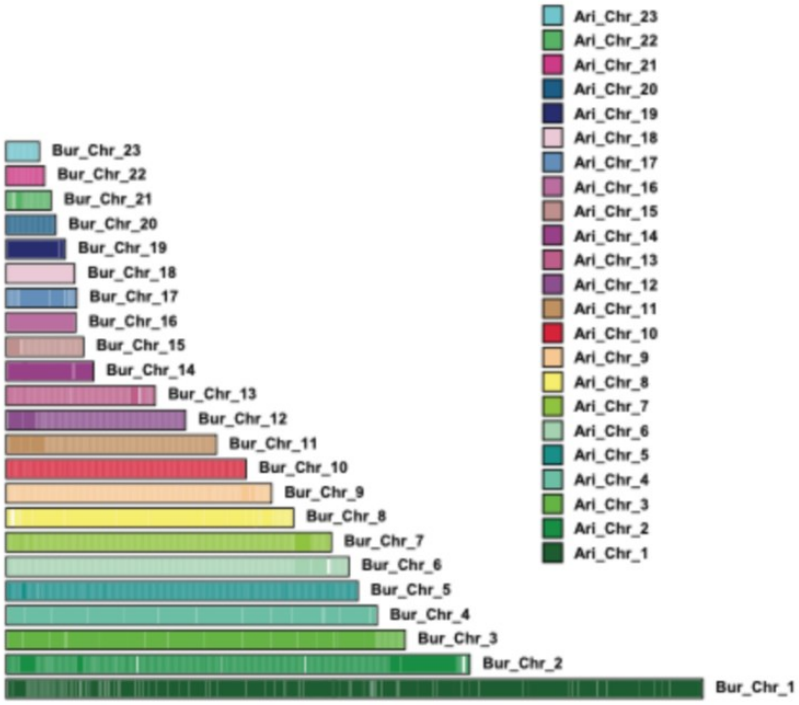

Figure 7: Synteny plot of *A. burti* and *A. arizonae* chromosomes. Generated by David Ho (unpublished data). Each large bar represents one of the 23 *A. burti* chromosomes, and the colored blocks within each bar represent *A. arizonae* scaffolds that are syntenic to specific regions of the *A. burti* genome.

Recent studies of Zhao et al., 2023 performed in synthetic allotetraploid wheat point out the significant correlation of sequence synteny in the sub-telomeric regions with meiotic chromosome

pairing irregularity. They point out that homeologous chromosome pairing is one of the major mechanisms of genome instability in allopolyploids causing rapid changes in the karyotypes. This shows the importance of considering different *Aspidoscelis* hybrids in regard to the mechanisms leading to ploidy elevated oocytes to maintain heterozygosity in the next generation.

I.IV. Emergence of ploidy elevated oocytes

The foundation of true parthenogenetic reproduction lies in the adaptation of the meiotic pathway, allowing the production of eggs with the same ploidy as somatic cells, thereby bypassing the need for male fertilization. In parthenogenesis, meiosis is modified to restore the original chromosome number through mechanisms such as premeiotic endoreplication, a process recently confirmed in rock lizards of the genus *Darevskia* (Dedukh et al., 2024). They based their conclusions on the presence of oocytes with duplicated genomes by comparing the number of bivalents between sexual and obligate parthenogenetic species only in the diplotene stage. Evidence for a ploidy elevation in earlier stages from earlier studies were contradicted by difficulties in identifying mis-paired chromosomes in pachytene stage (Dedukh et al, 2024).

However, in contrast to these findings considering the previous results by Newton et al., 2016, their observation that earlier stages of germline stem cells to zygotene and the majority of the cells in pachytene-like stage are 4c indicate the absence of a tetraploid germline and premeiotic endoreplication as the underlying mechanism in *Aspidoscelis*.

This work aims to reveal the pathway leading to the emergence of ploidy-elevated oocytes in obligate parthenogenetic species, enabling them to bypass the inability of homeologous chromosomes to synapse. To achieve this, immunostaining experiments were conducted to examine the overall structure and mechanisms within and around oocytes in lizard germinal beds, with a particular emphasis on synapsis patterns between identical chromosomes. This approach allows for the observation of nuclear dynamics during Prophase I in parthenogenetic species, mimicking a well-known phenomenon in plants-cytomixis. Additionally, species with varying ploidy levels were included to highlight differences in genome composition. This study confirms that the newly identified tetraploid species, *A. townsendae*, maintains high heterozygosity and tetraploidy parthenogenetically over generations (Cole et al., 2023). Special attention is given to the tetraploid *Sono*, due to its “balanced” genome composition and the implications this has for meiotic pathways and ploidy maintenance in subsequent generations.

II. MATERIALS AND METHODS

Table 1 gives an overview of how many lizards were included for which method. Several lizards were used in more than one approach.

Table 1: Overview of lizards used in this work.

Procedure	**# Lizards**
gDNA extractions	113
Genotyping (Blood smears)	129
Cloning + Sanger Sequencing	9
RADseq	108
FACS	18
Germinal bed Isolation + IF	13

II.I. Isolation of whole intact germinal beds

To characterize meiotic Prophase I in *Aspidoscelis*, intact germinal beds were isolated of parthenogenetic diploid, triploid and tetraploid species. The germinal bed is a structure within the ovaries, where early stages of germ cell development take place (Fig. 4). To isolate the germinal beds, the lizards were sacrificed at an age range between 16 to 40 days. The lungs, heart, liver, brain and tail were collected in 1.5 ml Eppendorf tubes and were subsequently flash frozen in liquid nitrogen. The ovaries, which are attached to the adrenal glands, were collected and transferred into 1X phosphate buffered saline (PBS) pH 7.4 for further dissection under the Leica MZ16 Stereomicroscope. Dumont #4 and #5 fine forceps were used from here on, to keep the desired structures intact during the isolation process. The carcasses were stored in 5 ml tubes, flash frozen and placed, together with the organs, at – 80°C for long term storage. After successful isolations, the germinal beds were transferred to fresh 1X PBS to proceed with the immunostaining protocol.

II.II. Immunofluorescence

For this work, a variation of antibodies was used to visualize the synaptonemal complex before and after synapsis (SCP1 + SCP3), the ring canal structure (MKLP1), and F-actin (Phalloidin). Table 2 gives a detailed overview of the antibodies used in this work.

Table 2: Summary of antibodies and staining used for immunofluorescence of intact germinal beds.

Type	Antibody	Catalog ID	Supplier	Species	Clonality	Iso-form	Conc.	Dilution in 1%BSA/PBS
1°	anti- SCP1	GTX15087	Biozol	rabbit	Poly		1mg/mL	1:100
1°	anti-SCP3	Clone YZ3150	Lab stock	rabbit	Poly			1:500
1°	anti-MKLP1	sc-136473	Santa Cruz	mouse	Mono	IgG	0,2mg/mL	1.100
2°	AF-488	A32731	Invitrogen	rabbit	Poly	IgG	2mg/mL	1:300
2°	AF-635	A31577	Invitrogen	rabbit	Poly	IgG	2mg/mL	1:300
2°	AF-546	A11030	Invitrogen	mouse	Poly	IgG	2mg/mL	1:300
Staining kit	F-actin (Phalloidin)	ab112127	Abcam	mammals	-	-	-	-

After isolating the germinal beds in 1X PBS, they were transferred to 100% cold methanol fixative for 45 – 60 minutes at 4°C. Then washed twice for 5 minutes in 1X PBS and blocked in 1% bovine serum albumin (BSA) + 0.2% Triton X-100 in 1X PBS for two hours at room temperature. Samples were then incubated overnight at 4°C with primary antibodies (Table 2) in 1X PBS (+ 1% BSA). After that, samples were washed four times for 30 minutes each wash with 400µl 1X PBS (+ 1% BSA) and incubated at 4°C overnight with secondary antibodies. After four washes for 30 minutes each with 400 µl 1X PBS (+1% BSA) and one single wash with 400 µl of 1X PBS at room temperature, samples were incubated in 1µg/ml 4',6-diamidino-2-phenylindole (DAPI) in 1X PBS or 1µg/ml DAPI in 1X PBS + 1/1000 cytopainter phalloidin for at least three hours. A final wash was performed for 30 minutes with 1X PBS. Prior to imaging, germinal beds were mounted and sealed in a 35 mm glass bottom imaging dish (Ibidi, Cat. No: 81158), within a ring of vacuum grease filled with 1X PBS and covered with a 22 x 22 mm coverslip.

II.III. Confocal spinning disk microscopy

All isolated germinal beds were acquired at VisiScope 5 Elements spinning disc confocal microscope (Visitron Systems GmbH) built on a Nikon Ti2 stand and equipped with a CSU-W1 spinning disk Yokogawa and Prime BSI sCMOS camera (2048 x 2048 pixels, 6,5 µm pixel size, Photometrics. The CFI Plan Apo VC 60x (1.2 NA, water) objective was used to acquire Z-stacks with a step size of 0.3 µm with up to four different laser lines sequentially (laser power and exposure times were set individually) using the acquisition software VisiView (Version 6.0.0). The laser lines 405nm, 488nm, 561nm and 640nm and corresponding fluorescence emission filters ET460/50m (Chroma), ET525/50m(Chroma), FF01-623/32 (Semrock) and FF01-692/40 (Semrock) was used to capture fluorescence of DAPI, Alexa Fluor 488, Phalloidin 555 and Alexa Fluor 635 respectively. Images were processed in Imaris (Version 10.1.1) or ImageJ 1.54i (Schindelin et al., 2012).

II.IV. Quantification of DNA content

To specify the exact timepoint of the doubling of DNA content during germ cell development in parthenogenetic species, 321 cells, including somatic cells (n=119) and oocytes in different stages of meiosis (pachytene-like n=152; diplotene n=50), in whole-mount DAPI-stained germinal beds from four different hybrid species were examined. This quantification is based on the method described in Newton et al., 2016 with some modifications. For that, images in the DAPI channel from DAPI and SCP3 stained germinal beds were analyzed using ImageJ 1.54i software. As the high cell density prevented an automated 3D cell segmentation, the 3D DNA content was estimated by a simplified model assuming spherical cells. First, midsections of randomly picked somatic cells, and the nuclei of pachytene-like oocytes (identified by positive SCP3) and diplotene oocytes (identified based on morphology and missing SCP3 staining) were identified and selected manually with the oval or freehand selection tool. For each selected nuclei, the area, the mean and integrated intensity were measured in 2D, and cell radii were calculated. Then, the total 3D DNA intensity was calculated for spherical volume according to

$$I_{total} = \frac{4}{3}\pi r^3 \cdot I_{mean}$$

with r and I_{mean} being the radius and mean intensity determined from the 2D midsections.

The average values of the 3D intensity of the somatic cells were set as 2C in the diploid species, 3C in the triploid species and 4C in the tetraploid species. The DNA content of the nuclei from pachytene-like and diplotene oocytes were then determined relative to this somatic cell standard.

II.V. Ploidy analysis using DAPI stained erythrocytes

Unlike mammals, lizards and other non-mammalian vertebrates including birds, amphibians and fish have nucleated erythrocytes (Moller et al., 2016). This significant feature was used to determine the ploidy levels of the hybrid Sono's through all lineages and generations of the colony. As controls, blood smears of diploid *A. neomexicanus* and triploid *A. sonorae* were used on each slide. In total, 129 lizards were analysed following the procedure of tail clipping, blood smear preparation, DAPI staining, widefield imaging and quantification in ImageJ. After tail clipping, a small drop of blood was collected on a clean microscope slide and a cover glass was used at a 30-45° angle to the slide with the blood drop to quickly and smoothly spread the blood into a thin film over the microscope slide. The piece of tail was flash frozen in liquid nitrogen and stored at -80°C. After the blood smears were air-dried, the DAPI staining was performed in Coplin Jars. For that the slides were fixed in 95% EtOH solution for 3- 5 minutes and then air-dried. After that the slides were incubated in 1:5000 1mg/mL DAPI stain in 1X PBS in the dark for 10 minutes, followed by a quick wash in 1X PBS by dunking slides five times. After air-drying for around 20 minutes, slides were mounted with DAKO Fluorescent Mounting Media (Agilent) and were imaged on a widefield microscope. The Leica Thunder inverted widefield microscope was used with a 40x/0.95 air objective. Images were acquired with the LasX software (V3.7.6.25997) with transmitted light-Brightfield and with the DFT51010 Quadband filter cube (Ex:375-407) for DAPI with the following settings: exposure time 100ms; Light mode FIM 100%, Il-Fld 6; Laser power (390) 3%; BF Intensity 83, Aperture 4, Tl-Fld 22; gain list: low noise & high well, no binning. Quantification of blood smears was performed in ImageJ by splitting the channels and using the DAPI channel in the "Make Binary" function to select for nuclei. After questionable nuclei were removed, the area of nuclei was measured in the ROI manager and transferred to excel for further analysis. To confirm the accuracy of this method, a few samples including diploids, triploids and tetraploids, were measured in parallel on the BD LSRFortessa TM cell analyzer using propidium iodide staining (described in II.X).

II.VI. gDNA extraction

Genomic DNA of 113 lizards including specimens of eight different species was extracted and subjected to different sequencing approaches such as Sanger and RADseq. For that, high molecular weight gDNA was extracted from approximately 10- 200 mg of tail tissue using the Blood & Cell Culture DNA Midi Kit (Qiagen, Cat. No./ID: 13343). For each sample below 20 mg (G20 tip) Buffer G2 was prepared by combining 4 µL of RNase A to 2 mL of Buffer G2. For samples between 20 – 200 mg (G100-tip), 19 µL RNase A and 9.5 mL of Buffer G2 were combined. Samples were added to a with liquid nitrogen pre-cooled mortar and homogenized into a fine powder by adding up to three pours of liquid nitrogen. The prepared Buffer G2 and 100µL Proteinase K for G20 samples and 500 µL Proteinase K for G100 samples was added to the mortar. The mixture was transferred into a 50 mL rapid-spin conical tube and incubated at 50°C for a minimum of three hours up to overnight to lyse the tissue. For each sample, 20/G or 100/G genomic tips were equilibrated by adding 2 mL or 5 mL Buffer QBT. After tissue lysis the samples were centrifuged at 3.200 x g for 10 minutes at 4°C and the supernatant was directly transferred to a new tube, for vortexing at maximum speed for 10 seconds and added to the equilibrized genomic-tip and left to flow-through. After the solution has flowed through, 5 x 1 mL (G20) or 2 x 7,5 mL (G100) Buffer QC was added to the tips and left to flow-through to wash the samples. After the washing, the genomic tips, including the DNA, were placed over fresh 15 mL rapid-spin conical tubes and 2 x 1 mL or 5 mL pre-warmed Buffer QF was added to elute the DNA. 0.7 x RT Isopropanol and 1 µL GlycoBlue were added to each sample to precipitate the DNA. Tubes were centrifuged at 7500 x g for 15 minutes at 4°C, the supernatant removed, and the pellet washed with 2 mL fresh and cold 70% EtOH, vortexed briefly and again centrifuged at 7500 x g for 10 minutes at 4°C. The supernatant was removed without disturbing the pellet and air-dried for 10 minutes. Next, the DNA was resuspended in 75 µL of Qiagen EB Elution Buffer and dissolved at 55°C for 1 -2 hours. The samples were transferred to a DNA LoBind 1.5 mL tube and placed at 4°C overnight before quantification.

The Qubit BR dsDNA Assay Kit (Life Technologies) was used according to the manufacturer's specifications, for gDNA quantification. For that, 1 µl of sample DNA were added to 198 µl of buffer solution and 1 µl reagent.

II.VII. Cloning, Sanger sequencing and analysis

To confirm a new tetraploid parthenogenetic whiptail lizard species derived from hybridization among four bisexual ancestral species of *Aspidoscelis*, DNA sequencing data for adenosine deaminase intron 9 was used (Cole et al., 2023). PCR primers (281T: GTTTGAAATCTACATGCCAG and 282B: GCTTTGGTTTCCACAAACTA) were designed based on ADA cDNA from *A. arizonae* to amplify parts of exons 9 and 10 and the intervening intron from genomic DNA. The ADA gene sequences of *A. marmoratus* (GenBank ON661265) and *A. gularis* (GenBank ON661263) were used to check sequence identity of the primer annealing sites within these species (by David Ho). The region of interest was amplified by PCR for *A. exsanguis* (SIMR 22519), *A. gularis* (SIMR 007), *A. burti* (SIMR 12836) and two individuals of *A. townsendae* (SIMR 25022 and D500) with an Eppendorf Mastercycler X50s in 20-mL reactions containing 4 µL of 5X Phusion HF Buffer, 0.2 mM dNTPs, 0.5 µM of each primer, 20 ng of genomic DNA and 0.2 µL of Phusion DNA polymerase. The initial denaturation was set to 30 sec at 98 °C. Thirty cycles of 10 sec at 98°C followed by 15 sec at 59°C and 40 sec at 72 °C were used for amplification. The final extension was performed at 72 °C for 10 minutes. PCR products were run on a 1% agarose gel in Trisborate EDTA and purified with the QIA-quick Gel Extraction Kit (Qiagen, Cat. No. 28706) following the manufacturer's instructions. For that the DNA fragment was excised from the agarose gel with a clean, sharp scalpel. After weighing the gel slice, three volumes of Buffer QG were added to one volume of gel and incubated for 50°C for 10 min. After dissolving, one gel volume isopropanol was added to the sample and mixed and the sample was applied to the QIAquick column and centrifuged for 1 min. The flow-through was discarded and 500 µl of Buffer QG were added to the QIAquick column and centrifuged for 1 min. Again, the flow-through was discarded and for washing, 750 µl of Buffer PE were added to the column, let stand for 5 min, and then centrifuged again for 1 min. The QIAquick column was placed into a clean 1.5 ml microcentrifuge tube and was eluted by adding 50 µl of Buffer EB to the center of the QIAquick membrane, let stand for 4 min and finally centrifuged for 1 min.

The purified PCR products were cloned into the pCR 4Blunt-TOPO vector (Thermo Fisher, 450159), transformants were picked, and plasmid DNA was isolated for Sanger Sequencing. Sequence Alignments were created by Muscle (v 3.8.1551) within SnapGene Version 5.2.4 with the program's default parameters. The evolutionary history was inferred by the Maximum Likelihood and Tamura-Nei model in MEGA Version 10.1.8 (Kumar et al., 2018). The Tamura-Nei model was used with uniform rates among sites, using all sites (including gaps). Bootstrap resampling of 500 replicates estimated the statistical confidence in the branch points of the tree. Initial trees for the

heuristic search were obtained automatically by applying Neighbor-Join and BioNJ algorithm to a matrix of pairwise distances estimated by the Tamura-Nei model. The topology was selected by superior log likelihood values and the cutoff value for condensed tree was set to 55%.

II.VIII. Restriction-site associated DNA sequencing (ddRADseq)

To follow on genetic differences in the different lineages of the tetraploid Sono animals in the colony, RADseq was chosen to analyze a large number of loci across the genome. The RADseq library prep contains five major steps, including restriction digest with SbfI-HF and NlaIII, A1.X and A2.1 adapter ligation, size selection with Blue Pippin, the amplification of unique dual indices (UDI; P5/P7), the final pooling for sequencing and some pre-library prep steps such as adapter annealing and preparation of working stocks and was performed together with Valentine P. and David H.

All adapters (A1.X = including inline barcodes and SbfI overhang; A2.1 = adapters with NlaIII overhang) were resuspended to a concentration of 200 µM (Tab. 3).

Table 3: Overview of adapters used for ddRADseq.

Adapter name (Internal)	In-line barcode	Bp	Annealed Set	Volume for annealing	BLoli
A1.1a + A1.1b	GGTTGT	6	A1.1	10 µL each	8806 + 8807
A1.2a + A1.2b	ATGCCT	6	A1.2	10 µL each	8822 + 8823
A1.3a + A1.3b	CCAGCG	6	A1.3	10 µL each	9321 + 9322
A1.4a + A1.4b	TTCAGCA	7	A1.4	10 µL each	9323 + 9324
A1.5a + A1.5b	TAGGAAT	7	A1.5	10 µL each	9325 + 9326
A1.6a + A1.6b	AAGTTGA	7	A1.6	10 µL each	9327 + 9328
A1.7a + A1.7b	GCTCTAGA	8	A1.7	10 µL each	9329 + 9330
A1.8a + A1.8b	TGACAGCT	8	A1.8	10 µL each	9331 + 9332
A1.9a + A1.9b	CTTCCATGC	9	A1.9	10 µL each	9333 + 9334
A1.10a + A1.10b	GAGATCACG	9	A1.10	10 µL each	9335 + 9336
A1.11a + A1.11b	ATATGTACG	9	A1.11	10 µL each	9337 + 9338
A1.12a + A1.12b	ACCTAGGTGT	10	A1.12	10 µL each	9339 + 9340
A2.1a + A1.1b	NlaIII-overhang		A2.1	100 µL each	8830 +8831

For the adapter annealing reaction, 5 µL of 10X annealing buffer (containing 100mM Tris-HCl pH 8, 500 mM NaCl and 10 mM EDTA) and 25 µL water for adapters A1.X and 50 µL 10X annealing buffer together with 250 µL water for adapter A2.1 were used. Adapters were incubated in a thermocycler at 97.5 °C for 2.5 minutes, then cooled down at a rate of 1 °C per 30 seconds until the

solution reached a temperature of 21 °C and held at 4 °C. Then working stocks for all adapters at a concentration of 40 µM were created with 1X annealing buffer.

The restriction digest and the adapter ligation were performed in a 96-well plate and one A1.X adapter each was used for one row containing eight samples.

Restriction digest:

For the restriction digest, in total 250 – 500 ng of gDNA were digested with 0.25 µL of SbfI-HF, 0.5 µL of NlaIII and 3 µL of CutSmart Buffer for each sample in a 50 µL reaction (filled up with water to 50 µL). Samples were incubated for three hours at 37 °C, then heat inactivated 20 minutes at 80 °C and some samples were randomly picked and verified with the Tapestation before heading on to the next steps.

Adapter Ligation:

To each 50 µL digested DNA sample, 1.5 µl of A1.X and A2.1 working stock adapter together with 6 µL of T4 10X Ligase Buffer and T4 DNA Ligase (400U/µL) were added. Samples were incubated in a thermocycler at 23 °C for 30 minutes, followed by heat-inactivation at 65 °C for 10 minutes, then cooled down at a rate of 2 °C per 90 seconds to 23 °C. A Tapestation run was performed for a few samples to check if a shift in about 100 bp ligation was successful.

Pooling and DNA clean-up:

The uniquely labeled samples were pooled together across each row, to have eight pools containing 12 samples each. A DNA clean-up was performed using the Zymo Research DNA Clean & Concentrator – 5 Kit (Cat. No. D4004) following the manufacturer's instructions. Concentration of the pools were quantified with the Qubit BR dsDNA Assay Kit.

Size Selection using the Blue Pippin (Sage Science):

To select the desired fragments of 375 – 475 bp, the 1.5% Agarose Gel Cassette for targets between 200 bp – 1500 bp, including an internal marker (R2), was chosen. For each 30 µL sample 10 µl of R2 markers were added. As protocol "USE INTERNAL STANDARDS" was selected. Next steps were calibrating the optics, followed by cassette preparation and running the continuity test on the cassette. After loading the samples onto the cassette, the program runs for around 1 hour to select fragments of the desired length. After the run, the samples were in a total volume of 40 µL in Tris-

TAPS and were quantified with 2 µL with the HS ds DNA Qubit Assay and run on a D5000 tape on the Tapestation.

Amplification with Unique Dual Indices (UDI) P5/P7 and Bead CleanUp:

To attach the unique dual indices to each size-selected pool, each one was split into four times 20 ng reactions. To each reaction, 4 µL 5X Phusion Buffer, 0.4 µL 10 mM dNTPs, 1 µL of each 10 mM P5 and P7 primer, and 0.2 µL Phusion DNA polymerase were added and finally filled up with water to a total volume of 20 µL. The initial denaturation was set to 30 sec at 98 °C. Eight cycles of 10 sec at 98 °C followed by 30 sec at 65 °C and 30 sec at 72 °C were used for amplification. The final extension was performed at 72 °C for 10 minutes. The PCR products were combined and a 0.7x AMPure XP bead clean-up was performed. For that, 56 µL of fully resuspended AMPure Beads were added to each pool, pipetted up and down 10 times and incubated for 10 minutes at room temperature. Tubes were then placed on a magnet to pellet the beads including DNA and the supernatant was carefully removed. The beads were washed twice with fresh and ice cold 80% EtOH and after removing trace amounts of ethanol and air drying on the magnet for up to one minute resuspended in 32 µL of Qiagen Buffer EB. The final concentration was measured by the Genomic Core Facility via, Qubit and Bioanalyzer and pooled into one single pool prior to sequencing on Illumina NextSeq Mid Output single end 150bp (run 2022).

II.IX. Whole genome sequencing (WGS)

This method was not performed by myself, but it supports and expands the understanding of findings from my analyses, which is important for the overall interpretation.

gDNA was sheared with a Covaris E220 focused ultrasonicator (Parameters: Peak Incident Power (W)=75, Duty Cycle=10%, Cycles per burst=1000, Temperature=7°C, Water Level= -2, Treatment Time=52sec). DNA library preparation of sheared gDNA (Covaris) was performed using NEBNext Ultra II DNA Library Prep Kit for Illumina Version 7.0_9/22. Libraries were prepared with a starting amount of 250 ng of fragmented DNA and were amplified in 3 PCR cycles. Libraries were profiled in a High Sensitivity DNA on a 2100 Bioanalyzer (Agilent technologies) and quantified using the Qubit dsDNA HS Assay Kit, in a Qubit 4.0 Fluorometer (Invitrogen by Thermo Fisher Scientific), as well as the sparQ Universal Library Quantification Kit (Quantabio) on a QuantStudio 5 Real-Time PCR System (Applied Biosystems by Thermofisher Scientific).

All ten samples were pooled in unequimolar ratio (according to their expected ploidy levels) and sequenced on 2 NextSeq 2000 P4 300 Flowcells, PE for 2x 161 cycles plus 2x8 cycles for the dual index read.

II.X. DNA content in whole blood cell nuclei (FACS)

Another way of confirming ploidy is quantifying the DNA content in whole blood cell nuclei by propidium iodide staining and flow cytometry. Approximately 50 µL blood was isolated from the tail. The blood was immediately collected in 1,5 mL Eppendorf tubes containing 1 mL of citrate-dextrose solution (ACD, C3821, Sigma). The BD Cycletest Plus DNA kit from BD Bioscience (Cat. No. 340242) was used to isolate and stain the nuclei following the manufacturer's instructions. Blood cells were counted on a hemocytometer and cell density adjusted to 1 x 10^6 cells/mL in buffer solution (containing sodium citrate, sucrose, and dimethyl sulfoxide). The cell suspension was transferred into a round-bottom polystyrene test tube (Falcon 352008) and centrifuged for 5 minutes at 300 x g at room temperature in an Eppendorf 570R centrifuge with swing-out buckets. After decanting the supernatant, the cells were resuspended in 1 mL of buffer solution by vortexing at low speed. This washing step was repeated two times. After the washing, cells were counted again, and the concentration was adjusted to 5 x 10^5 cells/mL in buffer solution. The cell suspension was centrifuged at 400 x g for 5 minutes, the supernatant carefully decanted and 250 µL of Solution A (containing trypsin in a spermine tetrahydrochloride detergent buffer) was added. The solution was gently mixed and incubated for 10 minutes at room temperature. Then, 200 µL of Solution B (containing trypsin inhibitor and ribonuclease A in citrate stabilizing buffer with spermine tetrahydrochloride) was added, gently mixed and incubated for 10 minutes at room temperature. Last, 200 µL of ice-cold Solution C (containing propidium iodide and spermine tetrahydrochloride in citrate stabilizing buffer) was added, gently mixed and incubated in the dark at 2-8°C prior to measure on a cell analyzer. A minimum number of 10,000 events were collected on the BD LSRFortessa TM cell analyzer with a YG561 (561 nm) laser and 610/20 bandpass filter. The BD FACS-Diva v9.0.1 software was used for acquisition with identical instrument settings for all relevant samples. A quality check for the laser was performed before all measurements. FlowJo v10.8.0 was used for data analysis, with a gating strategy including forward scatter (FSC)-area/side scatter (SSC)-area and area versus height for doublet discrimination.

III. RESULTS

III.I. Emergence of ploidy elevated oocytes during meiotic Prophase I

In total, 17 germinal beds of specimens from diploid species *A. neomexicanus*, triploid species *A. uniparens* and two tetraploid species (*A. townsendae* and Sono) were examined for DNA content quantification of different oocytes and overall characterized, to bring light into the mechanism in Prophase I with respect to the emergence of ploidy elevated oocytes in parthenogenetic species.

To accurately determine the DNA intensity of different cell types in the germinal bed, a model was developed that considers the volume-to-intensity ratio. By integrating DAPI fluorescence intensity with nuclear volume (DAPI mean intensity * volume), this model offers a more reliable estimation of DNA content, especially for cells of varying sizes. The model considers the fact that volume and intensity do not always directly correlate due to factors like chromatin condensation and changes in nuclear morphology. Nevertheless, for the correct interpretation of non-ambiguous oocyte stages, it is crucial to consider both parameters additionally by itself. Each germinal bed was analysed for cells in pachytene-like and diplotene state, based on the definition published in Newton et al., 2016 (Fig. 4A). According to that, pachytene-like oocytes were selected by showing well-defined and extended positive SCP3 threads dispersed around the whole nucleus. Early diplotene oocytes were selected by the lack of a defined SCP3 staining and their overall bigger size. Somatic cells of the germinal bed are predominantly in G1 or G0. The median DNA intensity peak for somatic cells is defined as 2C, for a diploid species, and the DNA content for the other cell categories were determined relative to this somatic cell standard.

III.I.I. Characterization of oocyte variations in diploid *A. neomexicanus*

Based on Lutes et al., 2010 and Newton et al., 2016, it is known that in diploid parthenogenetic species, oocytes in diplotene stage contain twice as much DNA as in bisexual animals. Also, one rare event of ploidy elevated pachytene-like oocyte was observed in the study. No evidence of premeiotic endoreplication or replication between pachytene-like and diplotene stages has been found, and brought up the following question: How are these 8C cells in early diplotene oocytes generated?

To understand the mechanism of ploidy elevation, I set up immunostaining experiments using a subset of antibodies to characterize the structure of germinal beds during Prophase I in detail in the

diploid hybrid species *A. neomexicanus*. Figure 8 represents a maximum intensity projection of a germinal bed of *A. neomexicanus* stained with DAPI and SCP3. SCP3 is a critical component of the synaptonemal complex (SC) and marks the lateral elements along the chromosomes including regions near the telomeres. Different types of cells, including somatic cells, primary follicles, and oocytes of different stages are part of the germinal bed. The primary follicles are in a diplotene stage, leave the cortex and become previtellogenic follicles. During this transition, the follicles increase in size from approximately ~ 40 µm to ~ 3 mm (Newton et al., 2016). The distinct patterns of SCP3 staining of the nuclei are indicating the current stages of Prophase I of the oocyte (from leptotene-like to diplotene), as described in Newton et al., 2016.

All examined germinal beds were isolated from hatchlings in the age between 16- 40 days, because in hatchlings the number of oocytes is 8-fold higher than in adults (Newton et al., 2016).

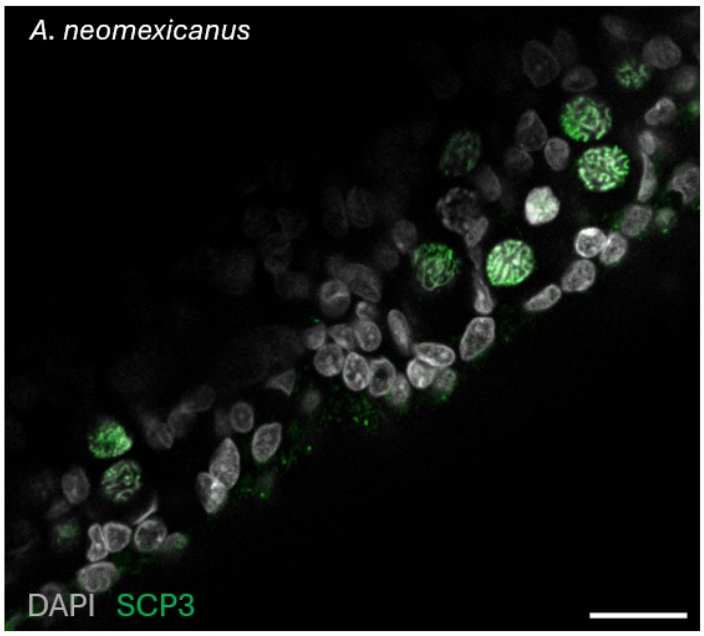

Figure 8: Maximum intensity projection of three planes of a germinal bed derived from diploid *A. neomexicanus* (D790) DAPI in grey, SCP3 in green. Scale bar 20 µm.

In total, the DNA content of 321 cells (37% somatic cells (n=119); 47% pachytene-like cells (n=152); 15% diplotene cells (n=50)) of eight germinal beds derived from seven different lizards, were quantified in this study. The quantification of DNA content of pachytene-like oocytes of diploid *A. neomexicanus* highlights the exciting heterogeneity, of 4C and 8C state cells (Fig. 9).

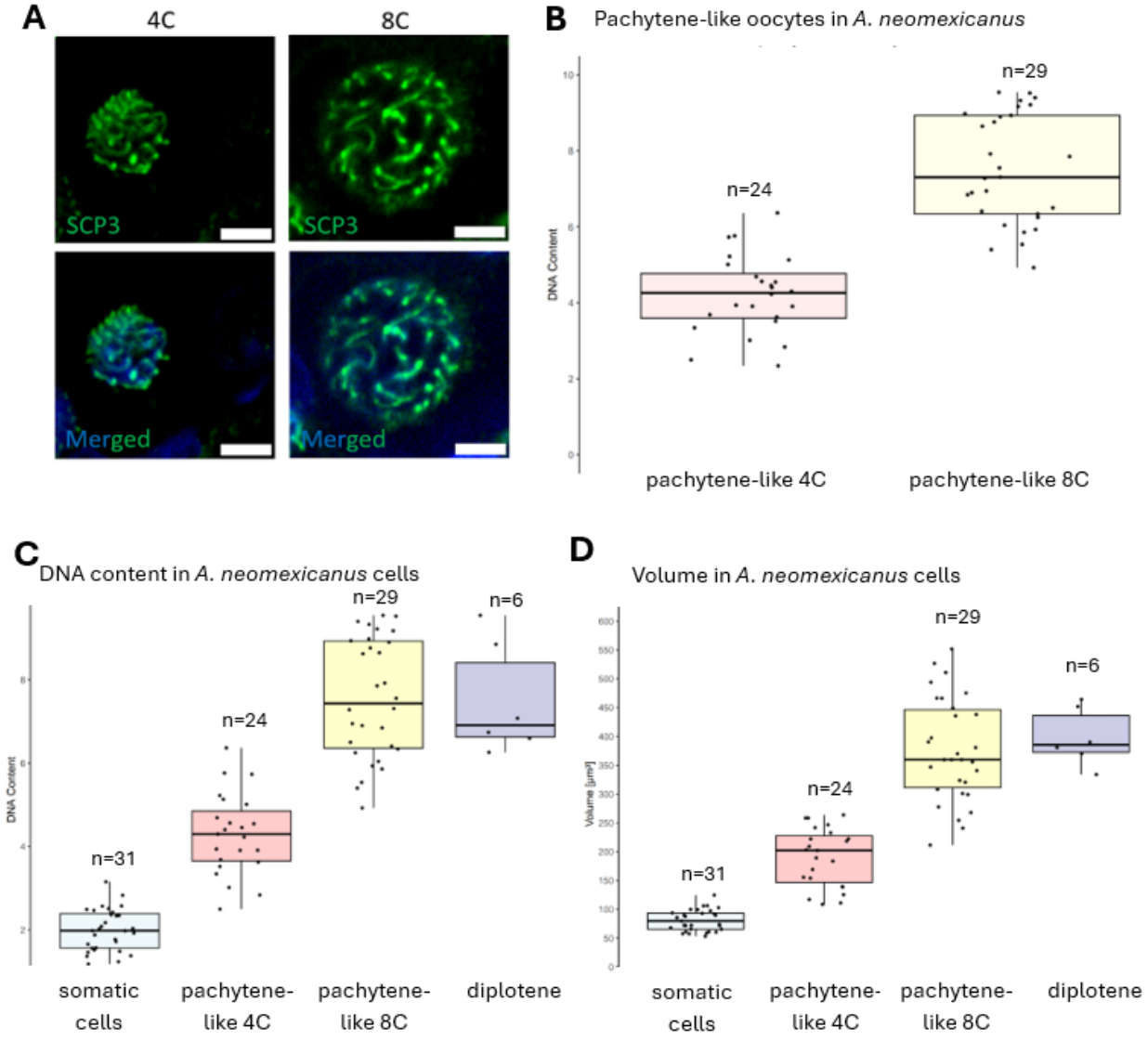

Figure 9: Quantification of cells in *A. neomexicanus* (D868, 25 days old and D790, 40 days old). 90 cells were analysed. **A:** Maximum intensity projection of two planes showing two pachytene-like oocytes of different sizes. SCP3 is green, DAPI is blue. Scale bar: 10 µm. Pachytene-like stage is defined by SCP3 positive chromosome threads. **B:** Quantification of DNA content considering the DAPI mean intensity * volume. **C:** Quantification of DNA content including somatic cells and diplotene cells with ImageJ normalized to the DNA content of the somatic cells. Standard deviation: somatic cells: 2 ± 0.4; pachytene-like 4C: 4.2 ± 0.9; pachytene-like 8C: 7.5 ± 1.4; diplotene 7.5 ± 1.2 **D:** Volume of cells: Standard deviation: somatic cells: 80µm^3 ± 17 µm^3; pachytene-like 4C: 190µm^3 ± 49 µm^3; pachytene-like 8C: 376µm^3 ± 87 µm^3; diplotene: 398µm^3 ± 45 µm^3.

45% of cells are in a 4C state indicating they have undergone DNA replication (as in normal pre-meiotic S-phase) but remain diploid. They have on average a cell volume of 190 µm^3 ± 49µm^3. 55% of cells show an elevated DNA content of 8C and on average a volume of 376 µm^3 ± 87µm^3 suggesting that ploidy elevation must have occurred. Including the measurements of diplotene

oocytes in this analysis (Fig. 9D), it reveals that all oocytes (n=6) exhibit a consistent DNA content of 8C, which aligns with previous findings.

The observation of a portion of pachytene-like oocytes, but all diplotene oocytes showing an elevated DNA content implied that the transition occurring from a 4C state to an 8C state during pachytene is a crucial step in the progression through meiosis in this parthenogenetic diploid species.

III.I.II. Morphology of oocytes

In the context of meiosis and particularly focusing on oocytes at pachytene-like stage, using Phalloidin staining can provide valuable insights into cell morphology, boundaries, and the overall architecture of oocytes. Phalloidin is a molecule that binds specifically to filamentous actin (F-actin), and if coupled to a fluorophore, visualizes the actin cytoskeleton, within the germinal beds. In oocytes, F-actin forms rich networks around the outer region of the oocyte (cortex) to maintain the oocyte's shape and regulate surface tensions. It also plays a role in controlling intracellular transport (Fig. 10, yellow arrows). It helps in visualizing different somatic cells, especially granulosa cells, which locate around the oocytes and provides nourishment and hormonal support. They are much smaller than the oocyte itself. Phalloidin also stains for perinuclear actin, which forms a dense network around the nuclei to assist in nuclear positioning and maturation processes (Fig. 10, white arrows).

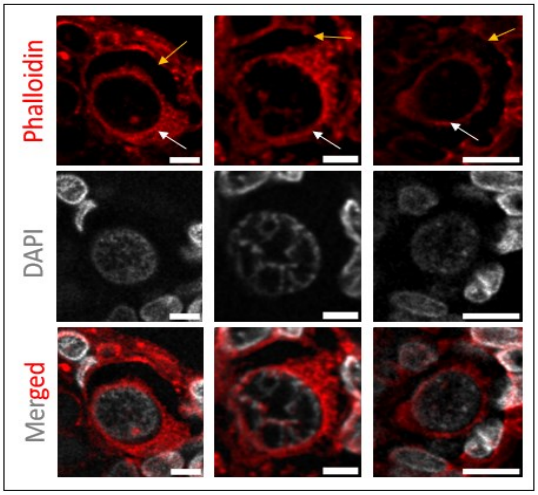

Figure 10: Characterization of Phalloidin staining in oocytes of *A. neomexicanus* (D868) at an age of 25 days. Maximum intensity projections show oocytes surrounded by somatic cells and including one nucleus. F-actin forms a rich network around the outer region of the oocyte (yellow arrow). The perinuclear actin forms a dense network around the nuclei within the oocyte (white arrow). DAPI in grey, Phalloidin in red. Scale bar 10 and 20 µm.

Overall, Phalloidin staining uncovers the structure and behavior of oocytes during Prophase I in parthenogenetic lizards and reveals the occurrence of oocytes with an altered morphology including empty, binucleated and polynucleated oocytes (Fig. 11).

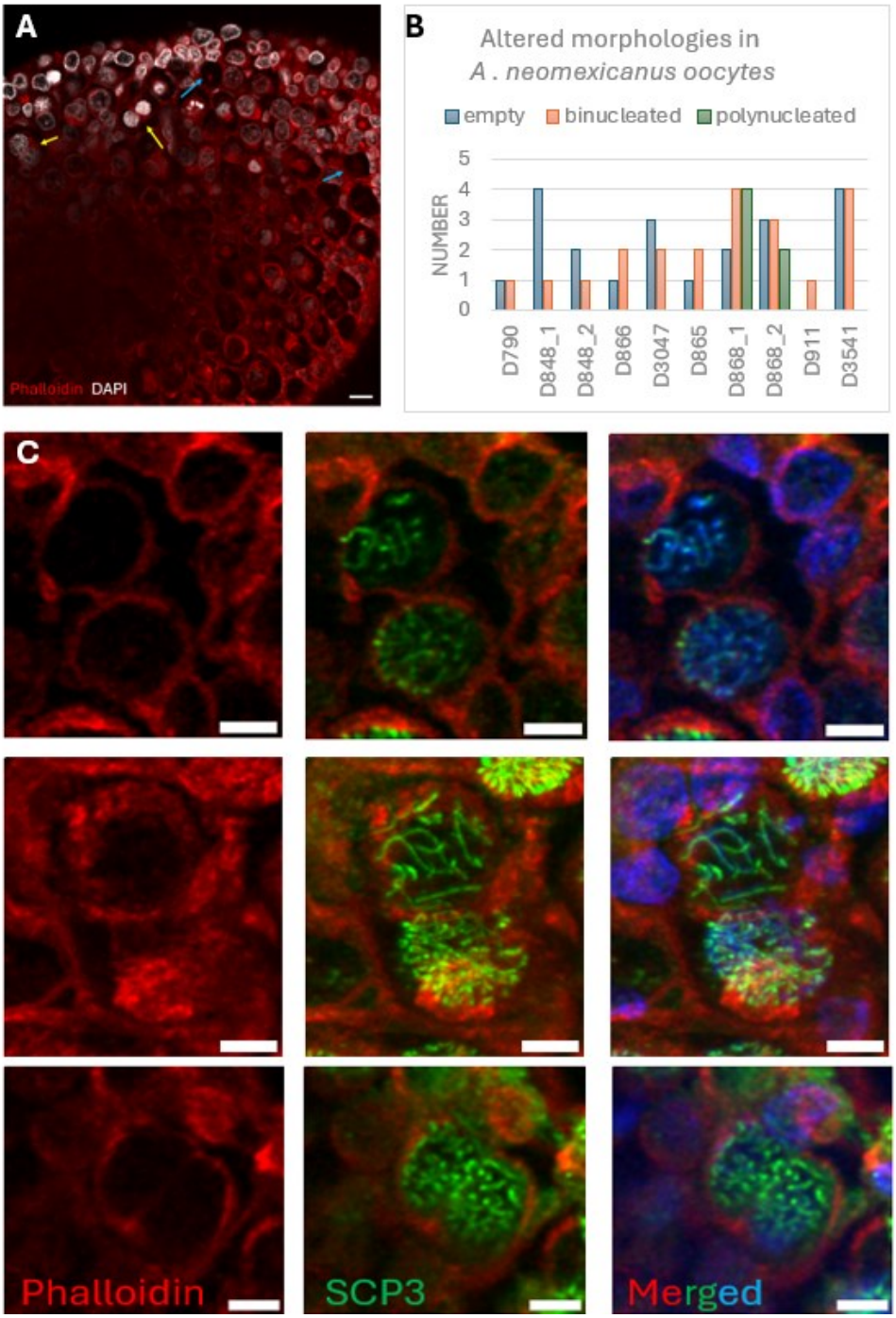

Figure 11: Morphology of oocytes in germinal beds. **A.** Maximum intensity projection of 10 planes of *A. neomexicanus* (D3541), at an age of 30 days. Yellow arrows mark binucleated oocytes, blue arrows mark empty oocytes. Phalloidin is red, DAPI is grey. Scale bar 20µm. **B.** Bar chart showing the occurrence of altered morphologies of oocytes in *A. neomexicanus*. Of ten germinal beds derived from eight specimens, the number of empty (blue bar), binucleated (orange bar) and polynucleated (green bar) oocytes is displayed **C:** Maximum intensity projections of a variation of binucleated oocytes of *A. neomexicanus* (D865) at an age of 25 days. The top panel shows the occurrence of two clear separated nuclei within one oocyte. The middle panel shows two nuclei in close contact within one oocyte. The bottom panel shows two nuclei fusing together within one oocyte. Phalloidin is red, SCP3 is green, DAPI is blue. Scale bar 10 µm.

Of the ten germinal beds examined derived from eight *A. neomexicanus* specimens, between one to four cases of binucleated oocytes, as well as empty oocytes, were observed per germinal bed (Fig. 11). Additionally, in the two germinal beds from specimen D868, two and four cases of polynucleated oocytes, each containing three to five nuclei, were identified. Panel 11A shows a maximum intensity projection of a whole germinal bed pointing out the occurrence of the different types of oocytes. The variation between binucleated oocytes reaches from clear distinguishable two nuclei within one oocyte (top), over to nuclei in closer distance to each other (middle) to fusion of two nuclei (bottom) (Fig. 11C).

Altered morphologies of oocytes lead me to the assumption that oocytes transition to an 8C state by migration and fusion of two nuclei within a binucleated oocyte.

III.I.III. Communicating nuclei

To gain insights on how binucleated and polynucleated oocytes arise, SCP3 staining was combined with Phalloidin and DAPI to follow nuclei dynamics. At the position where telomeres cluster, the SCP3 staining is more intense. It reveals that in bi- and polynucleated oocytes the tethering of chromosomes to the nuclear envelope (NE), also known as telomere bouquet, during early stages of prophase I, can be described as “orientated towards each other” (Fig. 12).

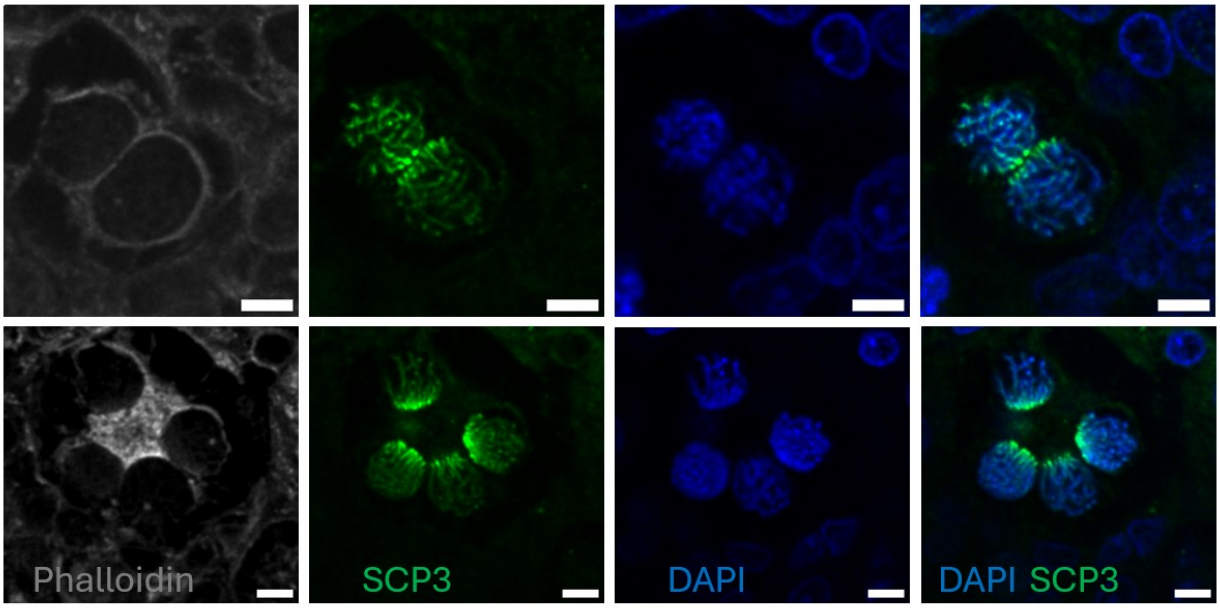

Figure 12: Telomere bouquet formation in *A. neomexicanus* (D868) at an age of 25 days. Maximum intensity projections of three z-stacks of telomere bouquets within one oocyte orientated towards each other. Phalloidin is grey, SCP3 is green, DAPI is blue. Scale bar: 10 µm.

In general, the clustering of telomeres has the important function to ensure proper chromosome pairing, synapsis and recombination, which is the basis for accurate meiotic division (Bass, 2003). The ending point of the bouquet stage is in early pachytene, where the telomeres disperse, and the chromosomes can be seen as well-defined continuous threads. In the diploid *A. neomexicanus*, also groups of up to five nuclei are showing this behavior of telomere bouquet formation with all telomeres orientated towards each other (Fig. 12, bottom panels).

Furthermore, "constricted" nuclei, which have the appearance of traversing through the cell wall or the cell boundary between two oocytes were detected (Fig. 13).

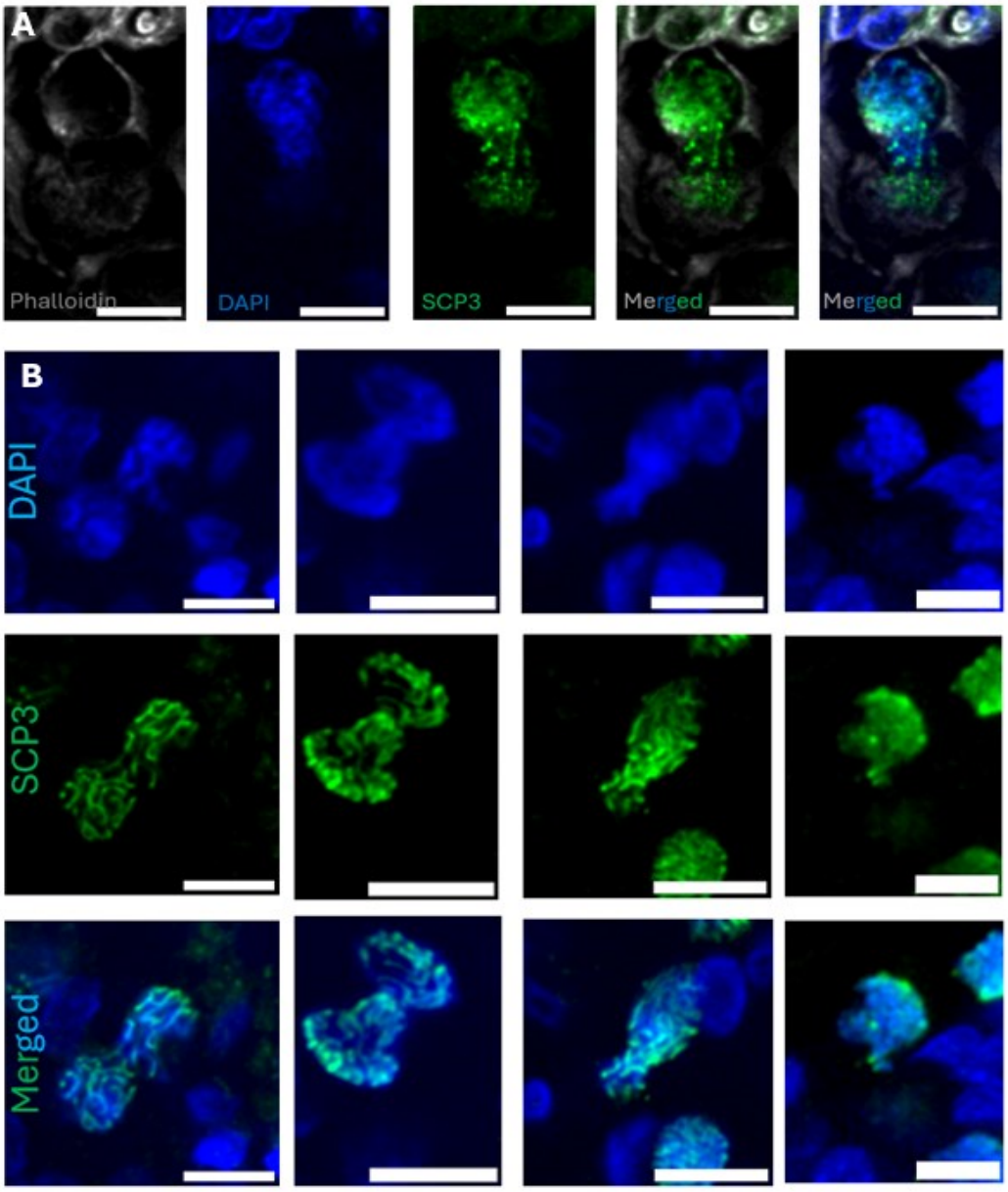

Figure 13: Constricted nuclei on the move. **A:** Maximum intensity projection of three planes of *A. neomexicanus* (D911) at an age of 32 days. Constricted nuclei in a binucleated oocyte. Nucleus is traversing from one cell into another. Phalloidin is grey, DAPI is shown in blue, SCP3 is shown in green. Scale bar 20 µm. **B:** Maximum intensity projections of *A. neomexicanus* D790 at an age of 40 days. Nuclei are traversing from one cell to another. DAPI is blue, SCP3 is green. Scale bar 20 µm.

The observations of nuclei with telomere bouquets orientated towards each other and nuclei appearing to move and squeeze between cells, indicate that nuclei actively try to find other cells to set the opportunity for transition to the 8C state. This led me to investigate which structures may be involved in the moving event.

III.I.IV. Nuclei on the move

During oogenesis in most sexually reproducing organisms, intercellular bridges, evolutionary conserved structures, allow neighboring cells to maintain a connection to each other. These connections are known as ring canals and facilitate the transfer of materials, such as nutrients, RNA or even organelles between the cells (Kline et al., 2018). This structure is well studied in the egg chamber of *Drosophila*, where ring canals connect several nurse cells to a single oocyte to support their development. During the process of oogenesis, the size of ring canals in *Drosophila* is changing dynamically depending on the needs of the cells they are connecting, as it is regulated by cytoskeleton elements, primarily actin. The size changes from 1-2 µm in the early development stage to up to 10 - 20 µm in late oogenesis (Hudson & Cooley, 2002).

In this work, Mitotic Kinesin-Like Protein 1 (MKLP1) was used to visualize the ring canals in lizard germinal beds, as this protein is a conserved component in the formation of ring canals and known for its role in cytokinesis during cell division. Several germinal beds of different animals were investigated regarding the occurrence and size of ring canals. Figure 14 shows a maximum intensity projection of a germinal bed, where many rings are visible in the cytoplasm (14A). Panel B shows the size difference of a ring canal compared to a pachytene-like nucleus. Of 63 ring canals measured, the average diameter of relaxed ring canals is around 1,9 µm (± 0,5). In panel C, a ring canal located between two oocytes is visible.

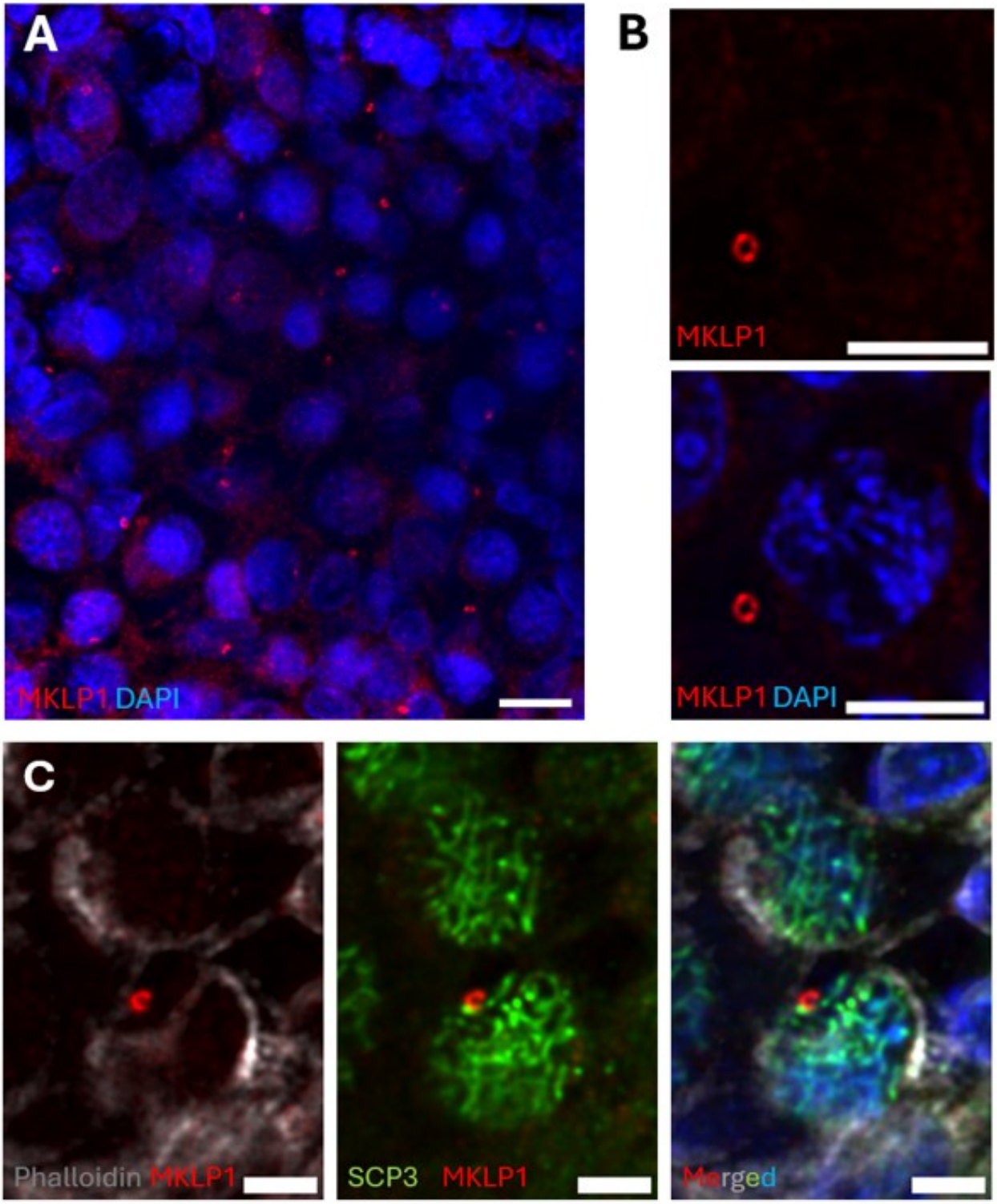

Figure 14: Maximum intensity projections of three z-stacks of ring canals in *A. neomexicanus* D790 & D911. **A:** Maximum intensity projection of a germinal bed with several ring canals in the cytoplasm. **B:** Size difference of a ring canal next to a nucleus. **C:** shows a ring canal between two oocytes. DAPI is blue, MKLP1 is red, SCP3 is green Phalloidin is grey. Scale bar: 10 µm.

In Figure 15A, a more detailed comparison of one relaxed ring canal can be seen. The diameter was measured in ImageJ with the Plot profile function and normalized to the DAPI intensity of the

MKLP1-channel. The canal is closely located to the nuclei, and it appears that the chromosomes are starting to traverse through the ring. In B the rare event of a nucleus moving through the ring canal is detected (Fig.15B, white arrow). During this moving event, the ring is stretched to more than double the size of the relaxed status. The plot profiles in the bottom panel were generated in ImageJ and point out the diameter of the rings.

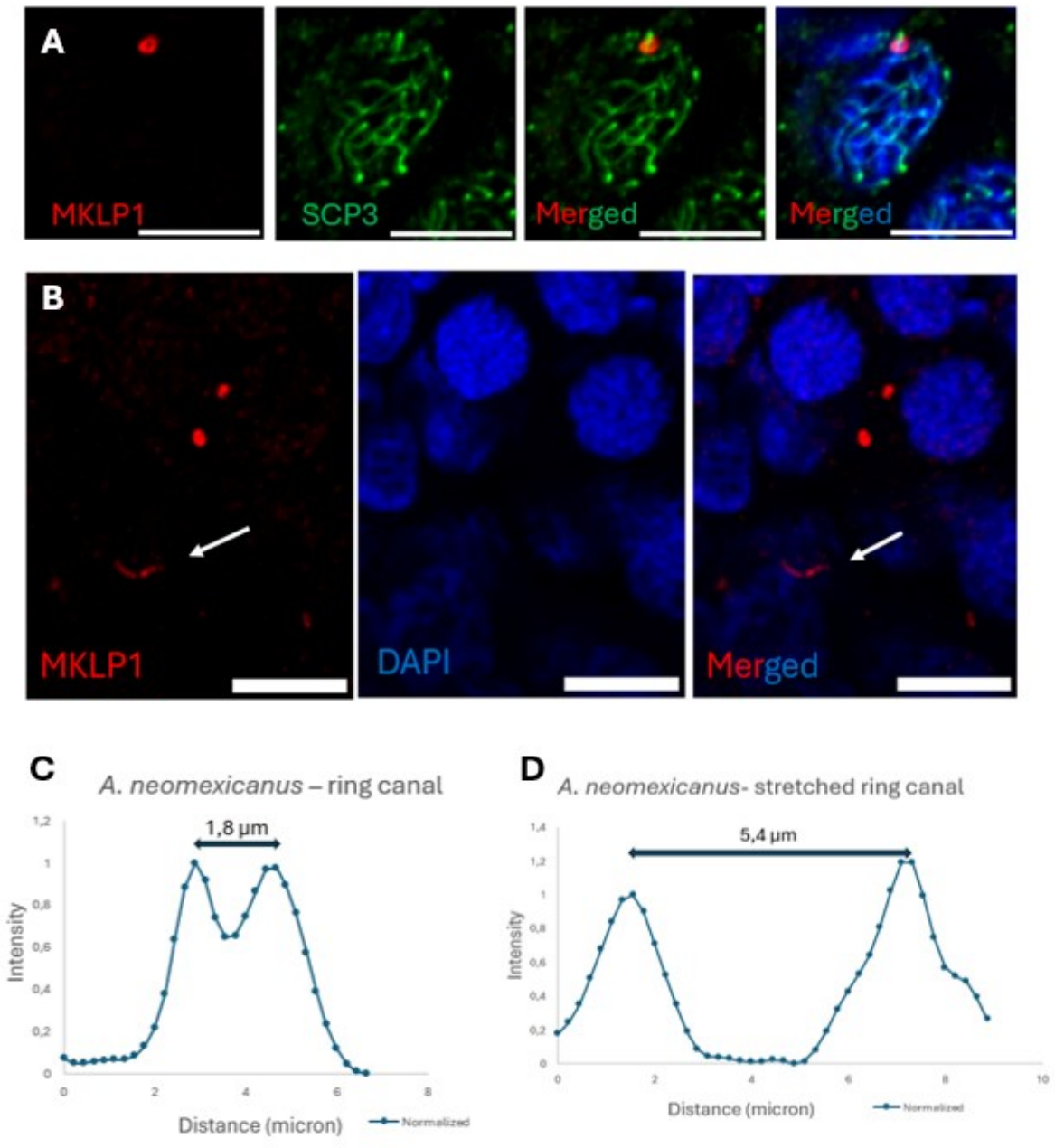

Figure 15: Ring canals in *A. neomexicanus* D848, at an age of 28 days. **A:** Maximum intensity projections of two planes of a ring canal in a relaxed state with chromosomes appearing to squeeze through. MKLP1 is red, SCP3 is green, DAPI is blue. Scale bar 10 µm. **B:** Stretched ring canal, while a nucleus is squeezing through (white arrow). MKLP1 is red, SCP3 is green, DAPI is blue. Scale bar 10 µm. **C:** Plot profile of a relaxed ring canal in *A. neomexicanus* show the diameter of the ring of 1.8 µm. **D:** Plot profile of a stretched ring canal in *A. neomexicanus* show the diameter of the ring of 5.4 µm. The plot profile generated with ImageJ shows the normalized MKLP1 intensity in relation to the distance in microns and was used to measure the diameter of the ring canals.

The observation of ring canals dispersed around the germinal bed, together with the occurrence of constricted nuclei and the detection of a nucleus traversing through a stretched ring, confirming the assumption of nuclei's traversing from one cell to another to elevate their DNA content.

The observations described here brought up the following model for the meiotic pathway in parthenogenetic species and is displayed for a diploid species. In parthenogenetic hybrid species the homeologous chromosomes are too distinct to each other, to continue with the normal pathway of meiosis. The differences prevent synapsis in the 4C state and lead to the accumulation of cells at the pairing state. At this stage telomere bouquets form and start to communicate to find other cells at the same stage. Some nuclei migrate and form a binucleated oocyte, where the two nuclei then fuse together. This leads to the occurrence of cells with an elevated DNA content, in pachytene-like and early-diplotene stage and the opportunity for identical chromosomes to synapse and to progress further through meiosis (Fig. 16).

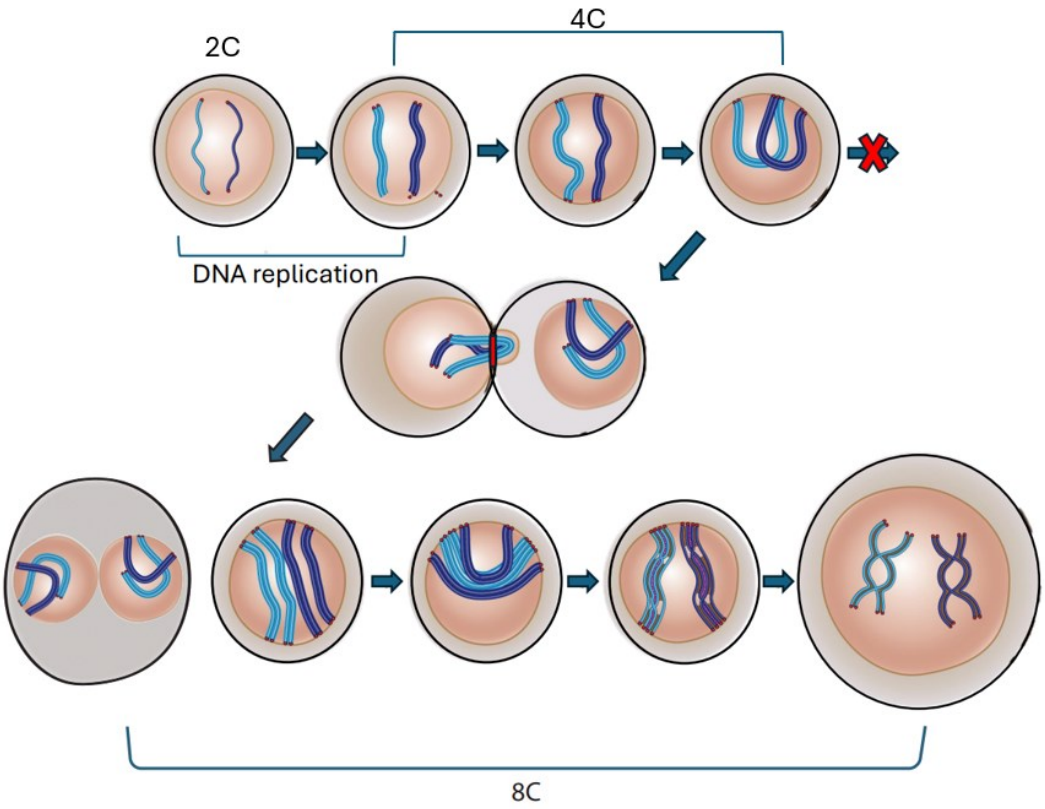

Figure 16: Model showing meiotic pathway in parthenogenetic species. The schematic shows how meiosis progresses from a 4C state after DNA replication, to the formation of binucleated cells to allow nuclei fusion, over to the rise of 8C elevated oocytes. The figure is adapted from former lab members.

III.II. The pairing of chromosomes

Following the results and the model described above, the next aim of this study was to determine the synapsis pattern occurring between chromosomes from *Aspidoscelis* species of different ploidy and genome composition. For a more detailed analysis of synapsis, the Synaptonemal Complex Protein 1 (SCP1) was considered, as it is a central element protein of the synaptonemal complex (SC) (Fig. 4, green region). SCP1 is running perpendicular to the paired chromosomes and ensures that the homologs remain close together during synapsis. The zygotene-like stage is the first stage when SCP1 starts to appear, because in this stage homologous chromosomes start to pair and SCP1 is visible as little stretches or dots. In pachytene-like, when synapsis is complete, the SCP1 staining reflects the fully formed synaptonemal complex (SC) and acts as long and smooth lines running the entire length of the paired homologous chromosomes. In combination with SCP3 (Fig. 4, red region) it can be used to define the status of synapsis of an individual oocyte.

It should be noted that both primary antibodies used in this work are from the same species (rabbit-derived), which raises concerns about potential cross-reactivity or nonspecific binding. The challenge in finding antibodies that work effectively in lizards is largely due to their evolutionary distance from common model organisms and the limited characterization of their proteins and I was not able to find another combination that worked. To minimize these complications, the protocol was adapted to include sequential staining, with blocking steps using bovine serum albumin (BSA) after staining with the first set of primary and secondary antibodies. This approach ensures that the second set of antibodies does not interact with the first. Furthermore, the SCP1 antibody was always applied in the first round, followed by SCP3 in the second round. The process of condensation, SCP3 localization to the axial filaments and synapsis and localization of SCP1 to the central elements proceeds rapidly. This makes it challenging to find cells that have threads of SCP3 on all chromosomes but not yet any SCP1 threads (oral communication with Peter Baumann in reference to gonochoristic species).

III.II.I Co-localization of SCP1 and SCP3 in triploid *A. uniparens*

For an initial overview, the DNA content of various cells from two germinal beds of *A. uniparens* (D3578 & D1143) were quantified. The genome of *A. uniparens* consists of two copies of *A. arizonae* and one copy of *A. burti* (Fig. 2). As it is a triploid species, its somatic cells are defined as 3C, corresponding to the 2C somatic cells in *A. neomexicanus*. Maximum intensity projections of representative oocytes show pattern of no co-localization of SCP1 and SCP3, partial co-localization of SCP1 and SCP3 and complete co-localization of SCP1 and SCP3 (Fig. 17). The cells were identified within a single germinal bed and imaged on a confocal microscope at similar z-planes, meaning they are positioned at comparable depths within the sample.

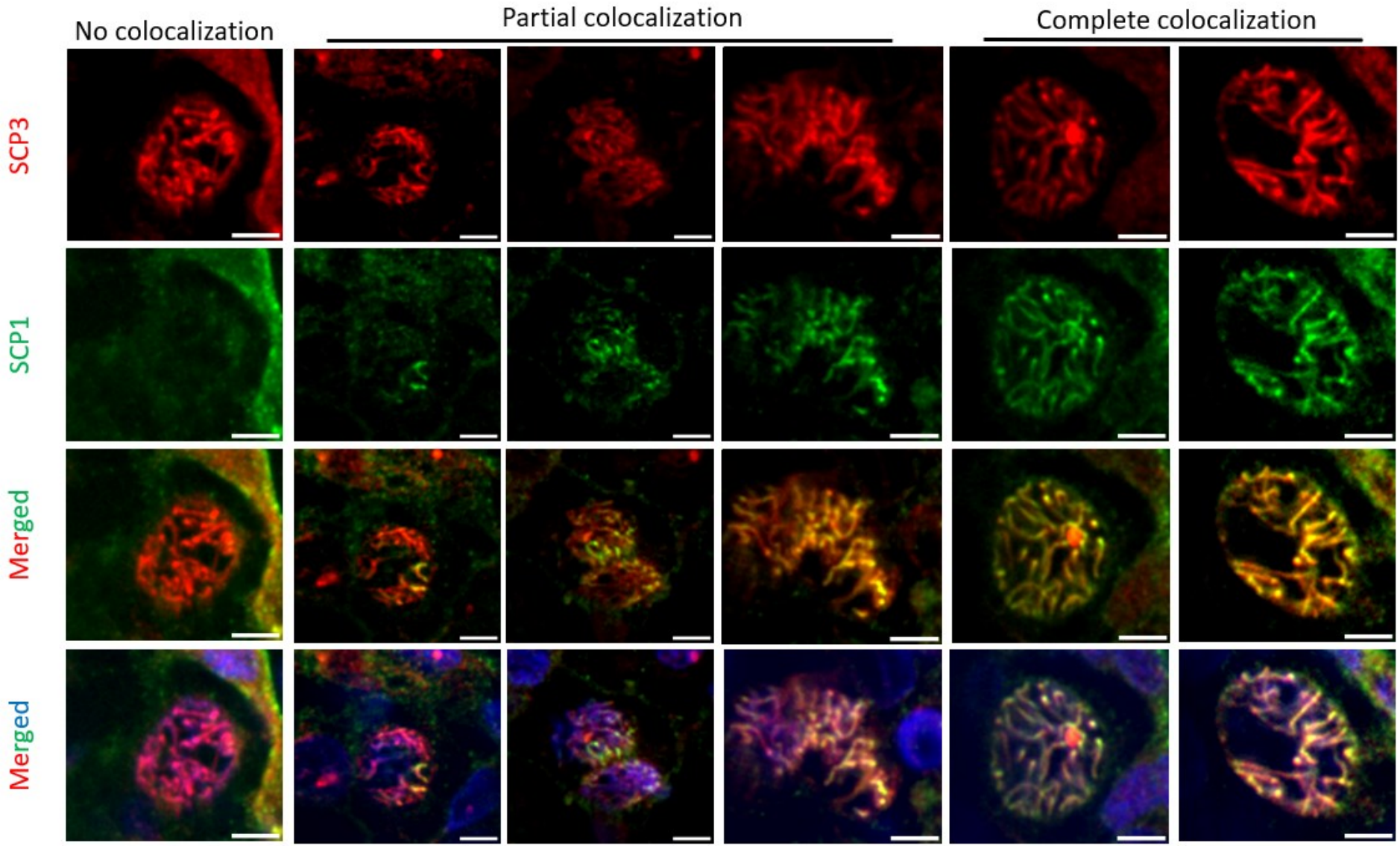

Figure 17: Maximum intensity projection of three planes showing co-localization of SCP1 and SCP3 in *A. uniparens* (D3578) derived from one germinal bed, at an age of 21 days. From left to right: No localization (SCP3 staining only) in a 6C state - pachytene-like oocyte, overview of three representative oocytes showing partial co-localization of SCP1 and SCP3 (in the last two cases in a binucleated oocyte), last two panels show complete co-localization of SCP1 and SCP3 in ploidy elevated oocytes (12C). SCP3 is red, SCP1 is green, DAPI is blue. Scale bar 5µm.

The quantification reveals a DNA content of around 12C for all diplotene oocytes (n=12) observed (Fig. 18A).

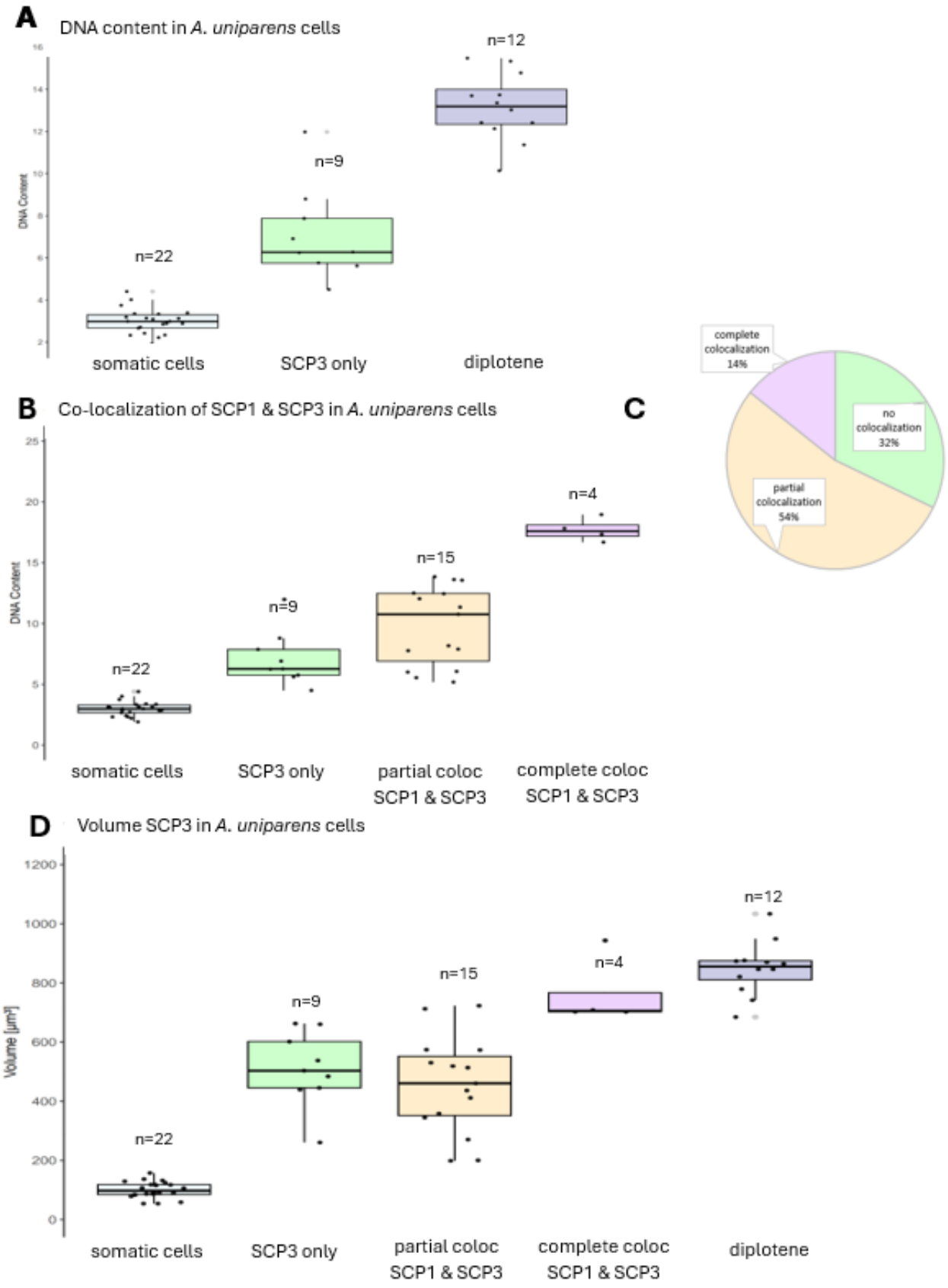

Figure 18: DNA content quantification of *A. uniparens* cells (D3587, 21 days old) and D1143 (16 days old). **A:** Of 43 cells analysed, 22 cells are somatic cells (3 ± 0.5). Nine cells could be identified as 6C pachytene-like oocytes based on the positive SCP3 staining only (7.1 ± 2). Twelve cells are identified as diplotene oocytes (13.1 ± 1.5). **B:** Co-localization pattern in *A. uniparens* (D3578). Pachytene-like cells showing partial co-localization of SCP1 and SCP3 (9.7 ± 3) and complete co-localization (17 ± 0.8) were added to the quantification. **C:** The pie chart shows the percentage of co-localization of the different cells. **D:** Volume of cells in *A. uniparens*: somatic cells (100 μm^3 ± 27 μm^3), SCP3 only cells (510 μm^3 ± 118 μm^3), partial co-localized cells (453 μm^3 ± 156 μm^3), complete co-localized cells (763 μm^3 ± 103 μm^3), diplotene cells (848 μm^3 ± 86 μm^3). Cells were quantified with ImageJ and normalized to the DNA content of the somatic cells.

Nine oocytes assigned as pachytene-like stage based on the SCP3 stained threads, show only a positive signal for SCP3 (Fig. 17 + 18). The absence of SCP1 indicates the absence of a synaptonemal complex in a 6C-state oocyte (32%). Furthermore, the presence of four cells (14%) showing complete overlap of SCP1 and SCP3, indicate that synapsis occurred. This implies that a prior DNA migration event happened and is confirmed by an elevated DNA content. Nevertheless, 15 cells (54%) show partial overlap of SCP1 and SCP3 (Fig. 17), which indicate that chromosome pairing occurs exclusively between the two identical pairs of chromosomes derived from *A. arizonae* in *A. uniparens*. The pachytene-like cells exhibit broadly diversified values of DNA content (Fig. 18B). When considering not just the volume-to-intensity ratio, which forms the basis of this model, but examine the volume alone, cells with partial colocalization have a similar volume to non-colocalized cells (SCP3-only) (Fig. 18C). The average volume for partially colocalized pachytene-like oocytes is 454 μm^3 (± 156 μm^3), compared to 510 μm^3 (± 118 μm^3) for pachytene-like oocytes showing no colocalization of SCP1 and SCP3.

The broadly diversified DNA content observed in oocytes with partial colocalization of SCP1 and SCP3 is attributed to higher intensity values measured in these cells. In cells undergoing partial synapsis, chromatin at synapsed regions becomes more condensed than in un-synapsed areas. This increased condensation leads to more localized and intense DAPI binding, resulting in elevated intensity values. This finding highlights the need to account for both intensity values and cell volume to accurately estimate the DNA content and point out the complexity of these cells.

The finding in *A. uniparens* of diplotene oocytes in a 12C state, aligns with the expectation that a ploidy elevation event is required for the continuation of meiosis, as described for diploid *A. neomexicanus*. The results are further confirmed by the observation of complete synapsis of identical chromosomes limited to DNA elevated cells and the absence of SCP1 or only partial synapsis in non-elevated cells.

III.II.II. Co-localization of SCP1 and SCP3 in tetraploid *A. townsendae*

For a first overview, the DNA content of various cells from a single germinal bed of *A. townsendae* (D3513) were quantified according to the same model. The genome composition of this tetraploid hybrid comprises of four distinct genomes of four ancestral sexual species (Fig. 2). As *A. townsendae* is a tetraploid species, its somatic cells are defined as 4C, corresponding to the 2C somatic cells in diploid *A. neomexicanus* and the 3C somatic cells in triploid *A. uniparens*.

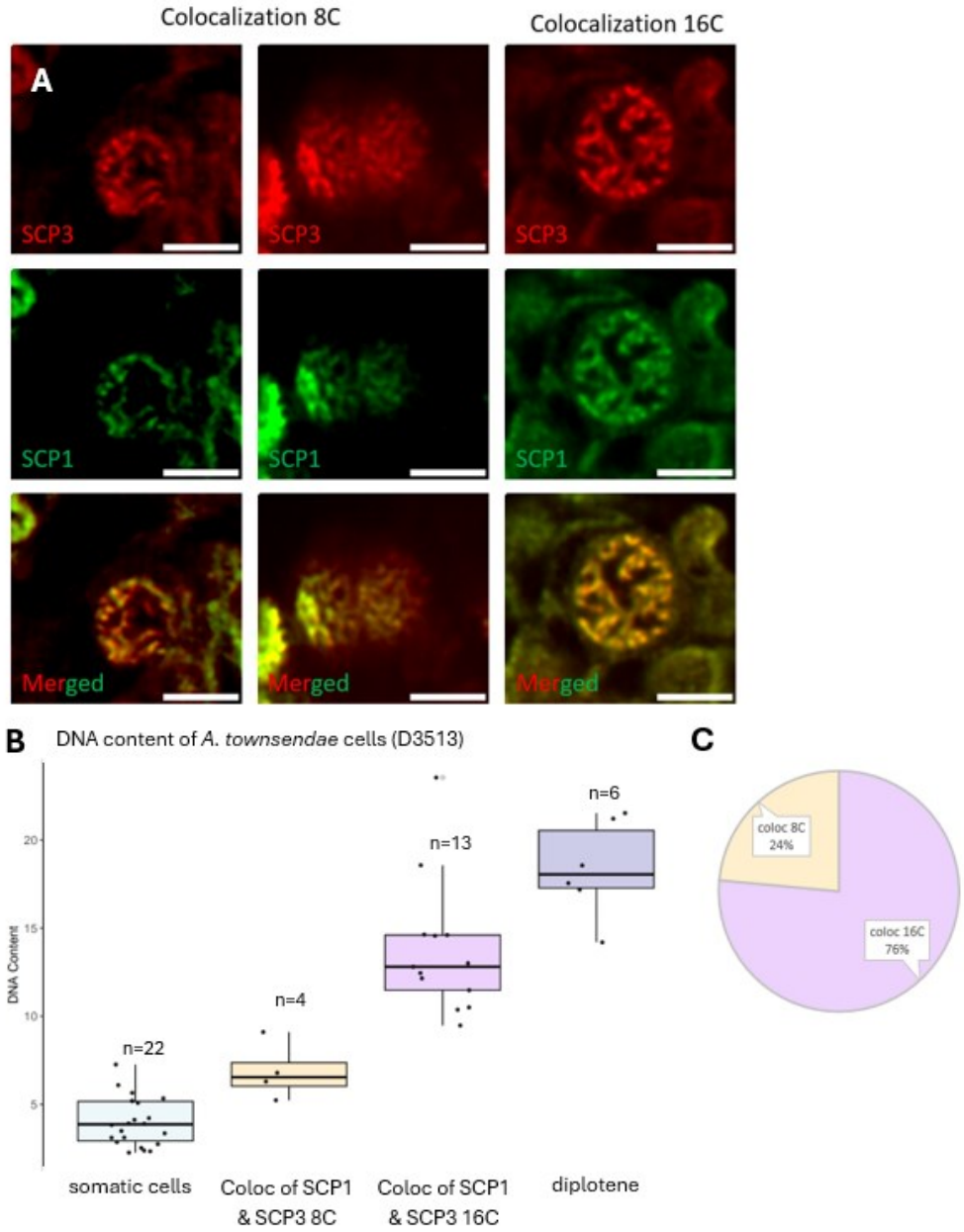

Figure 19: DNA quantification in *A. townsendae* (D3513) at an age of 31 days. **A:** Maximum intensity projection of 8C and 16C pachytene-like oocytes showing co-localization of SCP1 and SCP3 in *A. townsendae*. All cells were acquired under the same settings and can be found in one germinal bed. SCP3 is red, SCP1 is green, DAPI is blue. Scale bar 10 µm. **B:** Of the 45 analysed cells, 22 cells are somatic cells (4 ± 1.3), 13 cells show complete co-localization of SCP1 and SCP3 and an elevated DNA content (13 ± 3.6), four cells, including two cells part of a binucleated oocyte, indicating an 8C state (6.8 ± 1.4) and 6 cells could be identified as 16C diplotene oocytes (18.3 ± 2.5). **C:** The pie chart on the right shows the percentage between 8C and 16C pachytene-like oocytes. Cells were analysed with ImageJ and normalized against the 4C somatic cells.

All diplotene oocytes observed (n=6) exhibit an elevated DNA content of 16C (Figure 19B). Of the SCP3-positive stained cells in this germinal bed, 76% of the pachytene-like oocytes show complete colocalization of SCP1 and SCP3 proteins in an elevated DNA state, indications for the formation of the complete synaptonemal complex (Fig. 19A, 19B). In contrast, 24% of the pachytene-like oocytes show co-localization in an 8C state (Fig. 19B). Notably, two of these cells are part of the same oocyte (Fig. 19A, middle). Each nucleus in this oocyte shows approximately an 8C DNA content, with faint SCP1 staining, except at the periphery where synapsis begins. This suggests that the two cells fuse together within the oocyte to enable identical chromosome pairing, which would not occur without this fusion.

The other two cells in this 8C pachytene-like group display partial co-localization of SCP1 and SCP3 (Fig. 19A, left panel), confirming the inability of homeologous chromosomes from four distinct genomes to pair properly.

Further investigations of two other germinal beds from the same species but different specimens (D3514) revealed that, despite the animals being hatched on the same day, the developmental stages of their germinal beds varied slightly. This variation resulted in diverse colocalization patterns observed across different samples of the same species (Fig. 20).

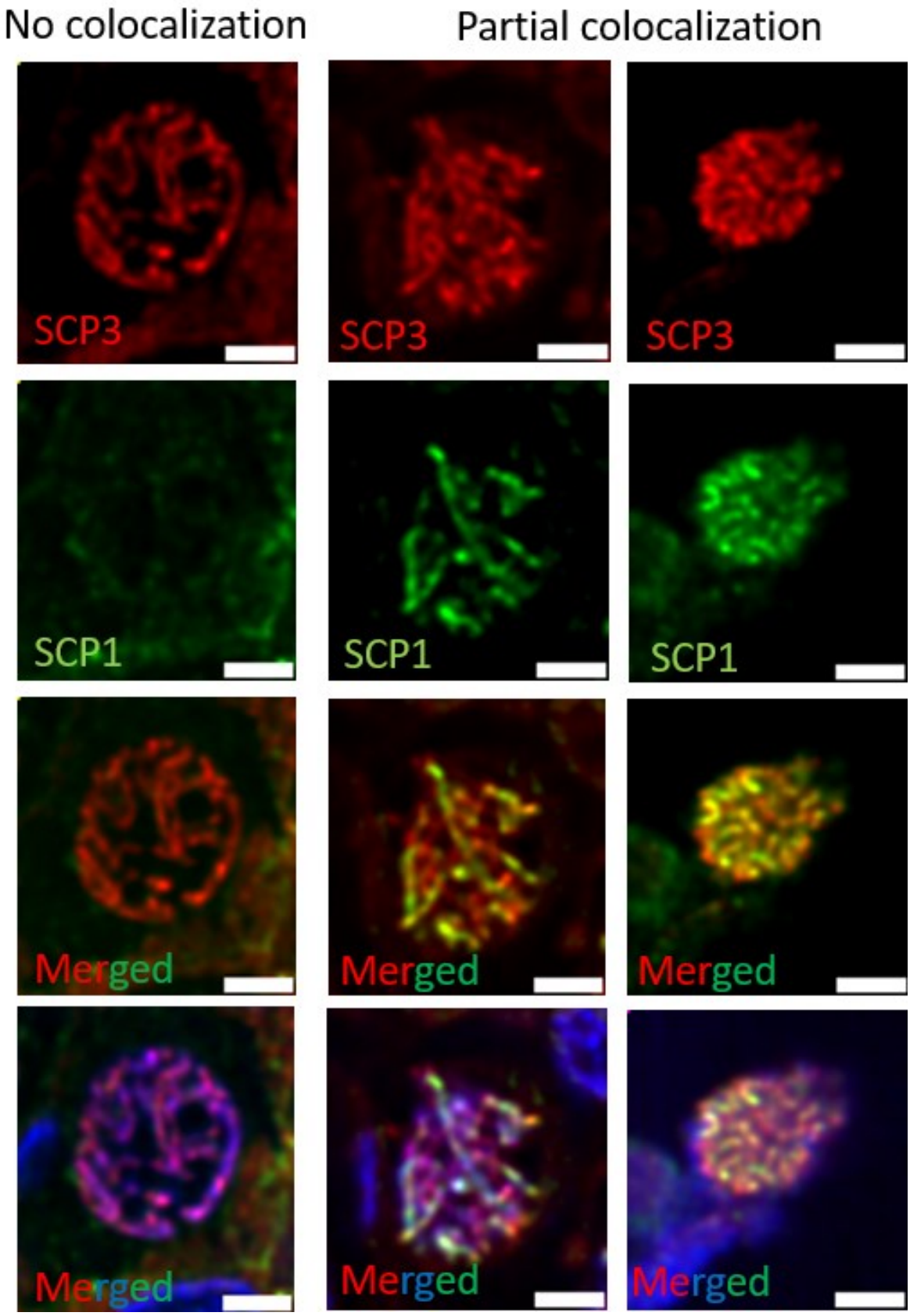

Figure 20: Maximum intensity projection of a single stack showing co-localization patterns of SCP1 and SCP3 in pachytene-like oocytes from *A. townsendae* (D3514) at an age of 31 days. **Left:** No colocalization of SCP1 and SCP3 visible, indicating the absence of the synaptonemal complex. **Right:** Two cases of partial co-localization of SCP1 and SCP3 in pachytene-like oocytes are shown. SCP3 is red, SCP1 is green, DAPI is blue. Scale bar 10 µm.

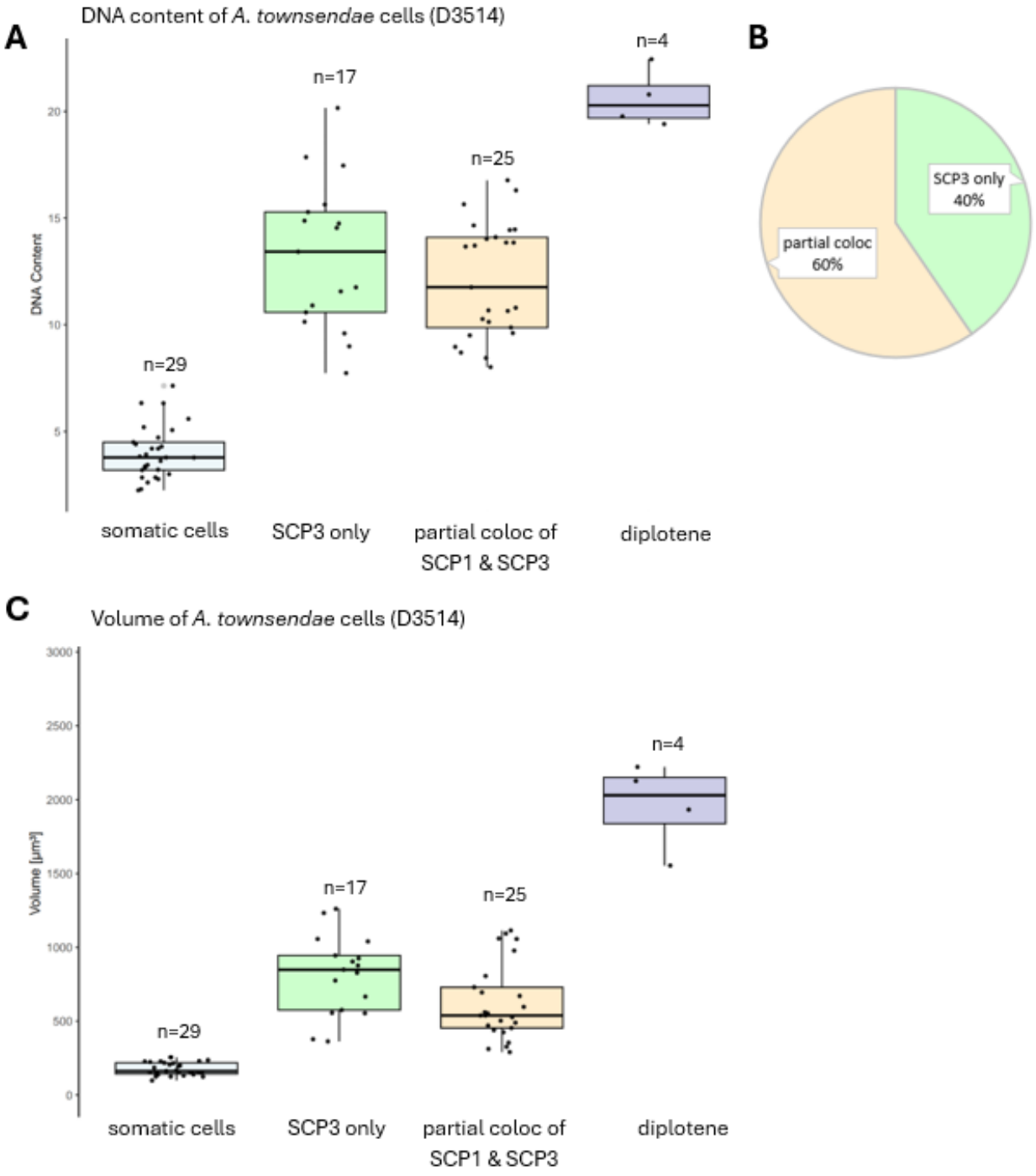

Figure 21: Quantification of DNA content and volume in *A. townsendae* (D3514) cells. **A:** Of the 80 analysed cells, 29 cells are 4C somatic cells (4 ± 1.2). 45 cells are in a pachytene-like state and positive for SCP3. Of these, 17 cells are only SCP3 positive (13.2 ± 3.3). 25 cells indicating partial co-localization of SCP1 and SCP3 (12.1 ± 2.6). Both cell categories show a similar 3D DNA content. Four cells could be categorized as diplotene cells (20 ± 1.1). Cells were analysed with ImageJ and normalized against the 4C somatic cells. **B:** The pie chart shows the percentages of pachytene-like oocytes. **C:** Volume of *A. townsendae* cells is shown: Standard deviation: somatic cells (177 μm^3 ± 43 μm^3), SCP3 only cells (810 μm^3 ± 258 μm^3), partial co-localized pachytene-like oocytes (623 μm^3 ± 251 μm^3), diplotene oocytes (1958 μm^3 ± 255 μm^3).

First, all diplotene oocytes show an elevation in DNA content; the same pattern as observed in all other species and specimens. Of the pachytene-like oocytes, 40% show SCP3-positive chromosome threads, indicating the complete absence of SCP1 (Fig. 21A). In contrast, the remaining 60% of pachytene-like oocytes show partial co-localization of SCP1 and SCP3 (Fig. 21A). The DNA content of both pachytene-like cell categories show a similar broader distribution of DNA content indicating no ploidy elevation, while in contrast the diplotene oocytes indicate a ploidy elevation (Fig. 21A). Seeing the size for the cell categories alone, the average volume of the non-colocalized pachytene-like oocytes lies at 810 μm^3 ±258 μm^3 (Fig. 21C). The average volume of the partial colocalized pachytene-like oocytes lies around 623 μm^3 ±251 μm^3 (Fig. 21C). Comparing this with the average volume of the diplotene oocytes of 1958μm^3± 255 μm^3, it clearly confirmed that no DNA doubling has occurred in the pachytene-like oocytes of both categories.

The results of the DNA content analysis of tetraploid *A. townsendae* (D3513 & D3514) point out that DNA elevation is only observed in diplotene cells and pachytene-like cells showing complete co-localization of SCP1 and SCP3. Without prior DNA doubling, only partial co-localization of SCP1 and SCP3 or no co-localization at all is observed. This confirms that due to the distinct genome composition, of harboring four genomes each of four ancestral species, the homeologous chromosomes are unable to synapse. This aligns with the observations made for triploid *A. uniparens*.

III.II.III. Variation of oocytes in tetraploid Sono

The next investigation includes the tetraploid Sono hybrid, due to its genome composition, consisting of two genomes each from *A. arizonae* and *A. burti* (Fig. 2). This "balanced" genome composition gives the possibility of homeologous chromosome pairing even without ploidy elevation. The observation of the heterogeneity in pachytene-like oocytes, with both elevated and non-elevated DNA states is consistent (Fig. 22).

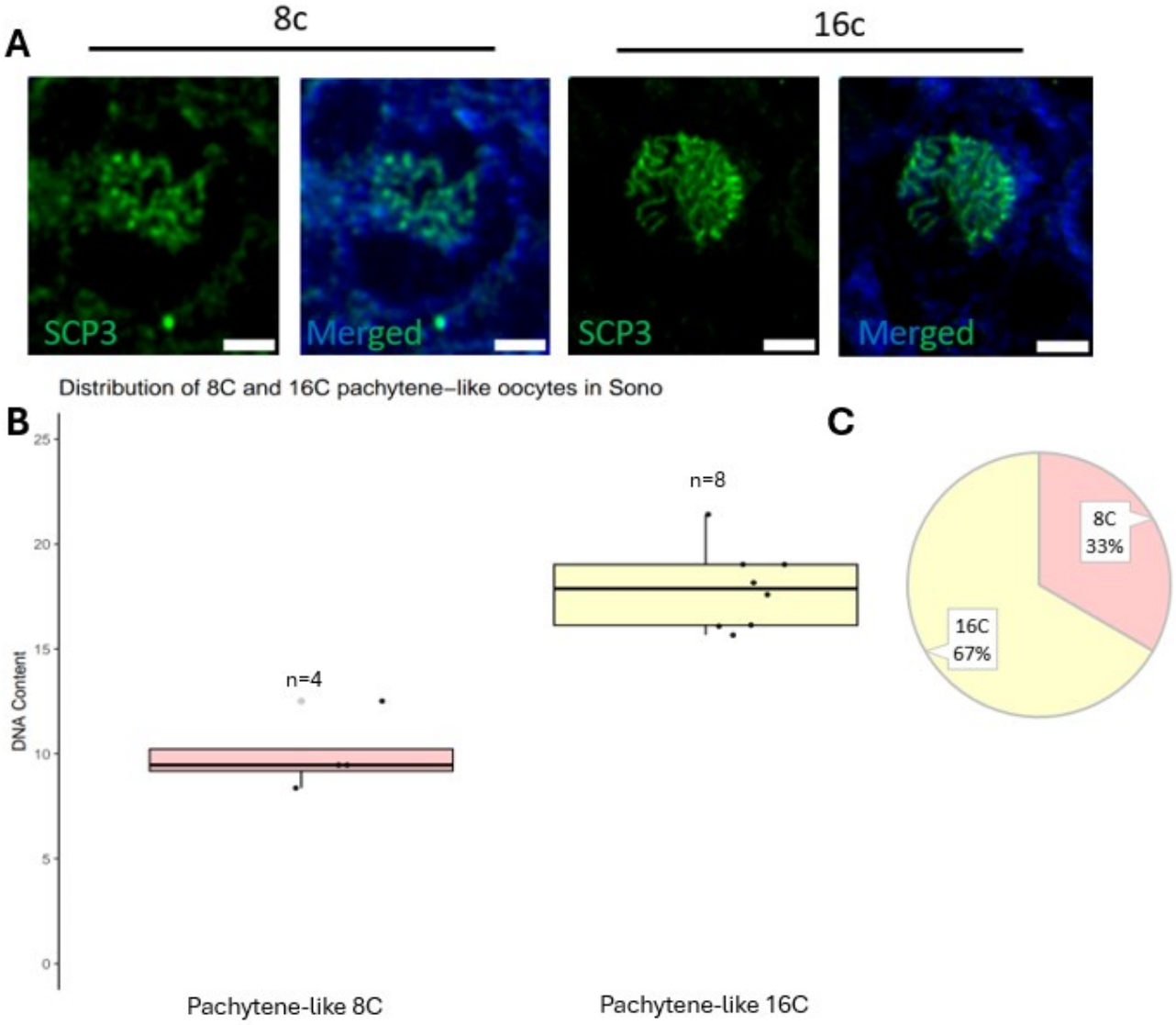

Figure 22: Distribution of pachytene-like oocytes in Sono (D1355) at an age of 21days. **A:** Maximum intensity projections of three z-stacks of pachytene-like oocytes in an unelevated (left) and elevated state (right). SCP3 is green, DAPI is blue. Scale bar 10 µm. **B:** DNA content of the 12 pachytene-like oocytes. 4 cells indicate no ploidy elevation (9.9± 1.5), and 8 cells indicate a ploidy elevation (17.8 ± 1.8). Cells were analysed with ImageJ and normalized against the 4C somatic cells **C:** The pie chart shows the percentages of both cell categories.

Among the twelve pachytene-like oocytes analyzed, 33% display an non-elevated DNA content, while 67% display an elevated DNA content (Fig. 22B). The clear difference in size and chromosome density is visible in Figure 22A.

More strikingly, two distinct types of diplotene oocytes were observed (Figure 23). Figure 23A illustrates the maximum intensity projection of diplotene oocytes in both unelevated and elevated states, where the size difference is evident. The right panel shows both types of diplotene oocytes in close proximity within the germinal bed.

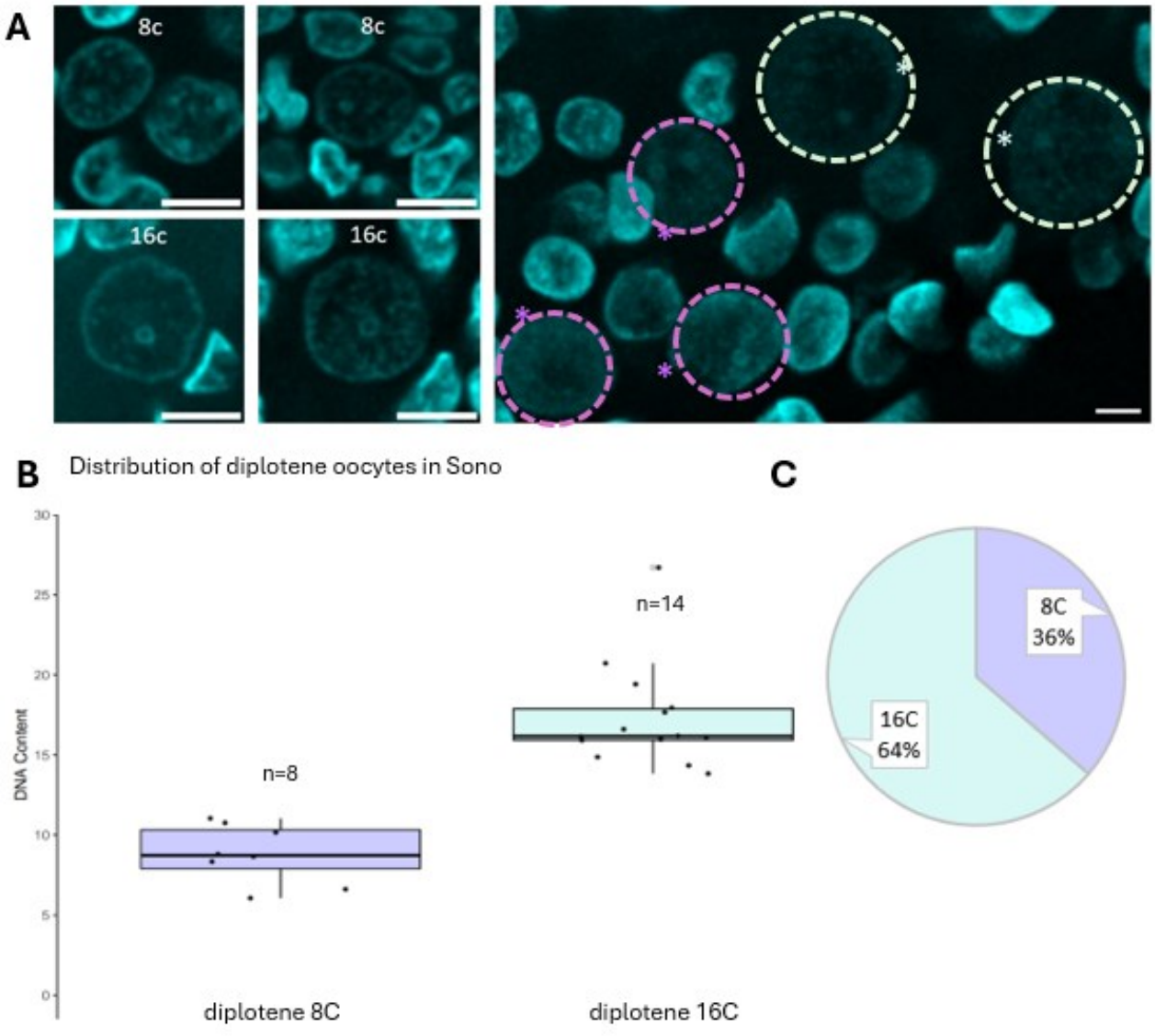

Figure 23: Distribution of diplotene oocytes in Sono (D1355). **A:** Maximum intensity projections of three z-stacks of diplotene oocytes. 36% indicate an 8C state (purple asterix), while 64% indicate a 16C state (cyan asterix). DAPI is cyan. Scale bar 10 µm for small panels, 20 µm for big panel on the right. **B:** DNA content quantification of 22 diplotene oocytes: 8 cells are diplotene 8C (8.8± 1.7), 14 cells indicate an 16C state (17.3± 3.1), Cells were analysed with ImageJ and normalized against the 4C somatic cells. **C:** The pie chart shows the percentages of both cell categories.

Of the 22 diplotene oocytes quantified, 64% are in an elevated 16C state, while 36% were much smaller and indicate an 8C state. This is a key finding in this study and is likely due to the "balanced" genome composition, consisting of two genomes each from *A. arizonae* and *A. burti*. The ability of homeologous chromosomes to pair between the two similar genomes eliminates the need for a migration event to continue meiosis. However, if a non-elevated 8C diplotene oocyte were to develop further, it would result in a ploidy reduction, leading to diploid rather than tetraploid offspring. As a matter of fact, we observed one such rare event in our lizard colony, which will be discussed in the next chapter.

It is important to note that due to technical difficulties early in this study, SCP1 staining in Sono germinal beds primarily resulted in a grainy pattern with significant background noise. Additionally, time constraints at the end of the study limited the number of successful experiments. Consequently, the only available data for Sono stained with both SCP1 and SCP3 comes from a single specimen containing seven oocytes, which show an inconclusive staining pattern for both proteins. However, given the small number of cells and the high likelihood of staining artifacts in this specimen, this analysis is not included.

The key findings from this chapter include the observation of a series of events in parthenogenetic species that enable oocytes to migrate through ring canals into neighboring oocytes. There, oocytes fuse together and double their DNA content to facilitate synapsis between identical chromosomes. Otherwise, due to the distinct genome composition, as the case for *A. neomexicanus*, *A. uniparens*, and *A. townsendae*, homeologous chromosomes are unable to pair. Additionally, in the 'genome-balanced' tetraploid Sono, both elevated and non-elevated diplotene oocytes were observed. This suggests that a nuclear migration event is not always necessary for meiosis to proceed. These findings present an alternative pathway for hybrids with balanced genome compositions. Overall, they underscore the need for further characterization of these hybrids, particularly in how genome composition influences ploidy elevation and maintenance.

III.III. Genotyping of new tetraploid lineages

To further follow on the influence of genome composition on ploidy dynamics, the two tetraploid species *A. townsendae* and Sono, were characterized in more detail (Fig.2).

III.III. I. *Aspidoscelis townsendae*

To confirm that *A. townsendae* is a tetraploid species and maintains their ploidy over several generations, flow cytometry was used to compare the DNA content in nucleated erythrocytes of F_5 and F_6 *A. townsendae* with different species of *Aspidoscelis* of known ploidy (Fig. 24). *Aspidoscelis townsendae* individuals show similar DNA content to *A. neavesi*, the first known and described tetraploid *Aspidoscelis* reproducing through parthenogenetic cloning (Cole et al., 2014).

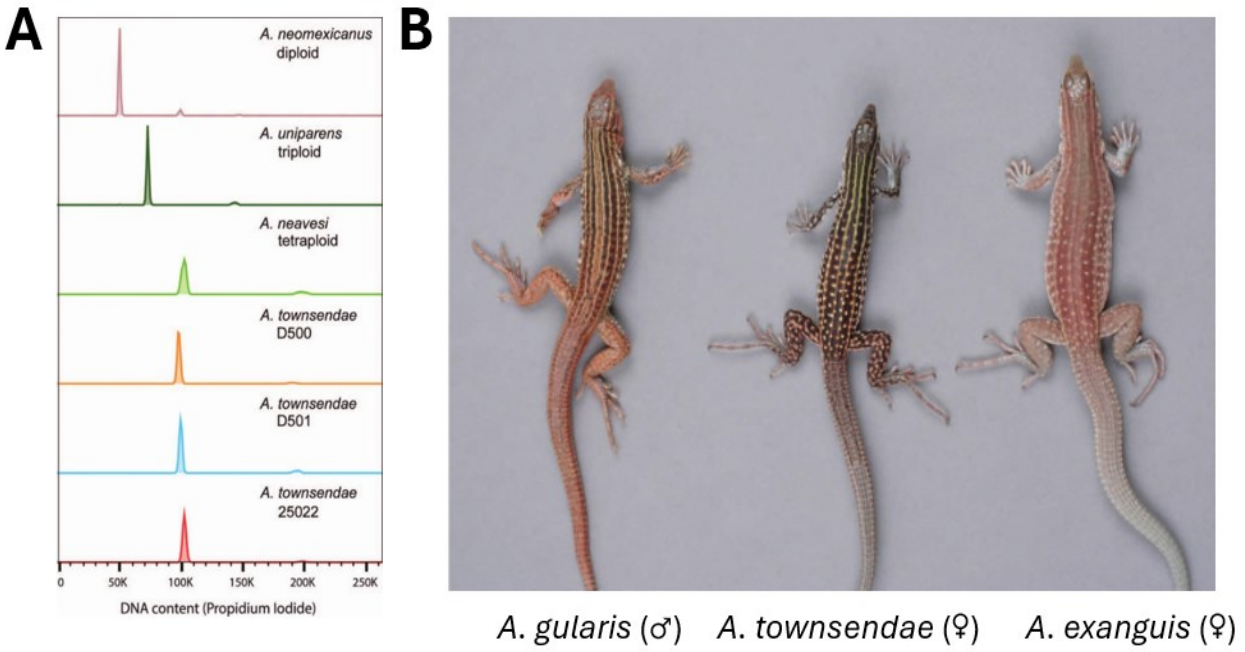

Figure 24: A. DNA content in whole blood nuclei determined by propidium iodide staining and detection by flow cytometry. *A. neomexicanus* (coral), *A. uniparens* (dark green) and *A. neavesi* (light green) were used as representatives for respective levels of ploidy. The three individuals of *A. townsendae* represent the 5th (25022) and 6th (D500 and D501) generation. Number of events scored by flow cytometry were 10,986 (*A. neomexicanus*), 10,931 (*A. uniparens*), 11,633 (*A. neavesi*), 10,524 (D500), 11,137 (D501) and 10,548 (25022). **B.** is showing representatives of *A. gularis* male (left) and *A. exanguis* female (right) and their F1 hybrid *A. townsendae* (middle). Figure adapted from Cole et al., 2023.

The further characterization of the evolutionary history of *A. townsendae* by DNA sequencing data for adenosine deaminase (ADA) intron 9 confirmed the presence of four distinct genomes (Fig. 25). In Figure F, Panel A an alignment of 40 sequences from *A. exsanguis* (22519) over 1,199 positions

was used to generate a Maximum Likelihood tree. The sequences clustered into three groups, where the color-coded boxes represent the ancestral species: *A. arizonae* (red), *A. burti* (blue), and *A. scalaris* (green; inferred because no *A. scalaris* genomic sequence was available). Number in parentheses represent the number of sequences in each cluster, and Maximum likelihood values are shown next to the branches. In B, 19 sequences of *A. burti* (12836) together with 21 sequences of *A. gularis* (007) were combined with the 40 sequences of *A. exsanguis* (22519) and aligned over 1,168 positions in a second Maximum Likelihood tree. The clustering of *A. burti* (12836) in two groups reflects a high degree of heterozygosity. The red and green boxes of *A. exsanguis* (22519) represent the ancestors of that species. In Panel C, 38 sequences of *A. townsendae* (25022) were added to the alignment from panel B and aligned to a total of 118 sequences over 1,118 positions to generate a third Maximum Likelihood tree. It shows that *A. townsendae* (25022) falls into four distinct groups belonging to four distinct ancestral species. In panel D, 41 sequences of another specimen of *A. townsendae* (D500) were added and aligned over 1,176 positions and generated the fourth Maximum Likelihood tree. It confirmed that tetraploidy is maintained over generations.

The multiple sequence alignment FASTA files used to generate the maximum likelihood trees are available on GitHub (2022).

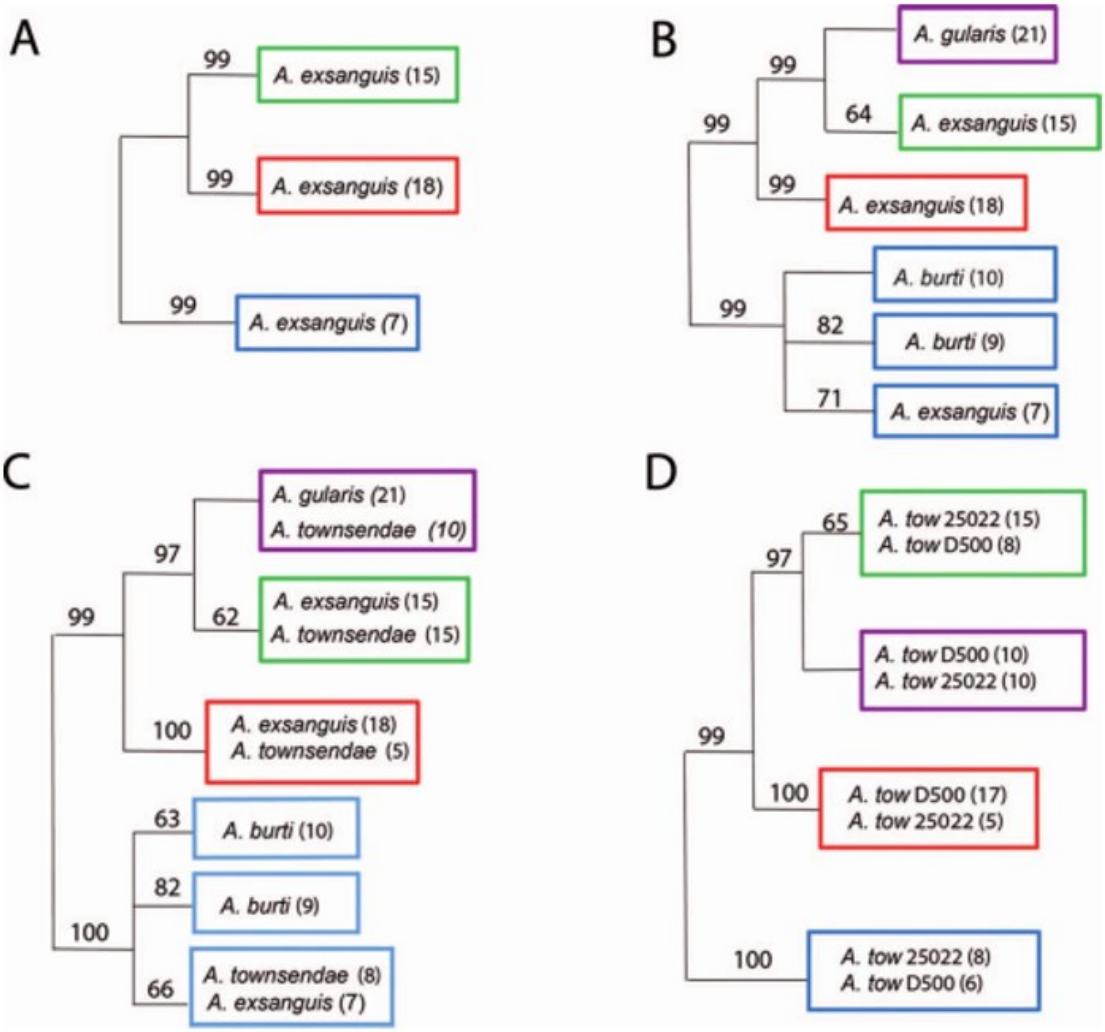

Figure 25: Sequence analysis of ADA intron 9 of *A. townsendae*. Maximum Likelihood trees confirm the presence of four distinct ancestral genomes. **A:** Alignment containing 40 sequences of *A. exsanguis* (22519) over 1,199 positions. **B:** Alignment containing 80 sequences of *A. exsanguis* (22519; 40 sequences), *A. burti* (12836; 19 sequences, blue), and *A. gularis* (007; 21 sequences; purple) over 1,168 positions. **C:** Alignment containing 118 sequences of *A. exsanguis* (22519; 40 sequences), *A. burti* (12836; 19 sequences, blue), *A. gularis* (007; 21 sequences; purple) and A. townsendae (25022; 38 sequences) over 1,118 positions. **D:** Alignment containing 159 sequences of *A. exsanguis* (22519; 40 sequences), *A. burti* (12836; 19 sequences, blue), *A. gularis* (007; 21 sequences; purple) and *A. townsendae* (25022; 38 sequences) and *A. townsendae* (D500) over 1,176 positions. The different color boxes represent the different ancestral species.

The analyses and results presented in this chapter constitute parts to the manuscript published by Cole et al. (2023).

III.III.II. Sono

Over a period of three years, 129 blood samples, including 106 samples of offspring from various Sono lineages, were examined for ploidy by measuring the nuclei area of DAPI-stained nucleated erythrocytes. This technique was developed because it requires less blood than other methods, such as whole blood cell measurements typically conducted using flow cytometry (FACS). Moreover, it is of great importance for assessing genome stability in hybrids, offering a less invasive and more animal-friendly approach while still providing critical insights into genomic integrity in the hybrid lizards studied.

The proof of principle that the method can distinguish between diploid, triploid and tetraploid species is shown in Figure 26. Panel shows that all Sono samples have a similar peak for DNA content as the tetraploid *A. neavesi*, indicating tetraploidy. The number of single-cell events counted ranged from 10,000 to 11,600. Figure 26B shows that measuring the nuclei area of DAPI-stained blood cells is consistent with the flow cytometry results: clustering into three distinct groups, corresponding to the ploidy levels (diploid, triploid, and tetraploid).

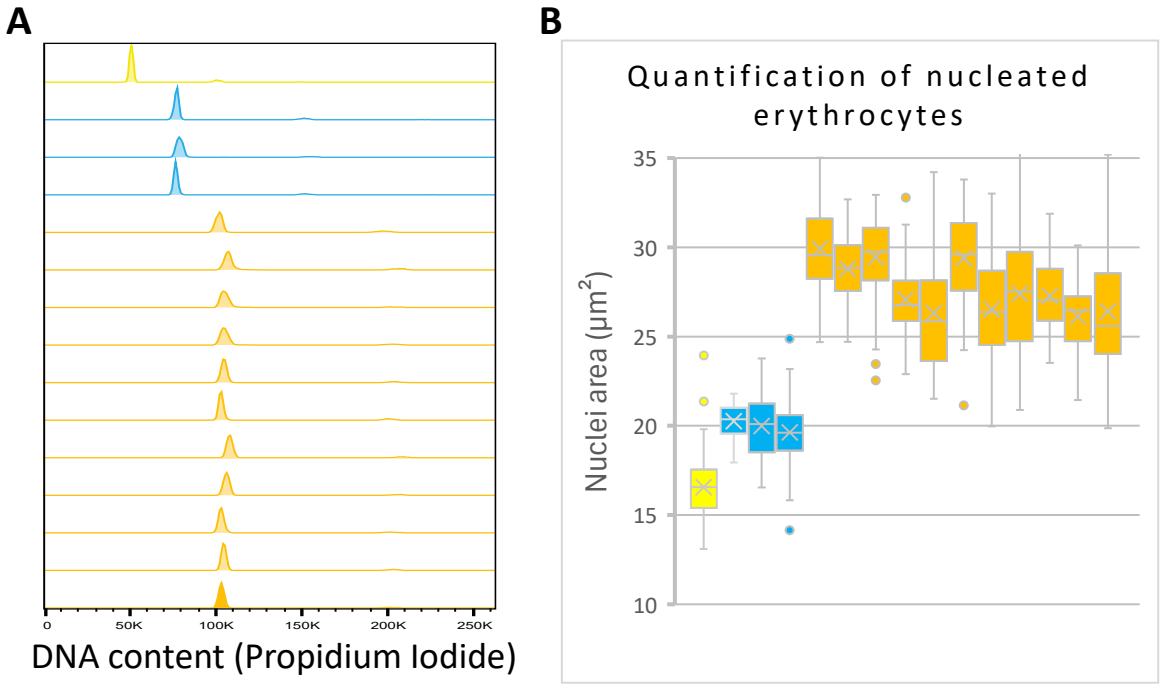

Figure 26: Comparison of flow cytometry (FACS) and area measurements of DAPI stained nucleated blood cells to distinguish between different ploidy levels. **A:** shows the results of flow cytometry. DNA content was stained with Propidium Iodide. The controls are represented by *A. neomexicanus* (diploid control), *A. uniparens* (triploid control), and *A. neavesi* (tetraploid control). Number of single cells counts from top to bottom: 11520; 11315; 10939; 10417; 11513; 11558; 10807; 11286; 11003; 11247; 10830; 10811; 10846, 10893 and 10631. **B:** shows the results of the same samples. DNA content was stained with DAPI, and area measurements of blood cell nuclei were performed in ImageJ. A minimum of 70 cells were measured per sample.

Quantifying 129 specimens from our colony reveal two distinct cases of ploidy loss in our colony (Fig. 28). One reduction from 4N to 2N and one reduction of 4N to 3N. The visual inspection of blood smears supports these quantitative findings (Fig. 27).

In figure 28, the first cluster (yellow) contains seven samples, including four diploid control samples from *A. neomexicanus*. The mean nuclear area for this cluster is 14.64 µm² ±1.83 µm². It reveals that three specimens of Sono fall into this diploid cluster, indicating the reduction in ploidy from 4N to 2N over two generations. The second cluster (blue) includes 18 triploid control samples from *A. sonorae*. The mean nuclear area in this cluster is 20.78 µm² ±2.65 µm², reflecting an intermediate nucleus size for triploid cells. Surprisingly, one Sono specimen (29988), clearly falls into this cluster, indicating a ploidy reduction from 4N to 3N. Considering the occurrence of non-elevated diplotene-like oocytes, a reduction from 4N to 2N could be expected, but this observation indicates even more divers genome dynamics occurring in Sono hybrids. The third cluster (orange) comprises tetraploid control samples from *A. neavesi* and 102 *Sono* specimens, with a mean nuclear area of 30.7 ± 3.94 µm². The larger nuclear size is consistent with the 4N ploidy level, confirming that the majority of Sono specimens in this group maintained their tetraploid status over generations.

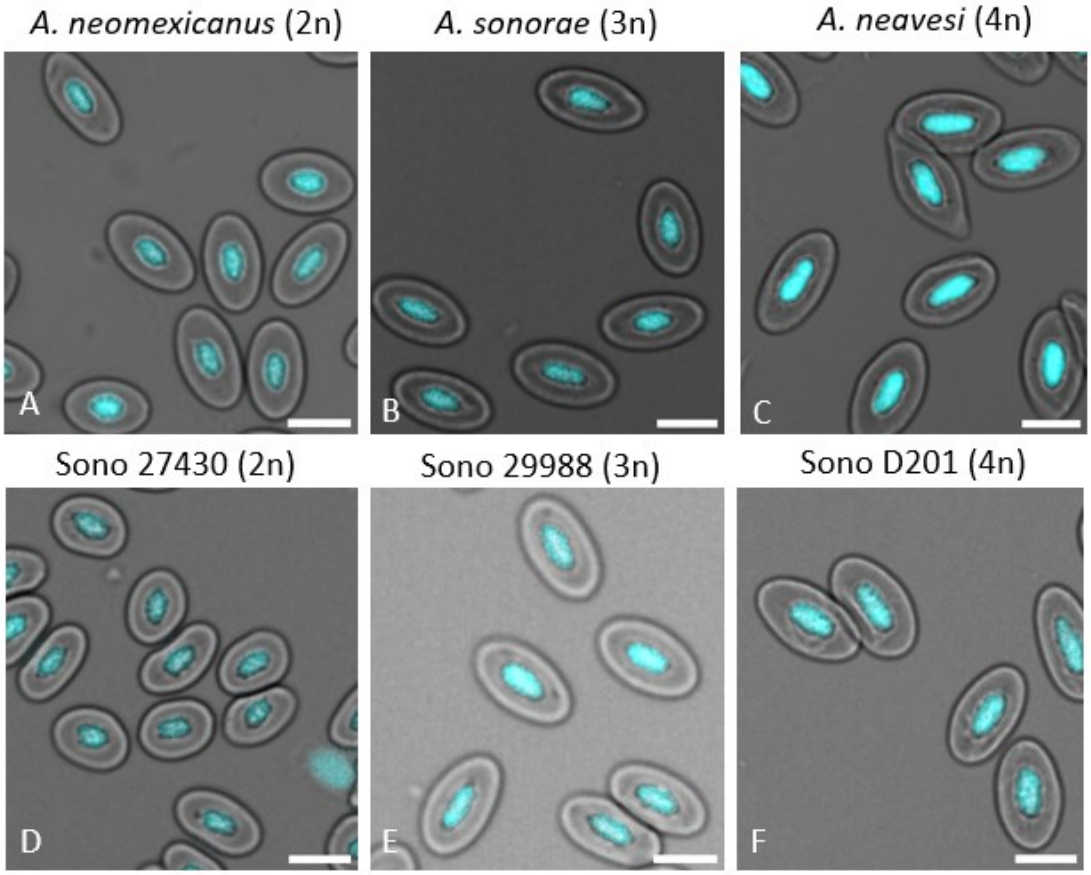

Figure 27: Widefield images of DAPI stained blood cells. Panel A-C show blood smears of the controls panel D to F show corresponding Sono specimens: **A.** *A. neomexicanus (*diploid), **B.** *A. sonorae* (triploid) and **C.** *A. neavesi* (tetraploid). **D.** diploid Sono (27430), **E.** triploid Sono (29988) and **F.** tetraploid Sono (D201). DAPI in cyan. Scale bar is 10 µm.

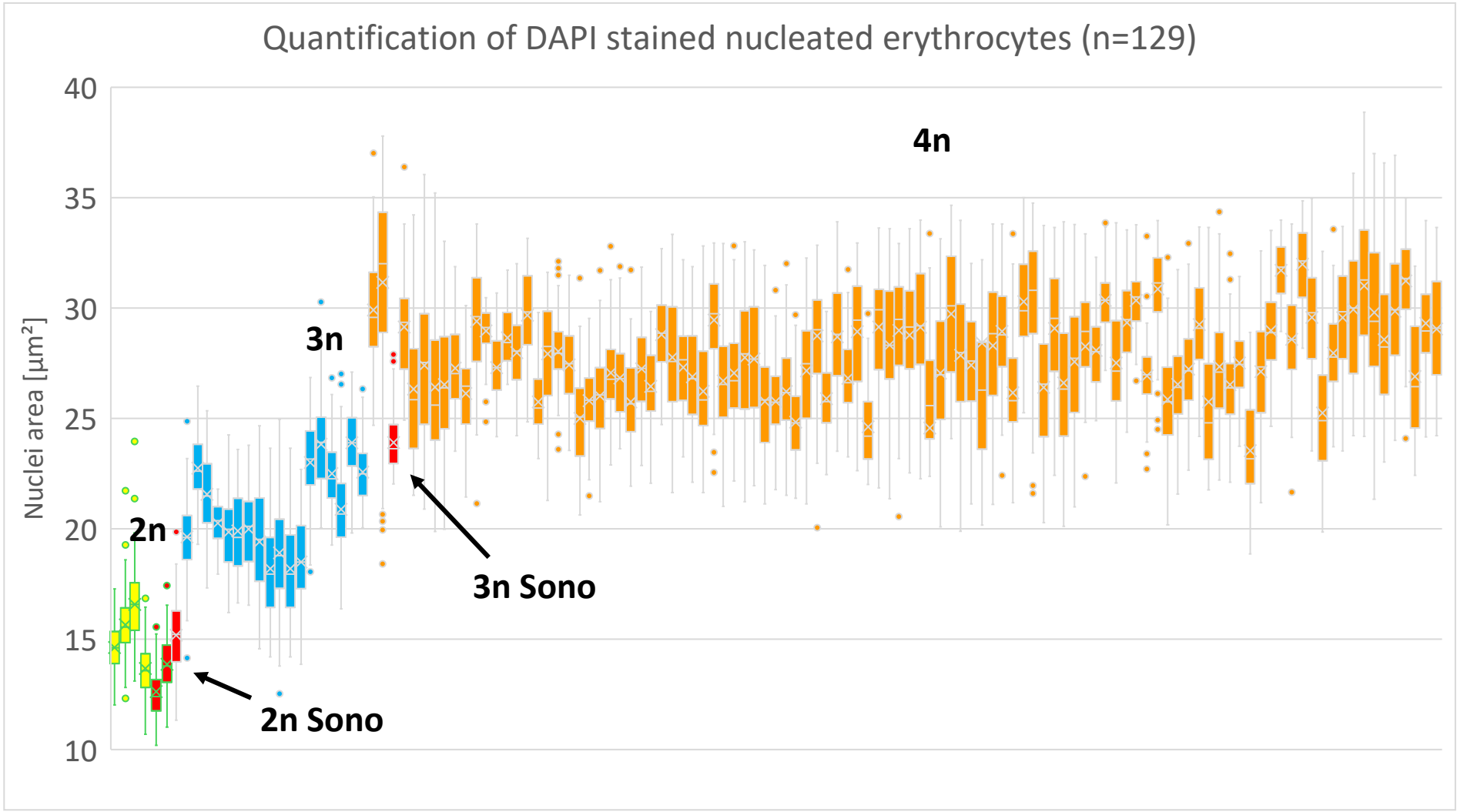

Figure 28: Quantification of DAPI stained nucleated erythrocytes of 129 specimens including *A. neomexicanus* (4), *A. sonorae* (18) and *A. neavesi* (1) Sono (106). Ploidy reduction events are shown with red boxplots. Standard deviations: diploid cluster 2N: 14.64 µm² ±1.83 µm²; triploid cluster 3N: 20.78 µm² ±2.65 µm², tetraploid cluster 4N: 30.7 ± 3.94 µm².

This analysis highlights the occurrence of two significant events of ploidy reduction between the second and third hybrid generations, originating from a specific clutch of three animals (Fig. 29, green circle). The pedigree of the animals involved, illustrating the genetic relationships and lineage connections (Fig. 29).

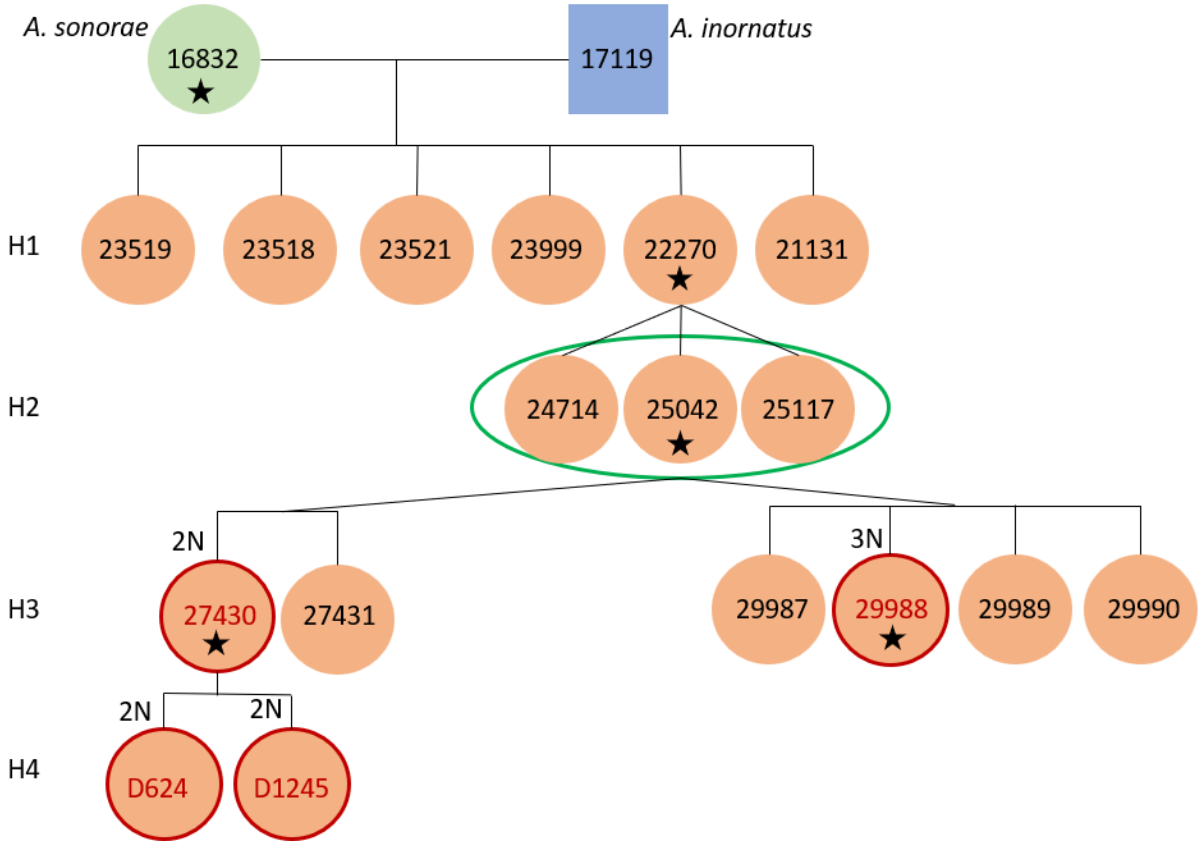

Figure 29: Pedigree showing the genetic relationship in the Sono colony starting from the parental species to follow the ploidy reduction events. Hybridization occurred between *A. sonorae* (16832) and *A. arizonae* (17119). In H1, specimen 22270 gave offspring to a clutch of three animals (within the green circle) from where two independent ploidy reduction events in generation H3 occurred. These animals are marked in red. The 2N-Sono (27430) gave offspring to two other diploid Sono animals in generation H4. The 3N-Sono (29988) has potential offspring, but further analysis is still ongoing. Individuals marked with stars were included in WGS.

The first observed case of ploidy reduction arises from a tetraploid H2 animal (one specimen from clutch highlighted in green). This animal gave rise to a diploid H3 animal, identified as 27430. Interestingly, despite being housed with an *A. arizonae* male since 2021, this animal continued to produce offspring from two independent clutches that also turned out to be diploid (D624 and D1245) in the next hybrid generation.

The other case of ploidy reduction also originates from the same H2 clutch and involves an animal identified as 29988, which exhibits a triploid DNA content based on the blood smear quantification (Fig.28). This animal, born in 2018, has been housed with various lizards over the years, potentially producing offspring. Analysis of the offspring is still in progress. The triploid nature of animal 29988 suggests a different pathway of ploidy reduction compared to the first case. The fact that this animal has a long history of interactions with mates and potential offspring makes it an interesting subject for further studies on the reproductive mechanisms and ploidy stability in hybrid animals including different sequencing approaches here.

Since the approach of Sanger sequencing, as performed for *A. townsendae*, did not provide sufficient information to determine which genomes were lost during the transition from H2 to H3 in the mentioned specimens, alternative sequencing methods were employed. These included in a first approach ddRADseq (double-digested Restricted site Associated DNA sequencing), a technique that allows for identification of genetic variations across the genome. It can provide insights into which segments of the genome might have been lost or altered during the reduction of ploidy (Hühn et al., 2022).

III.III.III. Sequence analysis to determine ploidy reduction

The double-digestion restriction-site associated sequencing (ddRAD-seq) library preparation was performed together with Valentine Patterson and David Ho following the steps of restriction enzyme digest of SbfI and NIaIII, adapter ligation, size selection of a desired fragment length of 375 to 475 bp and final amplification with a unique Illumina P7 index, as explained in more detail in the material and method section. The data analysis was performed by David Ho and included eleven Sono specimens and a triploid control of *A. sonorae* (ID 23988). Briefly, the 12 samples were demultiplexed based on their unique inline barcodes using the process_radtags command from Stacks (v. 2.62). The individual sample files were aligned to the concatenated *A. arizonae* and *A. burti* genomes and further processed with the populations command, which generated a variant calling file. Only sites with a genotype call for all samples were kept, resulting in 5106 SNPs. The principal component analysis (PCA) from the SNPs in figure 30 confirms that the method itself is capable of distinguishing between the closely related hybrids. The clustering in the different groups visible is based on genetic similarities between them. More closely related individuals arising from the same lineage cluster close together such as 29955, D612, D720 and D627 from lineage 22270 and D390, D52 and D570 from lineage 23999. The diploid individual D624 is the only diploid animal included in this analysis and does not cluster with the other Sono individuals. The Sono

individual 29988 is separated along PC1, which indicates more genetic variance between the other tetraploid individuals.

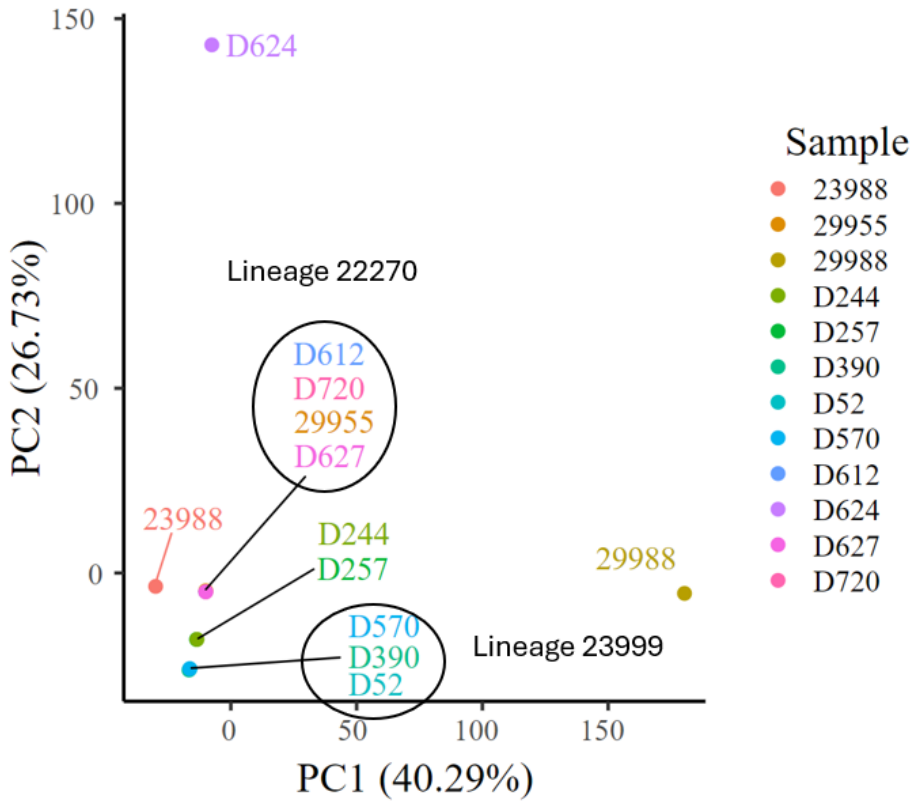

Figure 30: Principal component analysis (PCA) based on 5106 SNPs called across 12 samples. PC1 explains 40,29 % of the variance between the samples, whilst PC2 explains 26,73% of the variance. Of the 12 samples, the tetraploid Sono's cluster together demonstrating their higher genetic similarity. The Sono diploid is separated from the tetraploid cluster along PC2. The potential triploid Sono individual 29988 is separated along PC1. A second triploid animal was identified, *A. sonorae* (23988), however this individual clusters more closely with the tetraploid individuals.

After showing that ddRADseq is a tool which can provide lineage history over generations, a second sequencing run was performed in September 2024, including samples of 80 Sono individuals from different lineages, and 16 controls including *A. uniparens* (3), *A. arizonae* (3), *A. inornatus* (5), *A. sonorae* (4) *A. burti* (1). The analysis will be performed by David H. and is still ongoing.

The results of the blood smear analysis reveal two significant events of ploidy reduction, with ddRADseq confirming a substantial genetic variance of the 2N-Sono (D624) compared to other *Sono* individuals, as well as the potential 3N-Sono (29988). Together, these findings underline their unique genome composition and lead to further investigation through Whole Genome Sequencing

(WGS). WGS is used to elucidate the precise genome compositions of the involved animals and allow us to track the ploidy dynamics that lead to genomic loss in various scenarios.

The analysis was performed by David Ho including samples of five Sono individuals involved in the ploidy reduction process (marked with a star in the pedigree, Fig. 29). The first coverage plot (Fig. 31A) represents the coverage of the triploid *A. sonorae* (16832). Each point represents the average coverage within a non-overlapping 100 kb window. In blue the average of 15x coverage represents the 23 chromosomes of *A. arizonae*. In red the average coverage of 30x represents the 23 chromosomes of the *A. burti* genomes. As the aim of coverage per genome lays at 15x, it confirms the presence of two *A. burti* genomes and one *A. arizonae* genome and therefore triploidy for *A. sonorae* (16832). The second coverage plot (Fig. 31B) represents the coverage of the tetraploid Sono (22270). The average coverage of 30x for both, the *A. arizonae* and the *A. burti* genomes, confirming two genomes each referring to tetraploidy for this animal. The third plot (Fig. 31C) shows the average coverage of Sono 2N (27430). This sample was pooled double the expected concentration, during library prep, to overcome the risk of losing information in case the animal is not diploid (oral communication with David Ho). The coverage plot looks similar to the tetraploid 4N sample. That is not confirming diploidy, but confirms an equal genome composition, which makes diploidy highly likely, if the results of the blood smear quantification and ddRADseq are considered. In the final coverage plot (Fig. 31D), the coverage analysis of the other ploidy reduced sample, Sono 3N (29988), reveals chromosomal abnormalities and dynamics. Most chromosomes follow a 2:1 ratio, consistent with two genomes from *A. arizonae* and one from *A. burti*. However, chromosome 11 from *A. arizonae* appears to have triple coverage, while the reciprocal chromosome from *A. burti* shows reduced coverage. This indicates a structural abnormality or copy number variation specific to that chromosome.

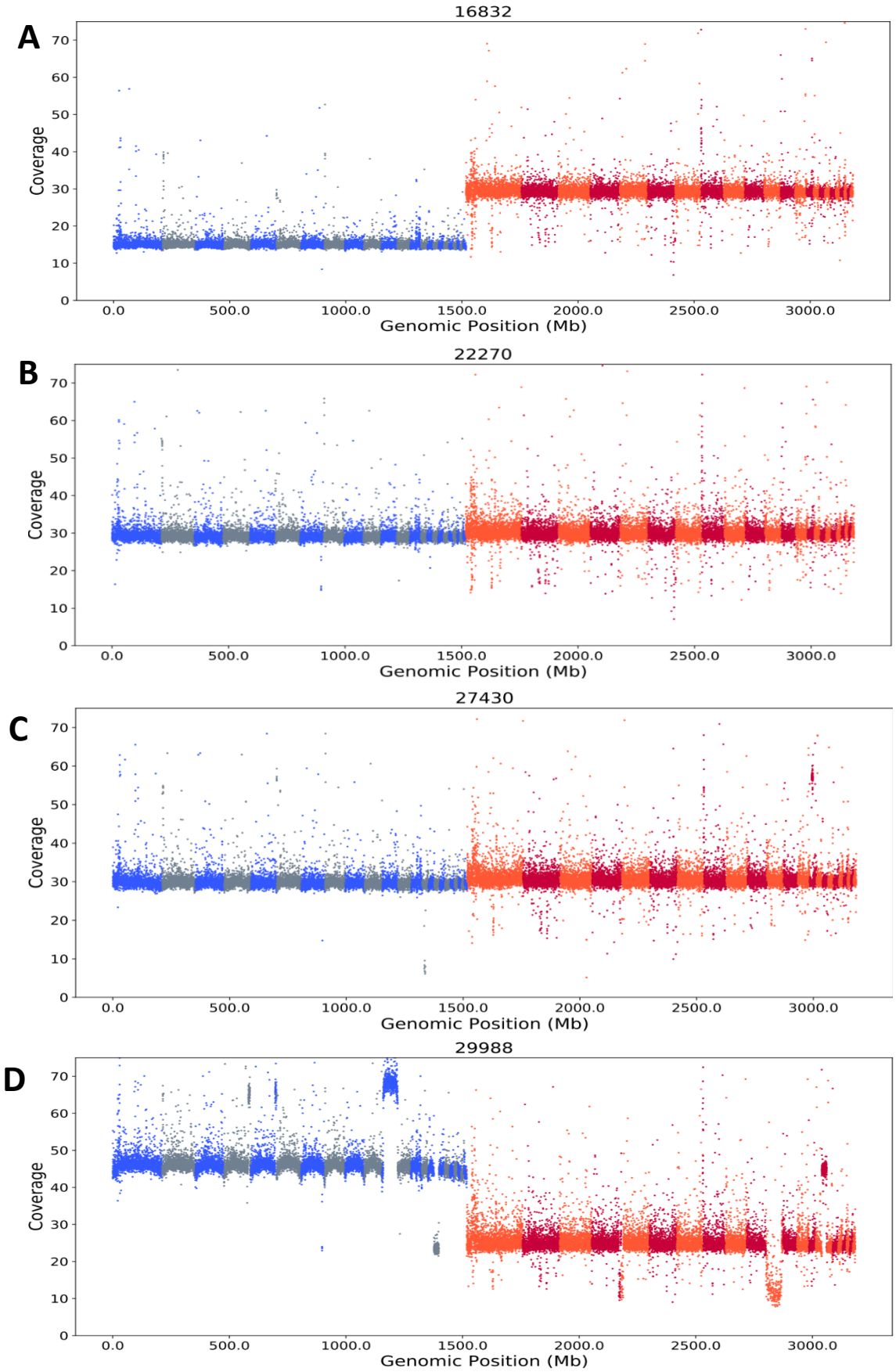

Figure 31: Coverage plots for (A) triploid control *A. sonorae* (16832), (B) tetraploid Sono 22270, (C) 2N-Sono (27430) and (D) 3N-Sono 29988. Each point represents the average coverage for a window size of 100 kb non-overlapping. Each genome was sequenced for an average coverage of x15. The *A. arizonae* chromosomes are represented in blue and *A. burti* chromosomes represented in red. Analysis was performed by David Ho.

The key findings from this chapter indicate that ploidy dynamics are more pronounced in the tetraploid Sono, which has a "balanced" genome composition, compared to *A. townsendae*. While *A. townsendae* consists of four ancestral genomes and maintains its tetraploidy across generations, two ploidy reduction events are observed in Sono. One event leads to diploid offspring, as already hypothesized in case of the progression of an 8C diplotene-like oocytes through meiosis. The second ploidy reduction event leads to most probably triploid offspring, which exhibit chromosome abnormalities, such as reduced and enhanced coverage of single chromosomes in a mainly 2:1 chromosome ratio for *A. arizonae*: *A. burti*.

IV. DISCUSSION

IV.I. The emergence of ploidy elevated oocytes

The presence of oocytes displaying heterogeneity in DNA content, with 55% of pachytene-like oocytes showing an elevated amount of DNA, but 100% of diplotene oocytes showing this ploidy elevation in *Aspidoscelis neomexicanus*, highlights a critical aspect of meiotic progression in parthenogenetic species (Fig. 9). These findings align with those reported in the work of Newton et al., 2016 and open the way to further characterize the mechanism behind the emergence of ploidy elevated oocytes. This study indicates that during oogenesis, in a parthenogenetic species, such as *A. neomexicanus*, the absence of male gametes, to increase the DNA content of oocytes at specific stages, requires an alternative mechanism to complete meiotic divisions. Herein, nuclear migration plays a key role in facilitating these processes. In this study, the number of detected ploidy-elevated oocytes in the pachytene-like state is higher as in the work of Newton et al., 2016. A possible explanation for this could be the individual variation between animals.

The observed pattern of two types of pachytene-like oocytes at different ploidy levels, along with all diplotene oocytes having a duplicated genome, in the diploid *A. neomexicanus*, is consistent with findings in triploid *A. uniparens* (genome composition AAB) (Fig. 18) and tetraploid *A. townsendae* (genome composition ABCD) (Fig. 19 & 21). This phenomenon was also observed in studies of three gecko genera *Hemiphyllodactylus*, *Heteronotia* and *Lepidodactylus* (Dedukh et al., 2022). In contrast, recently published work of rock lizards of the genus *Darevskia* by Dedukh et al., 2024 found evidence for exclusively endoreplicated oocytes in late diplotene, while oocytes in earlier stages contained the original ploidy level. A significant discovery in this study is that in tetraploid Sono (genome composition AABB), not only did the pachytene-like oocytes display varying ploidy levels, but the diplotene oocytes displayed this as well (Fig. 22 & 23). This suggests the possibility of a distinct adaptation in meiotic pathways in parthenogenetic *Aspidoscelis,* influenced by genome composition and that the mechanism of meiosis in asexual vertebrate species may not conform to a one-size-fits-all scenario (Dedukh et al., 2022).

Premeiotic endoreplication traditionally is considered as the primary mechanism driving asexual reproduction in earlier studies of reptiles such as rock lizards and geckos (Kupriyanova et al., 2021; Dedukh et al., 2022), but also in amphibians (Macgregor & Uzzel, 1964) and in natural clonal lineages of loaches (Itono et al., 2006) and other fish (Dedukh et al., 2024b).

This work offers a new observation for the mechanism leading to ploidy-elevated oocytes in parthenogenetic *Aspidoscelis* species. Newton et al. (2016) invalidated the theory of endoreplication occurring before Prophase I, demonstrating that most early-stage oocytes enter meiosis in a diploid state. Unlike many earlier studies on meiotic pathways in parthenogenetic vertebrates, which focused solely on comparison of single oocytes or chromosome patterns to explain the mechanisms of asexual reproduction (Kupriyanova, 2009, Spangenberg et al., 2020, Kupriyanova et al., 2021, Dedukh et al., 2022, Spangenberg et al., 2022), the long-standing research on *Aspidoscelis* extended the investigation to include the entire structure in which oogenesis occurs—the germinal bed.

Through analysis of intact germinal beds from various parthenogenetic *Aspidoscelis* species with differing ploidy levels, three significant findings emerged: (1) the presence of empty, bi-, or polynucleated oocytes; (2) oocytes in the pairing stage exhibiting telomere bouquets that appear to interact with one another; and (3) the movement of constricted nuclei through cytoplasmic bridges known as ring canals.

The accumulation of cells at the pairing stage as described by Newton et al., 2016 can be explained due to the fact that oocytes without a prior migration event are unable to synapse and are arrested, most probably by meiotic checkpoints. These checkpoints have the function of monitoring the fidelity of chromosome synapsis and DNA damage repair (Li et al., 2009). To prevent the next generation of defective gametes, these checkpoints cause the arrest and self-destruct of defective oocytes or a delay of progression to allow for repair mechanisms. In parthenogenetic *Aspidoscelis* oocytes, instead of being driven to apoptosis, the cells are accumulating at the pairing stage and begin to interact with other cells in the same stage. This can be observed in oocytes with telomere bouquets orientated towards each other (Fig. 12) preparing for nuclear fusion. This may be an event which is under positive selection in hybrids, where reproduction depends on elevated oocytes.

The process of nuclear migration through cytoplasmic bridges, often referred to as ring canals (Greenbaum et al., 2009), seems to act as a compensatory mechanism for the inability of homeologous chromosome to recombine. The doubling of DNA content allows oocytes to progress through meiosis, ensuring that ploidy is maintained and genetic stability preserved in the next generation. In obligate parthenogenetic species, this mechanism plays an essential role in maintaining genomic integrity and adaptability in the absence of sexual reproduction. These observations described above collectively suggest a series of events that resemble a pattern observed in the plant kingdom, known as cytomixis (Mursalimov, et al., 2013).

Cytomixis is described as “migration of the nuclei from one plant cell to another through intercellular channels of a special type”. This phenomenon has been observed in over 400 plant species belonging to 84 families, mostly in the microsporocytes in Prophase I (in tobacco and sweet pea), but also during telophase II and tetrad stage (in rape and wild turnip), with a high degree of variation also between different flowers of the same plant (Peng et al., 2003). Even if recently, there has been an increased interest in this phenomenon, its functional significance and genetics are not fully understood and effects on the course of meiosis are unclear (Greenbaum et al., 2009). In general, the rate of cytomixis is drastically increased in polyploids and hybrids, which leads to the hypothesis of cytomixies as a mechanism for stabilizing the newly arisen genomes (Mursalimov & Deineko 2018).

While cytomixis is a well-documented phenomenon in plants, it has not been reported in animals. However, the similarities of cytomixis compared to the observations made in parthenogenetic species of *Aspidoscelis* suggest an intriguing case of evolutionary convergence. This resemblance in nuclear migration mechanisms between distantly related lineages highlights how organisms might develop parallel strategies to maintain genomic stability and ensure successful reproduction without fertilization. Such convergence underlines the adaptive significance of these processes, offering a broader understanding of how parthenogenetic species overcome the challenges of asexual reproduction. The stabilization of newly formed hybrid genomes through nuclear migration may represent an adaptive mechanism to maintain ploidy balance and ensure meiotic progression, like its hypothesized role in plants (Fuentes et al., 2014).

IV.II. Effects of a “balanced” genome composition on homeologous chromosome pairing

This study reveals that a “balanced” genome composition, as it is the case for tetraploid Sono, allows for two sets of *arizonae* chromosomes to undergo homeologous pairing with each other. Similarly, the two sets of burti chromosomes can pair. DNA elevation is not essential in this type of tetraploid hybrid to progress further through meiosis. This is confirmed by the occurrence of diplotene oocytes with varying ploidy levels (Fig. 23), which is a key discovery in this study.

However, the fact that 64% of diplotene oocytes in Sono have undergone a nuclear migration event still leaves the task to examine the two ploidy classes of diplotene cells: What is the ratio between 8C and 16C diplotene cells? Does the ratio remain the same in primordial follicles and where do most 8C oocytes “disappear”?

The observation indicates that even with a balanced genome composition, nuclear migration plays a critical role in ensuring genomic stability and successful meiosis. In cases where a diplotene oocyte progresses without elevated DNA content, it may likely lead to the production of diploids rather than tetraploids in the subsequent generation. Such rare events were observed and further investigated in two different instances within our lizard colony (Fig. 27 & 28).

The offspring, where an H2-generation tetraploid Sono gave rise to diploid offspring (27430) in the next generation, indicates the loss of two genomes from one generation to the next. This aligns with the observed pattern, where an 8C diplotene oocyte without ploidy elevation progresses further through meiosis, ultimately leading to a reduction in ploidy. The lizard (27430) reached an age of around five years, showing no evidence for a reduced health. It was housed together with an *A. arizonae* male for the last three years and gave rise to at least two different clutches with diploid offspring (D624 and D1245) as shown in the relationship pedigree (Fig. 29) Specimen D624 died at a young age of 1,5 years, due to sickness (it had an enlarged gall bladder). Animal D1245 is around two years old however it hasn't produced any offspring as of yet. This could be an indication for reduced health and fertility in the following generations, however the number of these diploid offspring is too low to draw any concrete conclusion. The ddRADseq data confirmed that the diploid Sono (D624) indeed shows a great genetic variation to the other tetraploid Sonos included. The WGS of diploid Sono animal 27430 indicates an equal number of genomes of *A. arizonae* and *A. burti* (Fig. 31). This suggests that this "new variation" diploid Sono resembles the genome composition of *A. preopatae* (Fig. 2), a first-generation hybrid that served as the source for the tetraploid Sono. It is interesting to note that although the genome composition of this diploid Sono is identical to that of *A. preopatae*, they would be genetically distinct from each other.

The second instance of ploidy reduction of a tetraploid sono results in a Sono offspring resembling a triploid animal (Fig. 27 & 28). The Sono animal (29988) emerged from the same clutch as the 2N-Sono, and quantification of DAPI-stained erythrocytes indicated its triploidy (Fig. 28). As shown in the principal component analysis (PCA) obtained via ddRADseq, the animal clusters separately along PC1, indicating substantial genetic variance compared to the other Sono animals. The individual clustered away from the triploid *A. sonorae* (23988), which shares the same genomes (2x *A. burti*, 1x *A. arizonae*), but in a different genomic composition, indicating the variation between the triploid animals. The WGS results revealed an interesting pattern indicating a genome ratio of 2:1 for most chromosomes of *A. arizonae* to *A. burti* as seen in the fourth coverage plot (Fig. 31). That can be seen as an indicator for triploidy and explains the high variance to triploid *A. sonorae*, as this "new variation" triploid genome composition resembles the genome composition of *A.*

uniparens (Fig. 2). Notably, instances of chromosome abnormalities were also identified, such as on chromosome 11. It appears to be the case that chromosome 11 from *A. arizonae* (blue) has triple coverage, while the syntenic chromosome from *A. burti* (red) shows a reduction in coverage.

Possible explanations for the observed chromosomal abnormalities may arise from the complex synapsis patterns of homeologous chromosomes from different species. In intraspecific meiosis, homologous chromosomes align easily due to their structural similarity. However, in hybrids, homeologous chromosomes are quite similar but not identical, making their pairing during meiosis more challenging. Structural differences, such as copy number variations (CNVs), duplications, or translocations, complicate the proper alignment of these chromosomes. This misalignment typically triggers meiotic arrest, necessitating ploidy elevation to address these structural differences, as demonstrated in this study. Nevertheless, we can hypothesize that in rare cases, even after an elevation of ploidy, misarrangements may still occur among the high number of similar homeologous chromosomes present in a single oocyte.

Although Li et al., 2009 also noted that while the pachytene checkpoint is evolutionarily conserved across various organisms, including yeast and mammals, its effectiveness can quickly evolve. In rare cases this could lead to less stringent meiotic checkpoints in hybrids, as observed in triploid *Xenopus* species (Li et al., 2009). Therefore, misalignments not detected by the pachytene checkpoint would result in atypical synapsis patterns between the similar but non-identical homeologous chromosomes in hybrids, potentially causing unequal distribution of genes or chromosome fragments. These could lead to the described chromosomal abnormalities, as seen in the triploid Sono animal 29988, but need further investigations.

IV.III. Synapsis of chromosomes

In this study, the combined staining of two proteins of the synaptonemal complex (SC), SCP1 and SCP3 (Fig. 4), in triploid *A. uniparens* and tetraploid *A. townsendae*, extends the findings of Newton et al. (2016) in other polyploid *Aspidoscelis* species.

In *A. uniparens*, the majority of pachytene-like oocytes (54%) exhibit indications of partial synapsis, as evidenced by the partial colocalization of SCP1 and SCP3 in a 6C state. This result can be explained by the species' genome composition, which consists of two *A. arizonae* genomes and one *A. burti* genome. The presence of two identical genomes facilitates the pairing of homeologous chromosomes between the two similar genomes, resulting in partial synapsis, but complete synapsis

is impaired. In 14% of pachytene-like oocytes, a prior nuclear migration event led to the duplication of the genomes, enabling complete synapsis, as visible by the full colocalization of SCP1 and SCP3 in a ploidy elevated state (Fig. 17 & 18). In contrast, 32% of pachytene-like oocytes show no evidence of nuclear migration, and the absence of SCP1 staining indicates that the synaptonemal complex has not formed. This suggests that even though *A. arizonae* and *A. burti* share a relatively recent common ancestor and a 1:1 syntenic chromosome pattern, their homeologous chromosomes are too distinct to allow for proper synapsis without prior genome duplication. This finding underlines the limitations of homeologous chromosome pairing in hybrid organisms and highlights the importance of ploidy elevation in ensuring proper meiotic progression.

The same pattern is visible in tetraploid *A. townsendae*. Complete synapsis of chromosomes was only observed in cells indicating an elevated ploidy state and therefore the presence of identical chromosomes (Fig. 19-21), while in cells with unelevated DNA content synapsis was detected only on a fraction of chromosomes or not at all. The observation of two other nuclei in an 8C state, being in the process of migration already sharing one cytoplasm in one oocyte, but showing synapsis, is a further confirmation of the cruciality of nucleus migration for successful synapsis.

IV.IV. Conclusion

This study reveals the mechanisms by which obligate parthenogenetic *Aspidoscelis* species complete meiotic division and maintain ploidy and heterozygosity across generations. We observed a series of events in which whole nuclei traverse through ring canals into neighboring oocytes to fuse with other nuclei in the same state. This leads to ploidy elevated oocytes at specific stages of meiosis, which is a necessary adaptation in the pathway to asexual reproduction, as synapsis in hybrids is often impaired due to their distinct genome composition.

Furthermore, this study points out the high level of ploidy dynamics in a “balanced” genome composition compared to the more distinct hybrids. For tetraploid Sono comprising a “balanced” genome composition, a ploidy elevation event is not necessarily needed to produce offspring, even when it is observed in most cases. Consequently, if an unelevated germinal vesical progress further through meiosis, it results in ploidy reduction in the next generation. This caused a new variation of diploid Sono, resembling the genome compositions of first-generation hybrid *A. preopatae*. Moreover, a second event of ploidy loss was observed in this hybrid, most probably caused by the misalignment of homeologous chromosomes during synapsis. In this case the new variation of triploid Sono resembles the genome composition of second-generation hybrid *A. uniparens*.

Altogether, this study presents a striking mechanism on how allopolyploid oocytes are generated to permit clonal reproduction in parthenogenetic species.

FUTURE DIRECTIONS

The “balanced” genome composition in tetraploid Sono, is the cause for two exciting events of ploidy loss in third generation hybrids detected in this work. These two new variations of Sono need further investigations, in the directions of computational science to unravel the ploidy dynamics within Sono on the genetic level.

The analysis of the ddRADseq data of 80 Sono individuals is still in progress and will be used to compare the genetic variation between the individuals. Through this, it will be possible to track the origin of the exact lineage history over generations. This will allow for the identification of potential offspring of Sono 29988 and to investigate if further individuals display chromosomal abnormalities or if this pattern is only rarely observed in Sono individuals.

Investigations of the germinal vesicles in Sono individuals, as well as ploidy level determination in Sono embryos, will be carried out to track the disappearance of the 8C diplotene oocytes throughout development.

Another interesting aspect will be the investigation of heterozygosity and fecundity rates between a single hybrid generation for all species. This will allow for an estimate if changes are more likely to occur in higher generation hybrids and how different these rates are to sexual species.

The design of a specific SCP1 antibody for lizards, as performed for SCP3 by Newton et al., 2016 and the inclusion of more animals especially Sono will be the next step in investigating the synapsis pattern of homeologous chromosomes on a cell biological level.

So far, the driving forces behind the nuclear migration events still remain unclear. The SUN protein of the LINC complex is essential for chromosome movements during Prophase I and warrants further investigation (Lee & Burke, 2018). Additionally, by using antibodies against alpha-tubulin and Dynein, this could provide valuable insights into the moving forces on a cell biological level.

ACKNOWLEDGEMENTS

REFERENCES

1. **Barley, A. J., Nieto-Montes de Oca, A., Manríquez-Morán, N. L., & Thomson, R. C.** (2022). The evolutionary network of whiptail lizards reveals predictable outcomes of hybridization. *Science*, *377*(6607), 773-777. https://doi.org/10.1126/science.abn1593
2. **Barley, A. J., Nieto-Montes de Oca, A., Manríquez-Morán, N. L., & Thomson, R. C.** (2024). Understanding Species Boundaries that Arise from Complex Histories: Gene Flow Across the Speciation Continuum in the Spotted Whiptail Lizards. *Systematic Biology*, syae040. https://doi.org/10.1093/sysbio/syae040
3. **Bass, H. W.** (2003). Telomere dynamics unique to meiotic prophase: formation and significance of the bouquet. *Cellular and Molecular Life Sciences CMLS*, *60*, 2319-2324.
4. **Britten, R. J.** (2002). Divergence between samples of chimpanzee and human DNA sequences is 5%, counting indels. *Proceedings of the National Academy of Sciences*, *99*(21), 13633-13635. https://doi.org/10.1073/pnas.172510699
5. **Cole, C. J.** (1979). Chromosome inheritance in parthenogenetic lizards and evolution of allopolyploidy in reptiles. *Journal of Heredity*, *70*(2), 95-102. https://doi.org/10.1093/oxfordjournals.jhered.a109224
6. **Cole, C. J., Dessauer, H. C., & Barrowclough, G. F.** (1988). Hybrid origin of a unisexual species of whiptail lizard, Cnemidophorus neomexicanus, in western North America: new evidence and a review. American Museum novitates; no. 2905.
7. **Cole, C. J., Taylor, H. L., Baumann, D. P., & Baumann, P.** (2014). Neaves' whiptail lizard: the first known tetraploid parthenogenetic tetrapod (Reptilia: Squamata: Teiidae). *Breviora*, *539*(1), 1-20. https://doi.org/10.3099/MCZ17.1
8. **Cole, C. J., Baumann, D. P., Taylor, H. L., Bobon, N., Ho, D. V., Neaves, W. B., & Baumann, P.** (2023). Reticulate Phylogeny: A New Tetraploid Parthenogenetic Whiptail Lizard Derived from Hybridization Among Four Bisexual Ancestral Species of Aspidoscelis (Reptilia: Squamata: Teiidae). *Bulletin of the Museum of Comparative Zoology*, *163*(7), 247-275. https://doi.org/10.3099/MCZ76
9. **Dedukh, D., Altmanová, M., Klíma, J., & Kratochvíl, L.** (2022). Premeiotic endoreplication is essential for obligate parthenogenesis in geckos. *Development*, *149*(7), dev200345. https://doi.org/10.1242/dev.200345
10. **Dedukh, D., Altmanová, M., Petrosyan, R., Arakelyan, M., Galoyan, E., & Kratochvíl, L.** (2024). Premeiotic endoreplication is the mechanism of obligate parthenogenesis in rock lizards of the genus Darevskia. *Biology Letters*, *20*(9), 20240182. **https://doi.org/10.1098/rsbl.2024.0182**

11. **Dedukh, D., Lisachov, A., Panthum, T., Singchat, W., Matsuda, Y., Imai, Y., ... & Srikulnath, K.** (2024b). Meiotic deviations and endoreplication lead to diploid oocytes in female hybrids between bighead catfish (Clarias macrocephalus) and North African catfish (Clarias gariepinus). *Frontiers in Cell and Developmental Biology*, *12*, 1465335. https://doi.org/10.3389/fcell.2024.1465335
12. **De Kretser, D. M.** (1994). The cytology of the testis. *The physiology of reproduction*, 1177-1290.
13. **Dessauer, H. C., & Cole, C. J.** (1986). Clonal inheritance in parthenogenetic whiptail lizards: biochemical evidence. *Journal of Heredity*, *77*(1), 8-12. https://doi.org/10.1093/oxfordjournals.jhered.a110176
14. **Fuentes, I., Stegemann, S., Golczyk, H., Karcher, D., & Bock, R.** (2014). Horizontal genome transfer as an asexual path to the formation of new species. *Nature*, *511*(7508), 232-235. https://doi:10.1038/nature13291
15. **Fujita, M. K., Singhal, S., Brunes, T. O., & Maldonado, J. A.** (2020). Evolutionary dynamics and consequences of parthenogenesis in vertebrates. *Annual Review of Ecology, Evolution, and Systematics*, *51*(1), 191-214. https://doi.org/10.1146/annurev-ecolsys-011720-114900
16. **Greenbaum, M. P., Iwamori, N., Agno, J. E., & Matzuk, M. M.** (2009). Mouse TEX14 is required for embryonic germ cell intercellular bridges but not female fertility. *Biology of reproduction*, *80*(3), 449-457. https://doi.org/10.1095/biolreprod.108.070649
17. **Ho, D. V., Tormey, D., Odell, A., Newton, A. A., Schnittker, R. R., Baumann, D. P., ... & Baumann, P.** (2024). Post-meiotic mechanism of facultative parthenogenesis in gonochoristic whiptail lizard species. *Elife*, *13*, e97035. https://doi.org/10.7554/eLife.97035
18. **Hudson, A. M., & Cooley, L.** (2002). Understanding the function of actin-binding proteins through genetic analysis of Drosophila oogenesis. *Annual review of genetics*, *36*(1), 455-488. https://doi.org/10.1146/annurev.genet.36.052802.114101
19. **Hühn, P., Dillenberger, M. S., Gerschwitz-Eidt, M., Hörandl, E., Los, J. A., Messerschmid, T. F., ... & Kadereit, G.** (2022). How challenging RADseq data turned out to favor coalescent-based species tree inference. A case study in Aichryson (Crassulaceae). *Molecular Phylogenetics and Evolution*, *167*, 107342. https://doi.org/10.1016/j.ympev.2021.107342
20. **Itono, M., Morishima, K., Fujimoto, T., Bando, E., Yamaha, E., & Arai, K. (2006).** Premeiotic endomitosis produces diploid eggs in the natural clone loach, Misgurnus anguillicaudatus (Teleostei: Cobitidae). *Journal of Experimental Zoology Part A: Comparative Experimental Biology*, *305*(6), 513-523. https://doi.org/10.1002/jez.a.283
21. **Jaron, K. S., Bast, J., Nowell, R. W., Ranallo-Benavidez, T. R., Robinson-Rechavi, M., & Schwander, T.** (2021). Genomic features of parthenogenetic animals. *Journal of Heredity*, *112*(1), 19-33. https://doi.org/10.1093/jhered/esaa031

22. **Kearney, M., Fujita, M. K., & Ridenour, J.** (2009). Lost sex in the reptiles: constraints and correlations. *Lost sex: the evolutionary biology of parthenogenesis*, 447-474. https://doi.org/10.1007/978-90-481-2770-2_21
23. **Kline, A., Curry, T., & Lewellyn, L**. (2018). The Misshapen kinase regulates the size and stability of the germline ring canals in the Drosophila egg chamber. *Developmental biology*, *440*(2), 99-112. https://doi.org/10.1016/j.ydbio.2018.05.006
24. **Kravets, E. A., Plohovskaya, S. H., Horyunova, I. I., Yemets, A. I., & Blume, Y. B.** (2021). Sources of chromosomal polymorphism of microsporocytes in species of Lilium L. and Allium L.: cytomixis, extra chromosomes, and chromatin diminution. *Cytology and Genetics*, *55*, 107-116. https://doi.org/10.3103/S0095452721020080
25. **Kumar, S., G. Stecher, M. Li, C. Knyaz, K. Tamura, and X. Mega.** 2018. Molecular evolutionary genetics analysis across computing platforms. *Molecular Biology and Evolution* 35(6): 1547–1549. https://doi.org/10.1093/molbev/msy096.
26. **Kupriyanova, L.** (2009). Cytogenetic and genetic trends in the evolution of unisexual lizards. *Cytogenetic and genome research*, *127*(2-4), 273-279. https://doi.org/10.1159/000303325
27. **Kupriyanova, L. A., Safronova, L. D., Sycheva, V. B., Danielyan, F. D., & Petrosyan, V. G.** (2021). Oogenesis (prophase 1 of meiosis) and mitotic chromosomes of parthenogenetic species Darevskia armeniaca (family Lacertidae). *Biology Bulletin*, *48*, 274-280. https://doi.org/10.1134/S1062359021030080
28. **Li, X. C., Barringer, B. C., & Barbash, D. A.** (2009). The pachytene checkpoint and its relationship to evolutionary patterns of polyploidization and hybrid sterility. *Heredity*, *102*(1), 24-30. https://doi.org/10.1038/hdy.2008.84
29. **Lee, Y. L., & Burke, B.** (2018, October). LINC complexes and nuclear positioning. In *Seminars in cell & developmental biology* (Vol. 82, pp. 67-76). Academic Press. https://doi.org/10.1016/j.semcdb.2017.11.008
30. **Lowe, C. H., & Wright, J. W.** (1966). Evolution of parthenogenetic species of Cnemidophorus (whiptail lizards) in western North America. *Journal of the Arizona Academy of Science*, *4*(2), 81-87. https://www.jstor.org/stable/40022375
31. **Lutes, A. A., Neaves, W. B., Baumann, D. P., Wiegraebe, W., & Baumann, P. (**2010). Sister chromosome pairing maintains heterozygosity in parthenogenetic lizards. *Nature*, *464*(7286), 283-286. https://doi.org/10.1038/nature08818
32. **Lutes, A. A., Baumann, D. P., Neaves, W. B., & Baumann, P**. (2011). Laboratory synthesis of an independently reproducing vertebrate species. *Proceedings of the National Academy of Sciences*, *108*(24), 9910-9915. https://doi.org/10.1073/pnas.1102811108

33. **Macgregor, H. C., & Uzzell Jr, T. M. (1964).** Gynogenesis in salamanders related to Ambystoma jeffersonianum. *Science*, *143*(3610), 1043-1045. https://doi.org/10.1126/science.143.3610.1043
34. **Manning, G. J., Cole, C. J., Dessauer, H. C., & Walker, J. M.** (2005). Hybridization between parthenogenetic lizards (Aspidoscelis neomexicana) and gonochoristic lizards (Aspidoscelis sexlineata viridis) in New Mexico: ecological, morphological, cytological, and molecular context. *American Museum Novitates*, *2005*(3492), 1-56. http://hdl.handle.net/2246/5661
35. **Moller, C.A., Gaál, T. and Mills, J.N.** (2016), The hematology of captive Bobtail lizards (*Tiliqua rugosa*): blood counts, light microscopy, cytochemistry, and ultrastructure. Vet Clin Pathol, 45: 634-647. https://doi.org/10.1111/vcp.12425
36. **Mursalimov, S. R., Sidorchuk, Y. V., & Deineko, E. V.** (2013). New insights into cytomixis: specific cellular features and prevalence in higher plants. *Planta*, *238*, 415-423. https://doi.org/10.1007/s00425-013-1914-0
37. **Mursalimov, S., & Deineko, E.** (2018). Cytomixis in plants: facts and doubts. *Protoplasma*, *255*, 719-731. https://doi.org/10.1007/s00709-017-1188-7
38. **Neaves, W. B., & Baumann, P.** (2011). Unisexual reproduction among vertebrates. *Trends in Genetics*, *27*(3), 81-88. https://doi.org/10.1016/j.tig.2010.12.002
39. **Newton, A. A., Schnittker, R. R., Yu, Z., Munday, S. S., Baumann, D. P., Neaves, W. B., & Baumann, P.** (2016). Widespread failure to complete meiosis does not impair fecundity in parthenogenetic whiptail lizards. *Development*, *143*(23), 4486-4494. https://doi.org/10.1242/dev.141283
40. **Peng, Z. S., Yang, J., & Zheng, G. C.** (2003). Cytomixis in pollen mother cells of new synthetic hexaploid amphidiploid (Aegilops tauschii× Triticum turgidum). *Cytologia*, *68*(4), 335-340. https://doi.org/10.1508/cytologia.68.335
41. **Reeder, T. W., Cole, C. J., & Dessauer, H. C.** (2002). Phylogenetic relationships of whiptail lizards of the genus Cnemidophorus (Squamata: Teiidae): a test of monophyly, reevaluation of karyotypic evolution, and review of hybrid origins. *American Museum Novitates*, *2002*(3365), 1-61. https://doi.org/10.1206/0003-0082(2002)365<0001:PROWLO>2.0.CO;2
42. **Schindelin, J., Arganda-Carreras, I., Frise, E., Kaynig, V., Longair, M., Pietzsch, T., ... & Cardona, A.** (2012). Fiji: an open-source platform for biological-image analysis. *Nature methods*, *9*(7), 676-682. https://doi.org/10.1038/nmeth.2019
43. **Spangenberg, V., Arakelyan, M., Cioffi, M. D. B., Liehr, T., Al-Rikabi, A., Martynova, E., & Kolomiets, O.** (2020). Cytogenetic mechanisms of unisexuality in rock lizards. *Scientific Reports*, *10*(1), 8697. https://doi.org/10.1038/s41598-020-65686-7
44. **Spangenberg, V., Arakelyan, M., Galoyan, E., Martirosyan, I., Bogomazova, A., Martynova, E., & Kolomiets, O.** (2021). Meiotic synapsis of homeologous chromosomes and

mismatch repair protein detection in the parthenogenetic rock lizard Darevskia unisexualis. *Molecular Reproduction and Development*, *88*(2), 119-127. https://doi.org/10.1002/mrd.23450

45. **Wright, J. W., Spolsky, C., & Brown, W. M.** (1983). The origin of the parthenogenetic lizard Cnemidophorus laredoensis inferred from mitochondrial DNA analysis. *Herpetologica*, 410-416. https://www.jstor.org/stable/3892537
46. **Zhao, J., Li, J., Lv, R., Wang, B., Zhang, Z., Yu, T., ... & Liu, B.** (2023). Meiotic pairing irregularity and homoeologous chromosome compensation cause rapid karyotype variation in synthetic allotetraploid wheat. *New Phytologist*, *239*(2), 606-623. https://doi.org/10.1111/nph.18953